FORMATION OF HYBRID CdSe-LOADED TiO_2 NANOTUBES FOR SOLAR-DRIVEN PHOTOELECTROCHEMICAL WATER SPLITTING PROCESS

LAU KUNG SHIUH

INSTITUTE OF GRADUATE STUDIES
UNIVERSITY OF MALAYA
KUALA LUMPUR

2016

FORMATION OF HYBRID CdSe-LOADED TiO_2 NANOTUBES FOR SOLAR-DRIVEN PHOTOELECTROCHEMICAL WATER SPLITTING PROCESS

LAU KUNG SHIUH

DISSERTATION SUBMITTED IN FULFILMENT OF THE REQUIREMENTS FOR THE DEGREE OF MASTER OF PHILOSOPHY

INSTITUTE OF GRAUDATE STUDIES
UNIVERSITY OF MALAYA
KUALA LUMPUR

2016

UNIVERSITY OF MALAYA

ORIGINAL LITERARY WORK DECLARATION

Name of Candidate: LAU KUNG SHIUH

Matric No: HGA 130006

Name of Degree: MASTER OF PHILOSOPHY

Title of Thesis: FORMATION OF HYBRID CdSe-LOADED TiO_2 NANOTUBES FOR SOLAR-DRIVEN PHOTOELECTROCHEMICAL WATER SPLITTING PROCESS

Field of Study: MATERIALS ENGINEERING (NANOTECHNOLOGY)

I do solemnly and sincerely declare that:

(1) I am the sole author/writer of this Work;
(2) This Work is original;
(3) Any use of any work in which copyright exists was done by way of fair dealing and for permitted purposes and any excerpt or extract from, or reference to or reproduction of any copyright work has been disclosed expressly and sufficiently and the title of the Work and its authorship have been acknowledged in this Work;
(4) I do not have any actual knowledge nor do I ought reasonably to know that the making of this work constitutes an infringement of any copyright work;
(5) I hereby assign all and every rights in the copyright to this Work to the University of Malaya ("UM"), who henceforth shall be owner of the copyright in this Work and that any reproduction or use in any form or by any means whatsoever is prohibited without the written consent of UM having been first had and obtained;
(6) I am fully aware that if in the course of making this Work I have infringed any copyright whether intentionally or otherwise, I may be subject to legal action or any other action as may be determined by UM.

Candidate's Signature Date:

Subscribed and solemnly declared before,

Witness's Signature Date:

Name:

Designation:

ABSTRACT

Solar hydrogen generation from water electrolysis is a key target for the development of sustainable hydrogen economy for future energy system. The formation of self-organized TiO_2 nanotubes without bundling is essential for high efficiency in photoelectrochemical (PEC) water electrolysis application. This research project demonstrated an efficient approach to enhance the solar-driven photoelectrochemical (PEC) water splitting performance by incorporating an optimum amount of CdSe species into TiO_2 nanotubes film. Based on the results obtained, highly ordered TiO_2 nanotubes (AR = 57.95, G = 379.04) were successfully synthesized through electrochemical anodization of Ti foil in ethylene glycol electrolyte containing 0.3 wt% of NH_4F and 5 wt% of H_2O_2 at 40 V for 1 h. Promising anodic TiO_2 nanotubes were further underwent heat treatment at 400 °C for 4 h. Continuous efforts have been exerted to further improve the PEC water splitting performance by incorporating an optimum content of CdSe species into TiO_2 nanotubes using chemical bath deposition technique. It was found that TiO_2 nanotubes soaked in 5 mM CdSe precursor for one hour at room temperature exhibited higher photocurrent density (~2.50 mA/cm^2) compared to pure TiO_2 nanotubes (1.45 mA/cm^2). The presence of CdSe at approximately 1 at% in TiO_2 showed an improvement of photocurrent density because it acted as an effective mediator to trap the photo-induced electrons and minimizes the recombination of charge carriers. In contrast, excessive CdSe content of 1.5 at% loading and higher on the wall surface of TiO_2 nanotubes resulted in poor PEC water splitting performance because independent layers acting as recombination centers for the charge carriers was formed.

ABSTRAK

Penjanaan hidrogen solar dari elektrolisis air adalah sasaran utama dalam pembangunan ekonomi hidrogen mampan bagi sistem tenaga masa depan. Pembentukan nanotiub TiO_2 yang tersususn tanpa pemberkasan adalah penting untuk kecekapan dalam penggunaan elektrolisis air fotoelektrokimia yang tinggi. Projek penyelidikan ini menunjukkan satu pendekatan yang cekap untuk meningkatkan prestasi elektrolisis air fotoelektrokimia yang didorongi oleh solar dengan penggabungan jumlah spesies CdSe yang optimum ke TiO_2 nanotube filem. Berdasarkan keputusan yang diperolehi, nanotube TiO_2 yang sangat tersusun (AR = 57.95, G = 379,04) telah berjaya disintesis melalui elektrokimia anodisasi filem Ti dalam glikol etilena yang mengandungi 0.3 wt% NH_4F dan 5 wt% H_2O_2 pada 40 V selama 1 h. Nanotiub TiO_2 anodik yang telah berjaya disintesis dirawati dengan suhu sebanyak 400 ° C selama 4h. Usaha yang berterusan telah dikenakan dalam peningkatan lagi prestasi pembelahan air fotoelektrokimia dengan menggabung kandungan optimum spesies CdSe ke atas nanotiub TiO_2 malalui teknik pemendapan mandian kimia. Ia telah mendapati bahawa nanotiub TiO_2 yang direndam di dalam CdSe pelopor dengan kepekatan 5 mM selama sejam pada suhu bilik menghasilkan ketumpatan arusfoto yang lebih tinggi (~ 2.50 mA / cm^2) berbanding dengan nanotiub TiO_2 tulen (1.45 mA / cm^2). Kehadiran unsur CdSe lebih kurang 1% pada filem nanotiub TiO_2 menunjukkan peningkatan ketumpatan arusfoto kerana ia bertindak sebagai pengantara yang berkesan untuk memerangkap elektron teraruh oleh cahaya dan mengurangkan penggabungan semula pembawa cas. Sebaliknya, kandungan CdSe yang lebih daripada 1.5 at% mentap pada permukaan dinding nanotiub TiO_2 melemahkan prestasi pembelahan air fotoelektrokimia dengan sebab pembentukan lapisan bebas yang bertindak sebagai pusat penggabungan semula pembawa cas.

ACKNOWLEDGEMENTS

I would like thanks University of Malaya (UM) and Nanotechnology and Catalysis Research Centre (NANOCAT) for offering me an opportunity and providing a conductive research environment with sufficient facilities to complete my research project

I would also like to express my deep and sincere gratitude to my supervisors, Dr. Lai Chin Wei and Prof Sharifah Bee Abd Hamid for giving precious advice, excellent guidance in minimum words and provided a good basis for the present thesis to complete of my Master Research Project. Their wide knowledge and logical way of thinking also have been of great value for me.

Many thanks go to all the technical staff in various laboratories that aided me throughout my work. They offered me their generosity and technical support whenever I faced difficulties when using the machines and equipment. In my daily work, I have been blessed with a group of friendly and helpful postgraduate colleagues. With their valuable suggestions and discussions, I was able to produce quality results and thesis.

Finally, I thank my family for the love and support given throughout all my studies at the university.

TABLE OF CONTENTS

LIST OF FIGURES

LIST OF TABLES

LIST OF SYMBOLS AND ABBREVIATIONS

atm	:	Standard atmosphere
at%	:	Atomic percentage
α	:	Absorption coefficient
cm	:	Centimeter
e^-	:	Electron
eV	:	Electronvolt
h	:	hour
h^+	:	Hole
hv	:	Photon energy
G	:	Geometric surface area factor
j_p	:	Photocurrent density
mA	:	Miliampere
ml	:	Milliliter
mm	:	Millimeter
mM	:	Milimolar
min	:	Minute
nm	:	Nanometer
s	:	Second
µm	:	Micrometer
V	:	Voltage
W	:	Watt
wt%	:	Weight percentage
λ	:	Radiation wavelength
θ	:	Diffraction angle

°C	:	Degree Celsius
0D	:	Zero-dimensional
1D	:	One-dimensional
2D	:	Two-dimensional
AR	:	Aspect ratio
C	:	Carbon
CB	:	Conduction band
Cd	:	Cadmium
CdSe	:	Cadmium selenide
DC	:	Direct current
DRS	:	Diffuse Reflectance Spectroscopy
EDX	:	Energy dispersive X-ray spectroscopy
EG	:	Ethylene glycol
F	:	Fluorine
FESEM	:	Field emission scanning electron microscope
H_2	:	Hydrogen
H_2O	:	Water
H_2O_2	:	Hydrogen peroxide
HF	:	Hydrofluoric acid
Li	:	Lithium
Na_2SeSO_3	:	Sodium selenosulphate
Na_2SO_3	:	Sodium sulphite
NH_4F	:	Ammonium fluoride
O2	:	Oxygen
•OH	:	Hydroxyl radicals
PEC	:	Photolectrochemical

PL	:	Photoluminescence
Pt	:	Platinum
Se	:	Selenium
Ti	:	Titanium
TiO_2	:	Titanium dioxide
UV	:	Ultraviolet
VB	:	Valence band
XPS	:	X-ray photoelectron spectroscopy
XRD	:	X-ray diffraction

CHAPTER 1: INTRODUCTION

1.1 Introduction

It is well known that energy shortage is one of the most intractable challenges humankind are facing in this era. The drastic demand of energy is evidenced by the depletion of fossil fuel resources and increasing price of oil and gas, which results from exponential global population growth plus economic prosperity. This has remarkable impact towards our future generation. Moreover, the increasing of fossil fuels utilization that cause global warming from greenhouse effect has further exacerbated this phenomena. According to Yu and Chen, the extreme climate change is also caused by the greenhouse gases from human activities. It has wrought ravage towards our homeland since several years ago (Yu & Chen, 2009). Many are actually aware that human activities like burning fossil fuels for electricity, transportation, industry, and agriculture will release enormous quantity of greenhouse gasses to the atmosphere. As a result, environmental destruction such as global warming, ocean acidification, ozone layer depletion has become a worldwide problem (Ghicov & Schmuki, 2009). Worse still, if this problem prolonged, all the inhabitants will eventually extinct due to the changes of weather and climate patterns of earth.

One of the approaches taken by many countries in minimizing environmental problems is via sustainable development. The scientists believed that sustainable development is an ultimate goal of this modern era reflecting coeval demand for economic, social, political and ecological improvement. Therefore, executing researches for generating green and renewable energy resource are prioritized. This is essential because renewable energy is sustainable. Moreover, the discoveries of alternative clean energy source is likewise crucial to enhance our quality of life and the environment (Kreuter & Hofmann, 1998).

Hydrogen (H_2) has been generally recognized as environmentally friendly fuel carrier and most likely the best replacement of fossil fuel as a green and sustainable energy. Since many are concerned about the rapidly depletion of traditional fossil fuels and the greenhouse effect caused by the combustion of fossil fuels, H_2 has been regarded as an attractive sustainable energy (Cortright *et al.*, 2002). However, the hydrogen gas used in industry is mainly obtained through high-energy consumption process from non-renewable resources (e.g., fossil fuels). The production processes are neither environmentally friendly nor economical (Turner, 2004). Therefore, there is a great interest in developing a promising solution to reduce the implementation and associated costs of the production of H_2. Since the pioneering discover by Fujishima and Honda (Fujishima & Honda, 1972) on the semiconductor-based photoelectrochemical (PEC) water splitting, it has drawn considerable development in this important field. The PEC water splitting has become a promising way for a sustainable and environmentally friendly production of H_2 under solar illumination. Hence, the scientists are getting more interested to power non-polluting vehicles by using H_2. The major manufacturers have also put in enormous efforts on the hydrogen-powered cars (H_2 fuel cell vehicle), whereas the production processes of hydrogen generation are environmentally hazardous. Therefore, there is a great demand in the generation of environmentally benign H_2 using renewable energy since the development of H_2 application technologies are growing rapidly (Bak *et al.*, 2001).

In order to satisfy our green energy demand, solar energy appear to be the most viable choice and abundancy as compare to other resources. The earth continuously receives 120,000 TW of energy from the sun. This figure dramatically exceeds the global primary energy consumption rate (17 TW per year) (Crabtree & Lewis, 2007). Thus, it signify that with very less amount of earth's surface (~0.1%) is covered with solar cells, it would satisfy up to 10% of our current energy needs. Accordingly, today less than 0.1% of the

global energy consumption generated from sunlight could be achieved. Furthermore, the existing solar cells possess low efficiencies and required expensive manufacturing cost. Hence, Moniz *et al.* suggested that innovations are still encouraged to produce solar cell harvest incident solar photons with greater efficiency and economic feasibility (Moniz *et al.*, 2015).

Among viable renewable H_2 production approaches, the use of photoelectrochemical (PEC) water splitting system has become one of the most promising methods to secure the future supply of green and sustainable H_2 energy (Grätzel, 2001; Liu *et al.*, 2011). The general term for the chemical reaction of separating water into O_2 and H_2 by utilizing a semiconductor photocatalyst to catalyse the reaction is called PEC water splitting process (Kubacka *et al.*, 2011; Ni *et al.*, 2007). Figure 2.1 illustrates the reaction of PEC water splitting by a semiconductor photocatalyst schematically. PEC solar cell employs a semiconductor photocatalyst to drive the chemical energy, which turns to a high-energy state by illumination ($h\nu$). Under illumination, two phenomena are involved: (a) photocatalysis in which optical energy provides activation energy for reaction to occur (Equation 1.1)(Galinska & Walendziewski, 2005); and (b) photoelectrolysis whereby optical energy is converted to chemical energy (Equation 1.2 & 1.3) as presented below:-

$$TiO_2 \xrightarrow{h\nu > Eg} TiO_2\,(e^- + h^+) \qquad \text{(Equation 1.1)}$$

$$2H_2O + 4h^+ \rightarrow O_2\,(gas) + 4H^+ \qquad \text{(Equation 1.2)}$$

$$2H^+ + 2e^- \rightarrow H_2\,(gas) \qquad \text{(Equation 1.3)}$$

Theoretically, PEC water splitting solar cell for hydrogen generation requires three main characteristic: (a) stability against photocorrosion in aqueous solution, (b) visible light photosensitivity, and (c) more electronegative conduction band related to H^+ reduction level (H_2/H_2O) (Bak *et al.*, 2002; Grätzel, 2001; Kubacka *et al.*, 2011). A

number researches have been done on semiconductor materials to fulfill the requirements of the PEC process. Unfortunately, such a semiconductor with the properties of stable, efficient light absorption system coupled with favourable semiconductor-redox energetic has remain undiscovered. However, several success has been reported by employing metal oxide semiconductor, especially titanium dioxide (TiO_2) (Aroutiounian *et al.*, 2005; Bak *et al.*, 2001; Macak *et al.*, 2007).

TiO_2 possess many unique properties that are hardly found in other semiconducting materials like ZnO, ZnS, GaN, etc. The advantage properties include low production cost, exceptional photocorrosion resistance, nontoxicity and strong photocatalytic activity. However, TiO_2 is still insufficient to work alone as a practical semiconductor for PEC cell due to its large band gap post by its polymorph (3.2 eV on the anatase) which has poor responsive towards visible light and undesired photogenerated electron-hole pairs recombination, which is thermodynamically favoured (Ni *et al.*, 2007). Since the process of electrons transfer to the conduction band of the oxide is a surface phenomenon, it is anticipated that the larger the surface area of the semiconductor, more photo-induced electrons can be transferred to the electrode. Therefore, it is inferred that one-dimensional (1D) nanostructure, such as nanotubular structure could enhance PEC water splitting process (Grimes, 2007; Mor *et al.*, 2006).

Continuous efforts have been exerted to improve equilibrium reactions by simultaneous control of oxidation and dissolution reactions to grow highly-ordered nanotubes by incorporating a controlled amount of adsorbed small band gap semiconductor cadmium-selenide (CdSe) into TiO_2 nanotubes. In fact, this CdSe dopants is one of the popular Group II-VI semiconductor materials being used to sensitize wide band gap semiconductors due to its wider absorption range (below 730 nm) as compared with CdS dopants where its absorption range below the wavelength of approximately 550

nm. The conduction band edge of a small band gap CdSe is higher than that of the TiO_2 which has large extinction coefficient strongly absorb visible light. The photogenerated electrons in the small band gap CdSe can be injected to the conduction band of the TiO_2 and thereby, contribute to increase solar energy conversion (Lopez-Luke *et al.*, 2008). Furthermore, band gap narrowing provides sites that slow down the recombination of charge carriers and improves visible light absorption. CdSe-loaded TiO_2 nanotubes forms a type II band alignment with TiO_2 which has large absorption cross sections, is thermally stable and do not easily photodegrade. As a result, the photocatalytic reaction can be initiated by any photoexcited electrons in the CdSe dopants which injected into TiO_2 and subsequently migrate to counter electrode for H_2 evolution. This type of heterostructured nanomaterial can facilitate charge separation by utilizing the visible or near-IR photons to prevent fast recombination (Wang *et al.*, 2009).

1.2 Problem statement

Since the early of last century, TiO_2 has immerged as one of the most widely studied and used materials due to its inherent merits of physio-chemical properties. To date, well-aligned 1D TiO_2 nanotubes synthesized through electrochemical oxidation reaction on a Ti substrate has been widely reported. However, TiO_2 nanotubes photocatalyst has yet not sufficient from becoming a potential material for PEC water splitting for H_2 generation application. The poor visible-light absorption and high recombination losses of charge carries have restricted the widespread use of pure TiO_2 nanotubes photocatalyst in PEC water splitting H_2 generation application. In fact TiO_2 nanotubes only works effectively under UV region (λ<400nm) where our solar energy only contains about 4-5 % of UV rays. Hence, utilization of visible spectrum from our solar energy (40-45 %) is essential that lead to the higher photoconversion efficiency in solar-driven water-splitting applications.

Besides, oxidation and dissolution reactions also draw significant influences on the structural characteristics of nanotubes and its properties during electrochemical anodization. Although fluoride (F^-) ions could enhanced the growth rate of TiO_2 nanotubes with desired length, pore diameter and wall thickness, dis-equilibrium reactions between oxidation and dissolution while anodization but the optimum amount of ammonium fluoride interact in the ethylene glycol electrolyte contain of H_2O_2 still remain to be addressed. In order to get the right dimensions and morphologies for better PEC water splitting performance, a controlled synthesis procedure for the production of well-aligned and highly ordered TiO_2 nanotubes still remain a great challenging. Generally, highly ordered TiO_2 nanotubes will lead to undesirable bundling problems, which prominently reduce the photoconversion efficiencies in water splitting system. Thus in order to manufacture high efficient solar-driven PEC water splitting system using TiO_2 nanotubes as a photoelectrode is very defiant unless above mentioned issues are addressed.

1.3 Research objectives

The objectives of this research are as follow:-

- To synthesize and characterize the hybrid CdSe–loaded TiO_2 nanotubes film via electrochemical anodization (e.g., composition of electrolyte, time, voltage) technique followed by chemical bath deposition technique (e.g., temperature, molarity of precursors, time).
- To investigate hybrid CdSe–loaded TiO_2 nanotubes based photocatalysts for water splitting hydrogen generation system under solar illumination (e.g., photocurrent density, amount of H_2 generation).

1.4 Outline of Research Work

The three main sectors in this research study includes synthesis of the CdSe-loaded TiO_2 nanotubes film, data collection and analysis for materials characterization as well as evaluation of PEC water splitting performance under solar illumination was presented and discussed below. This research study aims to achieve high PEC water splitting performance using synthesized CdSe-loaded TiO_2 nanotubes film under solar illumination.

1.4.1 Synthesis of CdSe-loaded TiO_2 Nanotubes Film

The CdSe-loaded TiO_2 nanotubes film was synthesized via chemical bath deposition technique. Ti foil was cut into the dimension of 50 mm × 10 mm and degreased by sonication in acetone for 30 min before rinsing with deionized water and subsequently dried in ambient condition before the anodization process. The anodization process was performed in a premixed ethylene glycol (EG) electrolyte consisting of hydrogen peroxide (H_2O_2) and ammonium fluoride (NH_4F). Ti foil served as anode anodized in two electrodes configuration whereas platinum rod served as cathode. In order to maintain a uniform current in the electrolyte, soft agitation (air bubbling) was applied near the Ti electrode. A DC power supply (CBS Scientific EPS-200X) was used to perform the anodization at desired potential and duration. Then, the as-anodized Ti foils was rinsed using deionized water and subjected to sonication for 1 min and further dried in ambient temperature. Heat treatment of annealing on as anodized nanotubes arrays plays an essential role to convert innate amorphous structure to the desired polymorph. It eventually determines their potential applications.

For the deposition of CdSe on TiO_2 nanotubes, two step procedures were involved. In the first step, both of the precursors of Se and Cd that are, sodium selenosulfite (Na_2SeSO_3) and $Cd(NH_3)_4^{2+}$ solution was prepared, which consequently allowed to react

with annealed anatase TiO_2 nanotubes by bathing it in the bath solution contained both Cd and Se ions precursors in the second step. The detail procedures used to prepare the samples are discussed in Chapter 3- Research Methodology.

1.4.2 Materials Characterization

The physical and chemical properties of CdSe-loaded TiO_2 nanotubes such as morphological, structural, chemical, optical, and electronic properties was characterized via various characterization techniques. The anodized sample's surface and cross-sectional morphologies was studied by Field Emission Scanning Electron Microscopy (FESEM), whereas the element analysis was performed by Energy Dispersive X-Ray Spectroscopy (EDX) analysis. Moreover, both Raman Spectroscopy and X- ray diffraction (XRD) was used to justify samples' phase transition. The Photoluminescence Spectroscopy (PL) determined the structural defect state that appeared within the anodic growth of CdSe-loaded TiO_2 nanotubes. UV-vis Diffuse Reflectance Spectroscopy (UV-vis DRS) was used to determine the optical properties of the CdSe-loaded TiO_2 nanotubes. Meanwhile, the elemental composition, chemical state, oxidation state and electronic state was determined and quantified by high sensitive X-ray Photoelectron Spectroscopy (XPS) from the sample surface. The principle and the measuring conditions of each measurement are discussed in Chapter 3- Research Methodology.

1.4.3 Photoelectrochemical Water Splitting Performance Evaluation

The PEC water splitting properties of the samples was characterized using a three electrodes configuration PEC water splitting solar cell, with CdSe-loaded TiO_2 nanotubes as the working electrode, platinum sheet as the counter electrode, and Ag/AgCl as the references electrode under solar irradiation by using a 150 W Xenon arc lamp, AM 1.5 with UV-visible-infra red wavelength range. 1 M KOH aqueous solution was used as electrolyte in the PEC cell. Three electrodes system was applied for electrochemical

measurements. All three electrodes are connected to the potentiostat operate by a controlling software NOVA. A linear sweep potential (LSP) swept from -1.0 V to 1.0 V at a scan rate of 5 mV/s was performed to measure the corresponding photocurrent. Water displacement technique was applied to collect the H_2 gas generated at platinum rod. As the H_2 gas is produced in the counter electrode in PEC water splitting cell, it bubbled up into inverted burette. By reading the gas level on the side of burette, the volume of H_2 gas was determined.

1.5 Outline of Thesis

This thesis is structured into total five chapters accordingly. Chapter 1 presents a brief introduction, problem statements, research objectives, research frame work and lastly a thesis overview. In Chapter 2, a comprehensive review on the synthesis methods of TiO_2 nanotubes arrays and functional application of TiO_2 nanotubes including solar H_2 generation production via the PEC water splitting reaction. Moreover, Chapter 2 encompasses literature review on the CdSe-loaded TiO_2 using different approaches as well as their potential applications. Chapter 3 details experimental procedures for this research. The specifications of the raw materials and research methodology to obtain hybrid CdSe-loaded TiO_2 nanotubes arrays are included. This epitomized also the characterization techniques and equipment employed in this study with brief explanation on the operation principles and their sample preparation. Chapter 4 presents the experimental results and the discussions on the formation of high aspect ratio CdSe-loaded TiO_2 nanotubes arrays. Three sections in total, first is regarding the growth behavior pure TiO_2 nanotubes arrays by varying anodic oxidation parameters (e.g., electrolyte composition, anodization time and applied voltage), 2) the formation of CdSe-loaded TiO_2 nanotubes arrays by chemical bath deposition, 3) the potential of CdSe-loaded TiO_2 nanotubes arrays and pure TiO_2 nanotubes arrays for solar energy harvesting

H_2 generation applications. Chapter 5 concludes this research and also some suggestions plus recommendations for the further research.

CHAPTER 2: LITERATURE REVIEW

2.1 Introduction

In 1991, Iijima's successfully discovered carbon nanotubes and since then generated unprecedented interest in the area of one-dimensional (1D) nanostructure in the field of nanotechnology due to its supreme molecular geometry properties with high surface area, distinct electrical properties like, high electron mobility, quantum confinement effect and high mechanical strength (Lieber, 1998; Rao *et al.*, 2006). Indeed, this breakthrough has triggered subsequent interests in photocatalysis research and made 1D TiO_2 nanostructure as an important component in many practical applications, including solar cells (Ji *et al.*, 2012), supercapacitors (Li *et al.*, 2014a), biomedical devices (Li *et al.*, 2015) and lithium-ion batteries (Chen *et al.*, 2010). In this research studies, TiO_2 photocatalyst has been chosen as a photoelectrode in water splitting system due to it offers excellent promise for hydrogen generation water splitting applications. TiO_2 posted its unique characteristics such as non-toxic in nature, environmental friendly material, strong oxidation ability, good photocatalytic property and high photocorrosion resistant hence, emerged as the leading candidate as an efficient PEC water splitting system (Fujishima *et al.*, 2000; Kudo & Miseki, 2009). However, its large band gap (3.0 to 3.2 eV) resulting in poor visible light response and the rapid recombination of electrons and holes pairs obviously hindrance to the widespread use of TiO_2 as a photoelectrode in water splitting system. Some ideas have been demonstrated by researchers on the improvement of the visible light absorption of TiO_2 (Lee *et al.*, 2010; Lee *et al.*, 2014b; Yang *et al.*, 2010b). This can be done by coupling TiO_2 with another small band gap of semiconductor, which will lead to additional electronic state in the band-gap and in turn affect the optical, electronic and functionality of TiO_2. Other than poor response of TiO_2 to visible light, the multi-component semiconductors are complex materials. It is a very challenging task or rather impossible to make an intuitive guesses on the material's properties in a research.

2.2 Historical overview of PEC water splitting

There is a significant increase in the exploitation of renewable energy sources in this era globally as to effectively alleviate the dependence on using fossil fuel. Sources that emerge as first priority and urgently needed are with the properties of high efficiency, economic and facile manufactured (Kreuter & Hofmann, 1998). Solar energy is one of those sources and which can be harvest through the excitation of semiconductor materials, later coined as semiconductor photocatalyst (Aroutiounian *et al.*, 2005; Tong *et al.*, 2012). Back to 1839, Becquerel first reported the work on semiconductor photocatalysis. In his design, the counter electrode was a silver chloride electrode. When under illumination of sunlight, it generated a voltage and an electric current. From this discovery many researcher have been inspired on the capturing sunlight energy and converting into electric energy as an alternative energy sources. Around 50 years later, Charles Fritts demonstrated photoelectric effect with approximately 1% efficiency through a developed material selenium and gold *pn* junction device. However, in the early of 20^{th} century, the literature regarding to the photocatalyst was still very limited.

An efficiency of 6% was achieved by a viable commercial *pn* junction solar cell designed by Bell Laboratories in 1954 brings revolution in the photovoltaic industry. Henceforth, initiated on the modifications to improve and make photovoltaic more approachability in the global energy market, especially silicon made solid-state junction devices (Okamoto *et al.*, 2011; Solanki, 2015). New generation of PEC water splitting cell has emerged to challenge this dominance where the photovoltaic system is integrated with an electrolyzer to produce clean and portable H_2 energy carrier. This has led in essential while facing operation issue of photovoltaic system during night time and the period of bad weather as chemical fuel in the H_2 form by the storage of energy (Barreca *et al.*, 2011; Currao, 2007).

H_2 fuel stored within a fuel cell can be utilized as clean energy and efficiently converted into electrical energy and it is available at all times. This cell is basically composed of a cheap and facile fabrication nanocrystalline material and together with other attractive properties like high flexibility and chemical stability in aqueous solution. In a PEC water splitting cell, these materials are expected to have high solar light irradiation to current response (Centi & Perathoner, 2009). The first reported on photoelectrochemical (PEC) water-splitting on a Titanium dioxide (TiO_2) electrode in 1972 by Honda and Fujishima has dragged the subsequent interests in photocatalysis research by scientists and researchers from all over the world on TiO_2 and made TiO_2 as an important component in many practical applications.

2.3 Basic principle of PEC water splitting

The process of PEC water splitting is a kind of chemical reaction catalyzed by a photocatalyst to separate water into O_2 and H_2 which also is known as solar-driven water splitting reaction (Equation 2.1). Figure 2.4 illustrated a general schematic diagram of the overall PEC water splitting reaction by a semiconductor photocatalyst.

$$2H_2O\ (l) \rightarrow O_2\ (g) + 2H_2\ (g) \qquad \text{(Equation 2.1)}$$

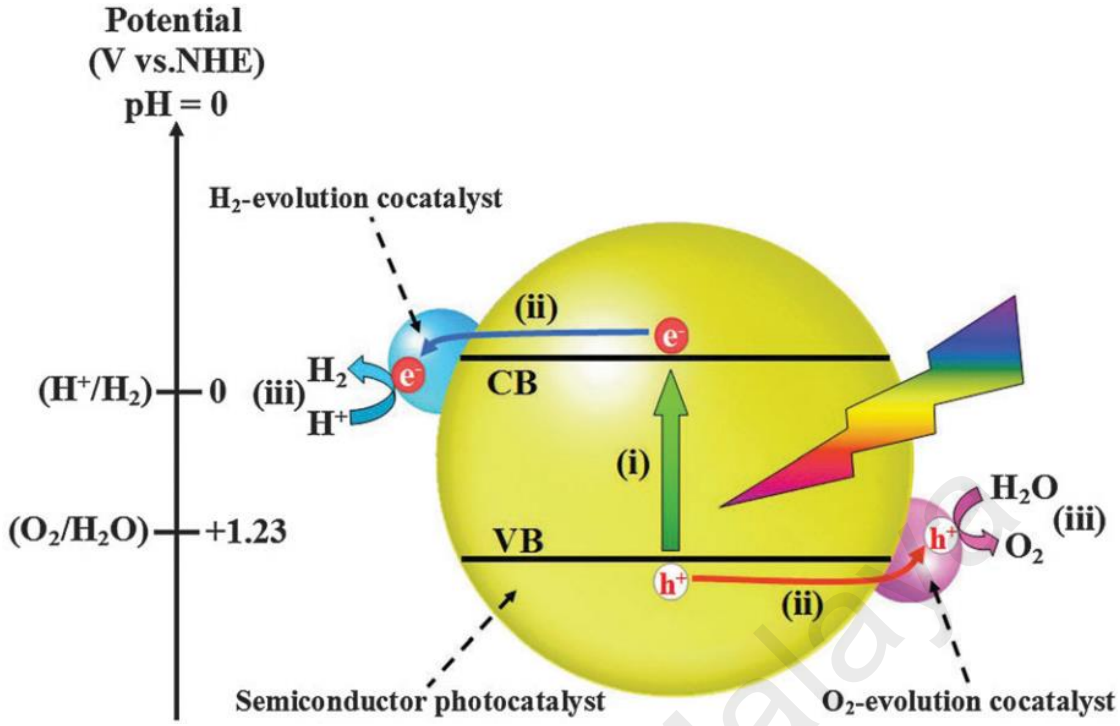

Figure 2.1: Schematic diagram of the photocatalyze PEC water splitting reaction by a semiconductor (Ran *et al.*, 2014).

The PEC water splitting reaction belongs to a thermodynamic uphill reaction with large Gibbs free energy change for the process ($\Delta G° = 237.2$ kJ mol^{-1}). It requires a minimum energy of 1.23 eV or 2.46 eV per molecule of H_2O. Therefore, higher photon energy is required to overcome the Gibbs free energy in order to perform the reaction (Moniz *et al.*, 2015). The mechanism of photocatalytic water splitting process can be described with two half reactions: (1) water oxidized to form O_2, : (2) proton reduction to hydrogen fuel, i.e. H^+/H_2 is 0 V and O_2/H_2O is 1.23 V which in line to the normal hydrogen electrode (NHE) (Kudo & Miseki, 2009).

$TiO_2 + 2\ h\nu \rightarrow TiO_2 + 2h^+ + 2e^-$ (Equation 2.2)

$2H_2O + 4h^+ \rightarrow O_2 + 4H^+$ (Equation 2.3)

$2H^+ + 2e^- \rightarrow H_2$ (Equation 2.4)

Semiconductor-based photocatalyst (i.e. n-type TiO_2) once triggered from an incoming photon with energy or greater than its band gap will be photoexcited and forms electrons and holes pairs. Photocatalyst absorbed photons and promotes electrons to the conduction band (CB) from the valence band (VB) by leaving a hole. Within the picosecond timescale these holes will then diffuse to the surface-electrolyte interface and then taking part in formation of O_2 and H^+ ions by oxidizing water molecules (Equation 2.3) whereas electrons move to the counter electrode through the external circuit. The reduction of H^+ ions to H_2 molecules (Equation 2.4) at platinum electrode is caused by electric field or under external bias. The lifetime and pathway of the photogenerated charge carriers are critically important which the energy conversion efficiency relies on how fast carriers recombine than the expected reaction. Hence, optimal efficiency can be attempted at the carriers ought to separate as far as possible, or as longer time as possible, on the surface of a photocatalyst (Moniz *et al.*, 2015).

Several factors are involved in determining the rate of hydrogen generation through light driven photocatalytic water splitting. First, photons that adsorbed by the material delivering enough energy to the reaction to form excited e–h. Second, activities of photoexcited charge carriers like separation, recombination, trapping and migration. Third, surface chemical reactions (utilizing the surface active sites to perform surface reaction for the evolution of H_2 and O_2). When the conditions are favourable, photoexcited semiconductor (catalyst) then generates electrons and holes pairs and take part in catalysis (Babu *et al.*, 2015).

However, photocatalysis is associated with unavoidable energy lost involving semiconductor photocatalyst under any solar energy. When solar light illuminates towards the photocatalyst, electrons and holes pairs are generated. These electrons and holes pairs might undergo rapid recombination and the dissipate energy is in the modality

of unwanted heat or photons (Grimes, 2007). Apart from electrons and holes recombination, energy lost also occurs via electrons transportation through lattice defects which act as charge carrier traps. Different crystal lattice structures (polymorphs) crystallinity (Jitputti *et al.*, 2008) and form of nanostructures in a material further affect the migration of the photogenerated charge carriers (Yan *et al.*, 2011; Yang *et al.*, 2014). Nevertheless, the efficient catalytic activity can be promoted by lowering the density of defects with the increasing of crystallinity. Modify the size of the photocatalyst to nanoscale by providing better diffusion path is essential for the movement of photogenerated electrons and holes pairs before they are trapped or recombined (Martinson *et al.*, 2006). Other possible reasons towards decreased photocatalytic activity are when electrons flows from the photoanode to the counter electrode or Joule heating resistant build up in external circuit when the electrons flow (Leung *et al.*, 2010).

2.4 Material selection for PEC water splitting

By considering the energy losses within the solar light driven photocatalytic activities for water splitting hydrogen generation, the materials used as the photocatalyst have to possess several properties relative to the band gap energy and electrochemical properties, which is shown as follows:

i. Band edge position: A materials with CB level more electronegative than reduction of H^+/H_2 level (E_{H_2/H_2O}) whereas, it's VB level should be more electropositive related to H_2O oxidation level (E_{O_2/H_2O}) in order to generate H_2 efficiently (Ni *et al.*, 2007).
ii. Band-gap: To utilize maximal of the solar light spectrum for photoexcitation on the materials, lower electronic band gap is necessary (Misra & Raja, 2010).
iii. Transportation of charge carriers: migration of photoexcited charge carrier with minimal recombination within the materials or losses when transferring from

photoanode to the counter electrode for high efficient H_2 generation (Grimes, 2007).

iv. Stability: The photocatalyst must be stable against photocorrosion in electrolyte under prolonged irradiation (Misra & Raja, 2010; Moniz *et al.*, 2015).

Hence, the electronic structure of a photocatalyst is important in determining its light-harvesting ability. These energetic levels (VB and CB) of each material play a critical part in PEC water splitting where ionization potential and electron affinity are corresponded by their band edges. Various semiconductors with their CB and VB edges related to vacuum and the normal hydrogen electrode (NHE) as standard for zero potential are illustrated in Figure 2.2. Each of the values is recorded in Table 2.2 for easy reference. Relatively, some of the materials shows wide band gap which poorly harvest the visible light spectrum. Altering band edges of the semiconductors remains as a great challenge in order to effectively increase the photocatalytic activity. Most of the semiconductors in Figure 2.2 with the VB edge are deeper than the O_2/H_2O oxidation potential, so the evolution of the O_2 is possible under illumination. In contrast, the evolution of H_2 is not possible for the semiconductors in Figure 2.2(b). This is because H_2/H^+ reduction potential is higher than their conduction band energy, the electrons excited at the conduction band has insufficient energy to reduce H^+ and form H_2 (Izumi *et al.*, 2009). Similarly, band gap of the semiconductors like MoS_2, Fe_2O_3 and WO_3 cover the whole visible region of solar spectrum but they are not considered as active materials. It is due to their unsuitable band energies as compare to NHE. Furthermore, the semiconductors in Figure 2.2(b) are also known as photocorrosive materials since their CB minimum does not reach the requirement of water splitting thermodynamically (Kudo & Miseki, 2009). It is important to note that the accessible of the flat band potential is essential criteria to fulfil the redox potentials of water splitting hydrogen production.

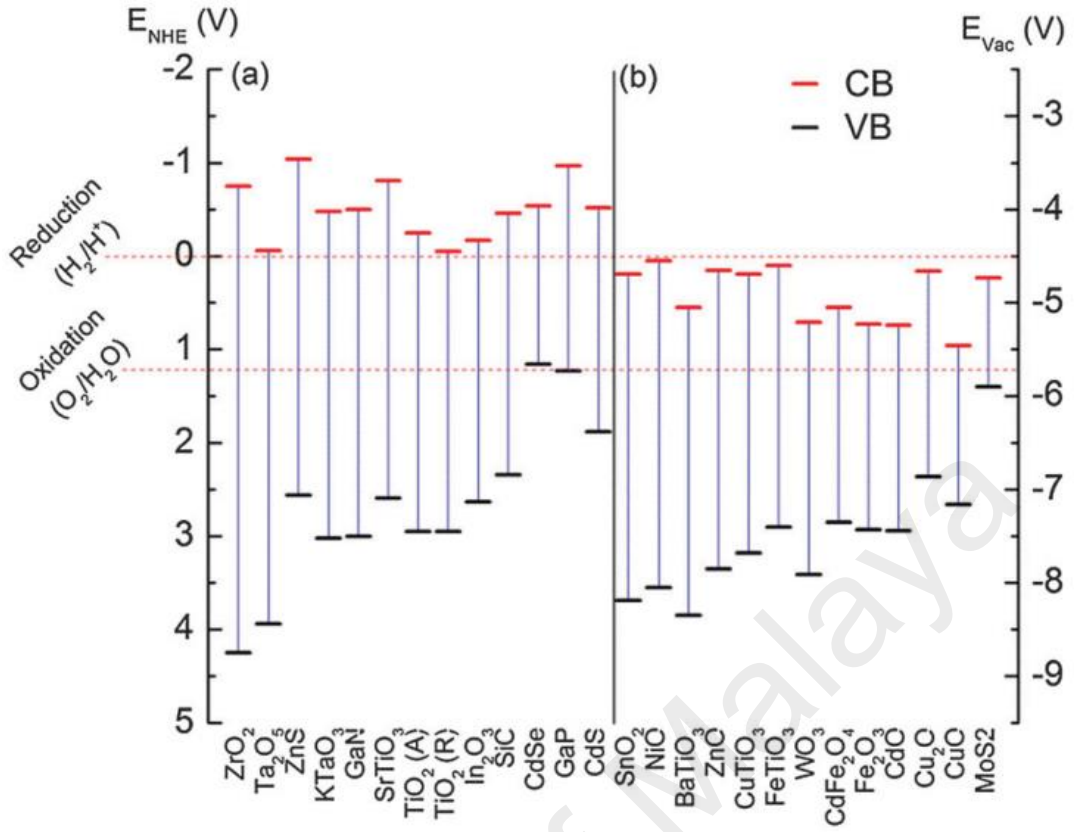

Figure 2.2: Thermodynamically (a) suitable and (b) unsuitable materials. Electronic structure of different semiconductors and the relative position of their band edge with respect to the NHE and vacuum (Vac) (Babu *et al.*, 2015; Castelli *et al.*, 2013).

Table 2.1: VB and CB of different semiconductors (Babu *et al.*, 2015)

Semiconductor	Band energy with respect to NHE (eV)			Reference
	CB	VB	Eg	
ZrO_2	-0.75	4.25	5.0	(Xu & Schoonen, 2000)
Ta_2O_5	-0.06	3.94	4.0	(Xu & Schoonen, 2000)
ZnS	-0.91	2.44	3.35	(Zhang *et al.*, 2011)
$KTaO_3$	-0.48	3.02	3.5	(Xu & Schoonen, 2000)
GaN	-0.5	3.0	3.5	(Gorczyca *et al.*, 2010)
$SrTiO_3$	-0.81	2.59	3.4	(Burnside *et al.*, 1999)
TiO_2 (A)	-0.25	2.95	3.2	(Burnside *et al.*, 1999)
TiO_2 (R)	-0.05	2.95	3.0	(Burnside *et al.*, 1999)
In_2O_3	-0.17	2.63	2.8	(Xu & Schoonen, 2000)
SiC	-0.46	2.34	2.8	(Chiu & Li, 2009)
CdSe	-0.54	1.16	1.7	(Kudo & Miseki, 2009)
GaP	-0.97	1.23	2.2	(Kudo & Miseki, 2009)
CdS	-0.52	1.88	2.4	(Xu & Schoonen, 2000)
SnO_2	0.19	3.69	3.5	(Xu & Schoonen, 2000)
NiO	0.05	3.55	3.5	(Xu & Schoonen, 2000)
$BaTiO_3$	0.55	3.85	3.3	(Xu & Schoonen, 2000)
ZnO	0.15	3.35	3.2	(Xu & Schoonen, 2000)
$CuTiO_3$	0.19	3.18	3.0	(Xu & Schoonen, 2000)
$FeTiO_3$	0.1	2.9	2.8	(Xu & Schoonen, 2000)
WO_3	0.71	3.41	2.7	(Xu & Schoonen, 2000)
$CdFe_2O_4$	0.55	2.85	2.3	(Xu & Schoonen, 2000)
Fe_2O_3	0.73	2.93	2.2	(Xu & Schoonen, 2000)
CdO	0.74	2.94	2.2	(Xu & Schoonen, 2000)
Cu_2O	0.16	2.36	2.2	(Xu & Schoonen, 2000)
CuO	0.96	2.66	1.7	(Xu & Schoonen, 2000)
MoS_2	0.23	1.4	1.2	(Xu & Schoonen, 2000)

2.5 Self-organized TiO_2 Nanotubes film's properties

Initially, the investigations of the photocatalytic activities were focused on 0D TiO_2 nanoparticles and they showed excellent photocatalytic performances in hydrogen production, solar cells, adsorbents and sensors due to their large surface area and broadened band gap (Han *et al.*, 2014; Liu *et al.*, 2012; Tang *et al.*, 2010). However, they also showed unavoidable disadvantages such as fast recombination of electrons and holes, slow charge carrier transfer and high recycling cost (Ge *et al.*, 2015b; Wu *et al.*, 2014).

The synthesis of 2D nanostructured materials was comparably complex and required harsh experimental conditions (Lee *et al.*, 2014a; Yao *et al.*, 2014). Recently, 1D self-organized TiO_2 nanotubes film have been extensively studied due to their distinctive advantages like large surface area, short lateral diffusion length which provides a unidirectional electrical channel for photo-induced charge carrier transfer, where TiO_2 grains are stretched in the tube growth direction. Thus, vertical transportation of charge carriers could be enhanced and improves the PEC water splitting performances due to the low recombination losses at the grain boundaries. (Roy *et al.*, 2011; Spadavecchia *et al.*, 2013). In order to get the right dimensions and morphologies, a controlled synthesis procedure for the production of self-organized nanotube arrays must be investigated and optimized by tuning the length, wall thickness, pore diameter, and intertube spacing through the anodization process. Maximizing the specific surface area of TiO_2 nanostructure film is also crucial. Highly ordered self-organizing TiO_2 nanotubes film is considered an ideal photoelectrode in the water splitting system because of their inner and outer wall surface area of nanotube that greatly increases the density of the active sites available for photon absorption. As a result, the use of TiO_2 nanotubes film in the present study is much better and effective to improve the PEC water splitting performance (Albu *et al.*, 2008; Grimes, 2007).

2.6 Formation of TiO_2 Nanotubes

Over the past few years, various synthesis methods to form 1D TiO_2 nanotubes have been explored including hydro/solvothermal method, template-assisted/sol-gel method, electrochemical anodization technique and etc. (Kasuga *et al.*, 1998, 1999; Lakshmi *et al.*, 1997; Sander *et al.*, 2004; Suzuki & Yoshikawa, 2004). In the following section, different approach to synthesis TiO_2 nanostructures will be reviewed.

2.6.1 Hydrothermal/Solvothermal method

Hydrothermal method has found to be the most used method for fabrication of 1D TiO_2 nanotubes conducted using a stainless steel vessel and heated at high temperature and pressure. The main advantages for this method include simple procedure and low production cost. Besides, many literatures reported that nearly 100 % conversion of the precursors to 1D TiO_2 nanostructured could be achieved within one single procedure under hydrothermal process. In 1998, Kasuga *et al.* first reported the preparation of TiO_2-based nanotubular materials by the hydrothermal method (Kasuga *et al.*, 1998, 1999). The authors reported that amorphous TiO_2 powder mixed in a highly concentrated NaOH solution (10 M) was treated at high temperature (110 °C) for 20 h, and no sacrificial templates were needed. Since then, many investigations have been carried out by controlling the processing parameters, such as temperature, treatment duration and caustic concentration in order to synthesize the desired dimensional nanotubes (Armstrong *et al.*, 2005; Bavykin *et al.*, 2004).

In fact, this hydrothermal synthesis can be achieved either through acid-hydrothermal or alkali-hydrothermal by referring to the nature of the reactants (Tian *et al.*, 2014). At the early stage, the reactants were composed of titanium salts and hydrochloric acid. Nevertheless, these reactants usually form TiO_2 nanorods structure rather than nanotubular structure. Thus, the applied reactants have been latter modified towards alkaline (high concentration of sodium hydroxide) approach with certain amount of TiO_2 nanoparticles in order to form TiO_2 nanotubes via dissolution–recrystallization mechanism (Tian *et al.*, 2014). In 2005 and 2006, both Tanaka and Peng *et al.* investigated the effect of hydrothermal conditions on nanostructure formation by using Ti substrate as a precursor through alkaline hydrothermal treatment (Peng & Chen, 2006; Tanaka *et al.*, 2005) Besides, Morgan and co-researchers have been reported that different morphologies and structures of TiO_2 such as nanoparticles, nanotubes, and nanoribbons

could be transformed accordingly by optimizing the caustic concentration and temperature treatment from Degussa P25 through alkaline hydrothermal treatment via the Kasuga method (Morgan *et al.*, 2008) gives the result consistent with the ones obtained by both Tanaka and Peng *et al.* It is evident that under specific hydrothermal condition, TiO_2 with different phases and morphologies can be transformed to nanotubes (Lim *et al.*, 2005; Nakahira *et al.*, 2010).

The solvothermal method is also a common synthesis approach similar to the hydrothermal method which is usually conducted in a stainless steel vessel with high temperature and pressure to fabrication of 1D TiO_2 nanotubes (Nam *et al.*, 2014; Wang *et al.*, 2013). Furthermore, these two methods are commonly use TiO_2 nanoparticles, $TiCl_4$ or tetrabutyl titanate as the precursor. However, the different where solvothermal with hydrothermal is it usually conducted in an organic solvent (ethanol, ethylene glycol, n-hexane, etc.), while the hydrothermal is done in water solutions (Hoa & Huyen, 2013). Wang *et al.* have successfully synthesized a bundle of both nanowires and open-ended TiO_2 nanotubes by the solvothermal method using ethanol and glycerol as solvents (Wang *et al.*, 2006). Besides, Zhao's group also successfully fabricated vertically aligned TiO_2 nanorods by the solvothermal method use as photoanodes for dye-sensitized solar cells with the discussion of the thermal treatment effect on their performances (Zhao *et al.*, 2014).

There are some drawbacks in this hydrothermal method. First, slow reaction kinetics leads to long reaction time. Second, varies length of nanotubes limits their wide range of applications. Thirdly, the diameters of the fabricated nanotubes are non-uniform on a large scale. Similar to the hydrothermal method, the understanding of the kinetic mechanism of each solvents towards the Ti precursors is the crucial part for the

solvothermal method in order to produce smaller range of high aspect ratio nanotubes which also limits its wide applications (Ge *et al.*, 2016).

2.6.2 Template-assisted/ Sol-gel method

The template-assisted method is one of the most prominent and well-established process to produce TiO_2 nanotubes by using TiO_2 precursor and then coated into a template. In this case, an anodic aluminium oxide (AAO) nanoporous membrane with arrays of parallel nanopores with a controllable diameter and length are commonly used as a potential template. This template is removed by chemical etching after the deposition of TiO_2 (Sander *et al.*, 2004). However, some precursors like tetrabutyl titanate or titanium isopropoxide mixed in acetic acid might need further treatment such as purging or hydrolysis process in order to form 1D TiO_2 nanotubes. In the last stage, the template was then removed by applying chemical etching method in order to obtain TiO_2 nanotubes. Several researchers have reported on the fabrication of TiO_2 nanotubes with controlled dimension by the template-assisted method (Hoyer, 1996; Lee *et al.*, 2011; Sander *et al.*, 2004).

Sol-gel synthesis is also widely employed due to its capability in controlling the textural and surface properties of the resulting TiO_2 nanotubes. In fact, this method is used primarily for the fabrication of mix-metal oxides, starting from a colloidal solution (sol). The sol acts as the precursor for the formation of integrated network (gel) or either discrete particles, which undergo various forms of hydrolysis and polycondensation reactions. The precursor typically is metal alkoxides, inorganic metal salts and metal-organic compounds, such as Titanium tetrachloride, alkoxide Ti solutions, polymeric bonded TiO_2) into a template and then undergo heat treatment at 150 °C or vigorous stirring in acetone to remove the template (Tan *et al.*, 2012; Xia *et al.*, 2003; Zhang *et al.*, 2002). Usually, sol-gel method is constructed by the combination of template-assisted

method to fabricate 1D TiO_2-based nanostructures. Joo *et al.* successfully synthesized TiO_2 nanorods with a diameter of about 5 nm by the sol–gel method (Joo *et al.*, 2005). Qiu and Attar *et al.* also reported the fabrication of 1D well-aligned TiO_2 nanotube arrays, nanorods and nanowires by a modified template-assisted sol–gel method (Attar *et al.*, 2009; Qiu *et al.*, 2006).

In summary, it was found that the preparation of TiO_2 nanotubes via template-assisted/sol-gel approaches involved high production cost and difficulties in template removal stage that might be damaged to the nanostructure (Hagen *et al.*, 2014; Shin *et al.*, 2004). In addition of that TiO_2 nanotubes formed by using titanium sol-gel precursor or template-assisted based process are all results in varies in length either heaping on together or loosen tubes dispersed in solution. With these drawbacks, it leads toward eliminations of many superiorities of the 1D directionality (Roy *et al.*, 2011).

2.6.3 Electrochemical Anodization method

Electrochemical anodization method has been brought into great interest in the development of 1D TiO_2 nanotube arrays due to its facile synthesis procedure. . In anodizing cell, Ti is used as an anode and it is connected to the positive terminal of power source, whereas platinum is used as cathode and being connected to the negative terminal of power source. A typical experimental setup of anodization process was shown in Chapter 3, Figure 3.2. The first literature was reported by Assefpour-Dezfuly and co-researchers about the use of electrochemical anodization technique to form TiO_2 porous in 1984. The authors reported that TiO_2 porous structure was synthesized via chemical etching in alkaline peroxide and then followed by electrochemical anodization in chromic acid solution (Assefpour-Dezfuly *et al.*, 1984). A report in 1999 by Zwilling and co-workers reported that self-organized porous TiO_2 could be obtained by anodizing a Ti-based alloy in an acidic, fluoride-based electrolyte. This research finding has make a

breakthrough of work undertaken on anodized Ti porous/tubular over the last two decades (Zwilling *et al.*, 1999). Since then, the electrochemical condition such as voltage, time, concentration of electrolyte, reaction temperatures, as well as pH of electrolyte have been studied extensively to control the morphological and structural of TiO_2 nanotubes. There are mainly five formation generations of TiO_2 nanotubes via electrochemical anodization technique have been reported so far and their details are summarized in Table 2.1.

Generally, the morphology of the self-ordered nanostructure is strongly affected by the type of electrolyte, pH, applied potential, time and temperature. In the first generation, hydrofluoric acid based water aqueous electrolytes are most commonly used in the fabrication of TiO_2 nanotubes. However, the length of the nanotubes obtained just merely a few hundreds nanometer (200 – 500 nm) which is insufficient to generate favourable photocurrent. However, further modifications have been done by using F-based inorganic and organic neutral electrolytes and showed longer and smoother nanotubes walls (Paulose *et al.*, 2007). Basically, the anodization voltage alters the morphology of the formed nanostructures, while the anodization time mainly affects the length of TiO_2 nanotubes. The temperature of anodization condition affects the dissolution rate. As a result, TiO_2 nanotube arrays are normally grown into optimum dimension at ambient condition (20–25 °C) (Ge *et al.*, 2016). Appropriate selection of anodization parameters for the TiO_2 nanotubes formation is the key to the successfull growth of high quality nanotubes.

By comparison, electrochemical anodization approach led to the formation of self-organized nanotubes array and compactly aligned perpendicularly with its metal (substrate) surface. All of the tubes are attached with the metal herein is electrical conductive. Controlled geometry and formation of dense nanotubes layer makes electrochemical anodization an extremely versatile parallel structuring process.

Table 2.2: Summary of the generations of TiO_2 nanotube arrays synthesized by electrochemical anodization method (Ge *et al.*, 2016)

TiO_2 nanotube arrays	**Electrolyte**	**Morphology**	**Ref**
1st generation: (HF electrolyte)	0.5 wt% HF	Short nanotube length: 200–500 nm, diameter: 10–100 nm, and wall thickness: 13–27 nm	(Zwilling *et al.*, 1999)
2nd generation: F-based buffered electrolytes	1 M $Na_2SO_4/(NH_4)_2SO_4$ + 0.5 wt% NH_4F	Rough wall with wing length: 0.5–2.4 mm, diameter: 100 nm, and wall thickness: 12 nm	(Macak *et al.*, 2005)
3rd generation: organic electrolytes containing F	0.5 wt% NH_4F + 2 v% H_2O in ethylene glycol	Smooth and ultra-long tube length: 5–1000 mm, diameter: 100 nm, and wall thickness: 12 nm	(Paulose *et al.*, 2007)
4th generation: fluoride-free electrolytes	0.01–3 M $HClO_4$	Disordered tube length: 30 mm, diameter: 20–40 nm, and wall thickness: 10 nm	(Hahn *et al.*, 2007)
5th generation: multiple-step anodization in organic electrolytes containing F ions	0.5 wt% NH_4F + 2 v% H_2O in ethylene glycol	Smooth and hexagonal tube length: 2–10 mm, diameter: 100 nm, and wall thickness: 15–20 nm	(Ge *et al.*, 2015a; Ye *et al.*, 2012)

2.7 Mechanism of formation of TiO_2 nanotubes

The TiO_2 nanotubes formation mechanisms are discussed in this section. It can be divided into three types or generations of the model of TiO_2 nanotubes formation via electrochemical anodization method. First reported by Choi *et al.* regarding the mechanistic formation model (Figure 2.1) of TiO_2 nanotubes based on the phenomena of the electrical breakdown of the TiO_2 in the formation of porous TiO_2 (Choi *et al.*, 2004). At the beginning of the process, anodization voltage was applied and formed a barrier layer of TiO_2 on the substrate and grows thicker with increased voltage. The barrier layer will then undergo crystal structure phase transformation into denser structure like anatase or rutile and induced high compressive stress in the oxide. When the electrical breakdown occurs, new pores were created with occurrence of sparking followed by immediate

passivation of these pores by oxide. Repetition of the breakdown and re-passivation at both pore tips and inside the pores occurs which eventually forms the nanotube arrays.

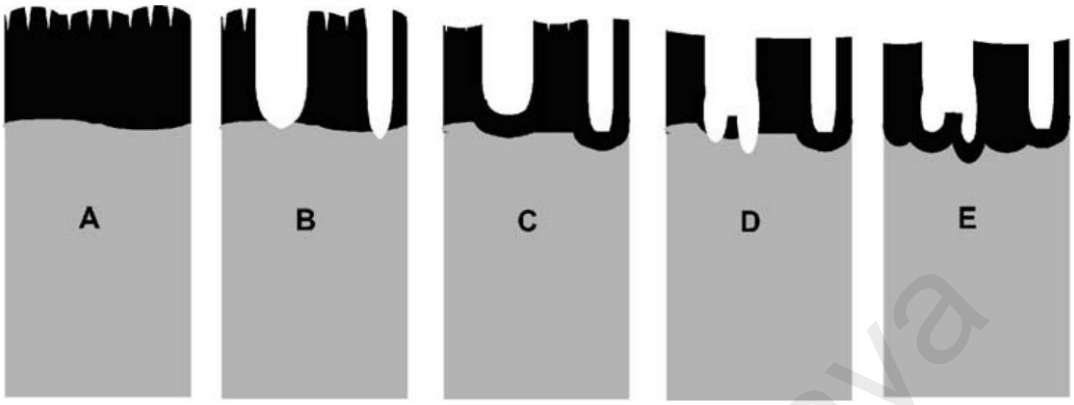

Figure 2.3: Schematic diagram of porous TiO_2 nanotube formation: (A) oxide growth to maximal thickness (B) burst of oxide by the formation of crystallites (pore formation), (C) immediate repassivation of pore tips, (D) burst of repassivated oxide, and (E) dissolution of the formed oxide and second repassivation (Choi *et al.*, 2004).

In 2006, another mechanistic model has been reported by Mor *et al.* where the first growth of the TiO_2 on the Ti substrate is due to the reaction of Ti metal with O^{2-} or OH^- ions from the electrolyte. A thin layer of oxide will then form on the surface as a barrier layer. Further oxidation of the Ti on the substrate surface to for thicker oxide layer is occurred through the migration of these anions through the oxide layer and reaching the metal/oxide interface where they react with the metal. Ti^{4+} cations from metal/oxide surface then subsequently ejected into oxide/electrolyte interface under application of an electric field. Formation of the small pits in the oxide layer at the oxide/electrolyte interface originate from the localized dissolution of the oxide layer making this barrier layer at the bottom of the pits relatively thin as the voltage was increased. The free O^{2-} anions in electrolyte migrate towards the metal/oxide interface, to interact with Ti metal to regain the oxide layer. Localized dissolution and oxidation will continuously lead to the growth of these pits into pores of various sizes and depths as the electric field distribution in the curved bottom surface of the pores (Mor *et al.*, 2006). A schematic diagram of evolution of nanotubes proposed by Mor *et al*. is presented in Figure 2.2

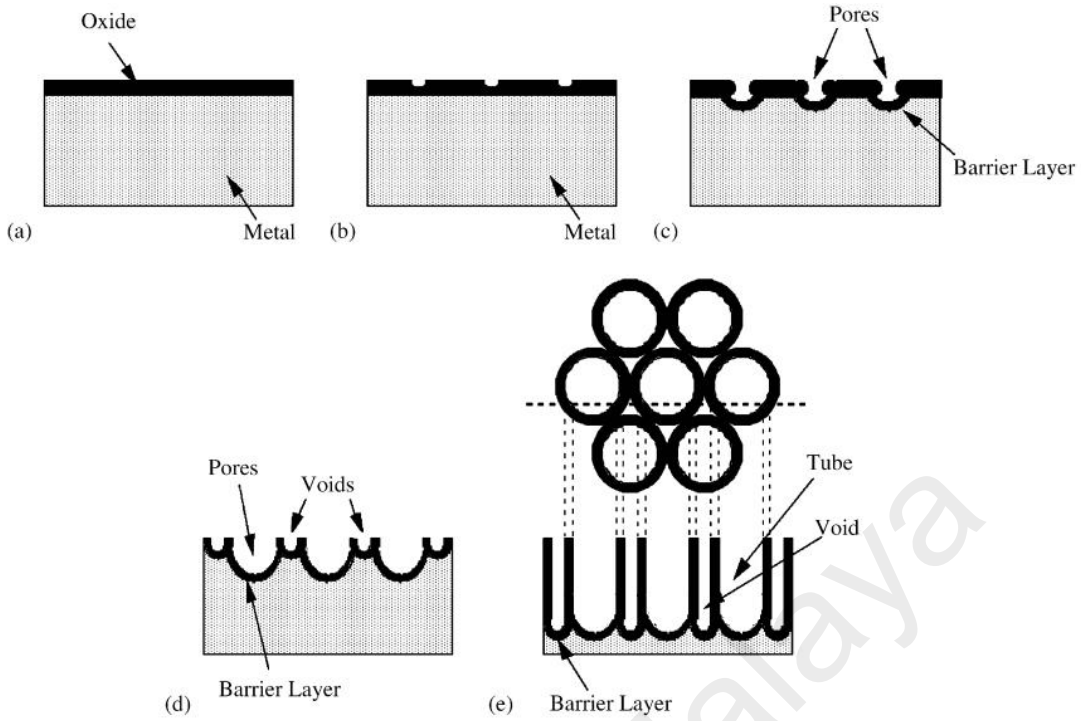

Figure 2.4: Schematic diagram of the evolution of a nanotube arrays at constant anodization voltage: (a) oxide layer formation, (b) pit formation on the oxide layer, (c) growth of the pit into scallop shaped pores, (d) metallic part between the pores undergoes oxidation and field assisted dissolution, and (e) fully developed nanotube array with a corresponding top view (Mor *et al.*, 2006).

Another more systematic and constructive mechanistic model by the team led by Patrick Schmuki involving chemical reaction equations were reported (Taveira *et al.*, 2005). In the report, a competition between the anodic oxide formation and the chemical dissolution of the oxide layer was discussed based on the formation of the nanotubes layer. As been reported by Mor *et al*, 2006 initial layer of oxide was formed due to the reaction of Ti metal with O^{2-} or OH^- ions from the electrolyte under an applied electric field (Equation 2.5).

$$Ti + H_2O \rightarrow TiO_2 + 2H^+ + 4e^- \quad \text{(Equation 2.5)}$$

$$TiO_2 + 6F^- + 4H^+ \rightarrow [TiF_6]^{2-} + 2H_2O \quad \text{(Equation 2.6)}$$

Random pits formed at the surface of the oxide layer were continuous dissolved by the fluoride ions and formed soluble fluoride complex of $[TiF_6]^{2-}$ left over initial pores under applied electric field (Equation 2.6). At the beginning of the anodization process, field-

assisted dissolution is dominating in the whole process while chemical dissolution is comparatively slow due to relatively large electric field across the thin oxide layer. Small random pits were found on the surface of the oxide caused by localized dissolution. These pits also act as pore forming centers and subsequently grew into pores. Field-assisted dissolution at the oxide barrier layer provides the high inwards driving force for the F^- ions to form soluble fluoride complex of $[TiF_6]^{2-}$ ions. The fluoride complex formation tendency leads to a permanent chemical dissolution (attack) at the pores also prevents precipitation of $Ti(OH)_xO_y$ layer from the Ti^{4+} ions migrated at the oxide/solution interface. During anodization, the continual growth of the oxide at the metal/oxide interface and chemical dissolution of the oxide layer at the oxide/electrolyte interface occurs simultaneously. When steady state was established, the growth rate of the nanotubes in length was identical to the thickness reducing dissolution rate of the outer interface of the oxide layer. In this situation the nanotube oxide layer just continuously ‘‘eats” through the titanium substrate without thickening of the oxide layer (Macak *et al.*, 2007).

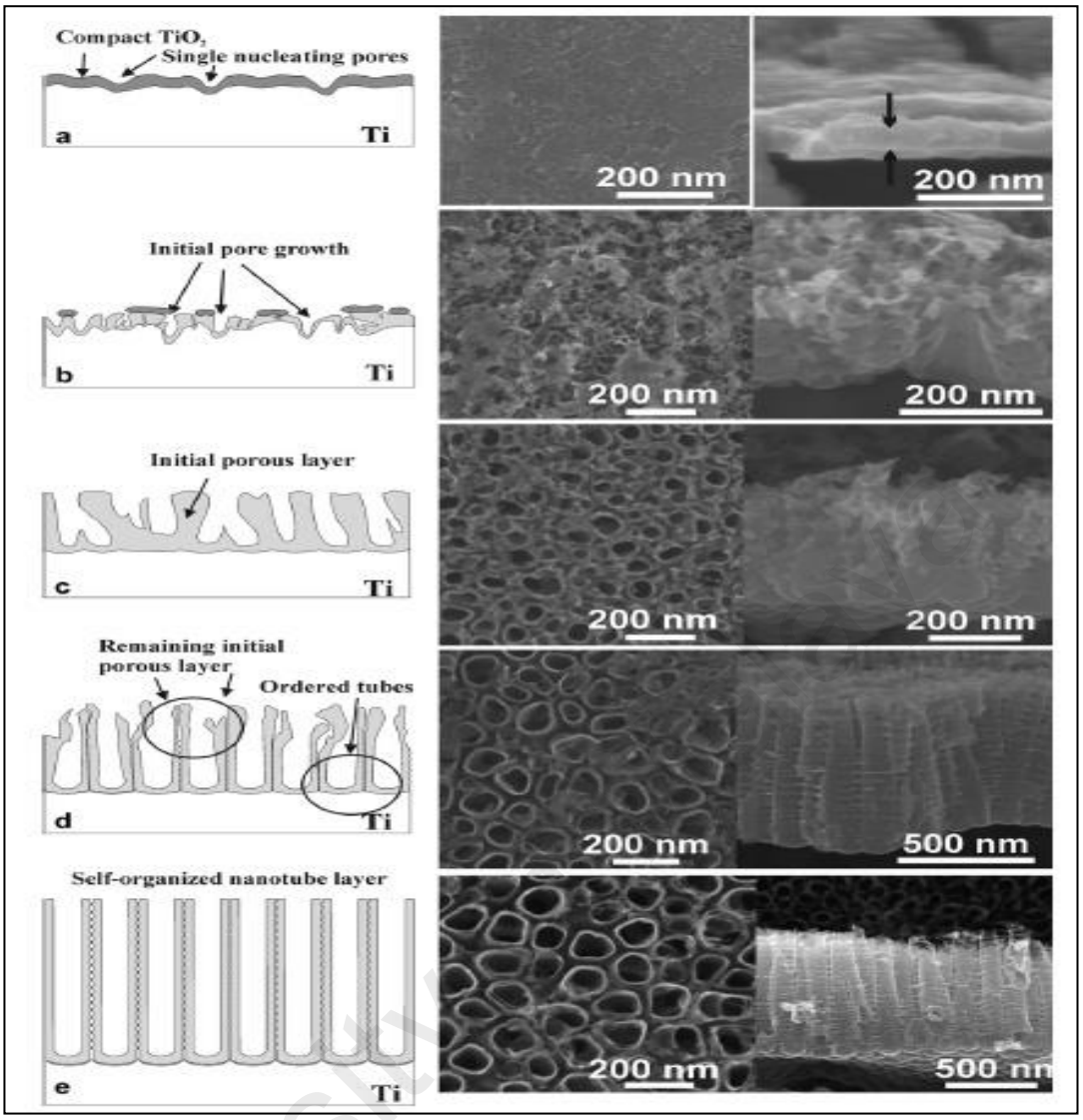

Figure 2.5: Schematic diagram (left column) and SEM sequence (top-views – middle column, cross-sections – right column) of different stages of the TiO_2 nanotubes layer formation. Anodization stopped after (a) 0 min, (b) 3 min, (c) 10 min, (d) 30 min, (e) 1 h from reaching 20 V in water/glycerol/0.27 M NH_4F after potential ramp from 0 to 20 V with a sweep rate of 250 mV/s (Taveira *et al.*, 2005)

2.8 Limitation of TiO_2 Nanotubes Film

In fact, TiO_2 has immerged as a promising photoelectrode in water splitting system for the hydrogen generation. However, an obvious hindrance to the widespread use of TiO_2 as a photoelectrode in water splitting cell is its large band gap energy that can only effectively function under the UV region ($\lambda < 400$ nm) (Khare *et al.*, 2013). Thus, the energy conversion efficiency from solar to hydrogen by TiO_2 photocatalytic water-splitting is still low, mainly due to the following reasons:

1. Recombination of photo-generated electrons and holes pairs: CB electrons can recombine with VB holes very quickly and release energy in the form of unproductive heat or photons (Martin *et al.*, 2013).
2. Fast backward reaction: Decomposition of water into hydrogen and oxygen is an energy increasing process, thus backward reaction (recombination of hydrogen and oxygen into water) easily proceeds (Martin *et al.*, 2014).
3. Inability to utilize visible light: The band gap of TiO_2 is about 3.2eV, and only UV light can be utilized for hydrogen production (Kitano *et al.*, 2007). Since the UV light which accounts for about 4% of the solar radiation energy while the visible light contributes about 50%, the inability to utilize visible light limits the efficiency of solar photocatalytic hydrogen production.

These drawbacks cannot be overcome by only optimizing the dimensions of TiO_2 nanotubes itself by controlling the processing parameter of electrochemical anodization as described in previous section. Therefore, considerable efforts have been exerted to minimize the recombination losses of charge carriers and extended the spectral response of TiO_2 to visible spectrum by incorporating an optimum amount of small band gap semiconductor, such as CdSe with TiO_2 nanotubes film. As a result, band gap narrowing effects for TiO_2 could expand the range of excitation light to the visible region and provide sites that can reduce the recombination loss of charge carriers (Fernandes *et al.*, 2016; Lv *et al.*, 2015; Su *et al.*, 2014).

2.9 Enhance the photoactivity of TiO_2 across entire UV-visible region

One-dimension (1D) TiO_2 nanotubular structure has drawn great interests in the application of PEC water splitting due to its excellent properties like high corrosion resistant, efficient charge transport and good photocurrent stability (Reyes-Gil & Robinson, 2013). In order to enhance the extension of its visible light absorption, various

studies on the modification of the methods or decorated with few percent of the other elements has been reported. Details of the foreign element doping on TiO_2 photocatalyst by several researchers and their findings are summarized in Table 2.3.

Chu et al has performed solar water splitting by using transferred TiO_2 nanotubes arrays on a transparent conductive oxide substrate. Two coreduction processes of flame and chemical reduction were applied to enhance the water splitting performance. First, rapid flame reduce (>1000 °C) anatase TiO_2 by generating oxygen (O^{2-}) vacancies and Ti^{3+}. These oxygen vacancies in TiO_2 act as new electron donors have not only enhance photocatalytic capability but also solar illumination absorption (Hu, 2012). Second, chemical reduction of TiO_2 nanostructure in $TiCl_3$ successfully introduce oxygen vacancies hence improved in photocurrent density. With the synergistically engineered from two processes, highest photocurrent density reported was ~2.0 mA/cm^2 which is ∼15% higher than the monoreduced sample (Cho *et al.*, 2015).

Besides that the improvement in photoelectrochemical water splitting can be done through modification of methods, but also the metal doping. Several successful cases were reported such as gold (Au) nanoparticles doped TiO_2 by Pu et al. In the report, Au nanoparticle decorated TiO_2 effectively enhanced the absorption of whole UV- visible solar spectrum as compare as bare TiO_2 with the photocurrent density recorded at 0V as 1.49 and 0.82 mA/cm^2 respectively. Pu and his teams also found that with the decoration of Au nanorods on the TiO_2 exhibited three times higher under visible light illumination (>430 nm, 73.3 mW/cm^2) than bare TiO_2 which recorded as 2.67 and 0.87 μA/cm^2 respectively (Pu *et al.*, 2013). Zhang and his team also reported in the Au doped TiO_2 nanotubes with the highest photocurrent density obtained as ∼150 μA/cm^2 when under illumination of visible light (Zhang *et al.*, 2012b). Another noble metal Ag also have been reported by Wu et al used to dope on TiO_2 nanotubes. Ag nanoparticles was assembled

by microwave-assisted chemical reduction onto anodized TiO_2 nanotubes. The recorded best hydrogen generation in the medium contain of ethanol (10 vt%) and H_2O under solar illumination is 1.34 μmol/cm^{2}h. It has been devoted by the sample soaked in 2 mM $AgNO_3$ solution with 3 min microwave irradiation (300 W) at 100 °C (Wu *et al.*, 2013).

Extensive investigation also have been reported in composing of nanocomposite metal oxides. ZnO has drawn certain interests in coupled with TiO_2. High electron mobility of ZnO improve the process of electron transfer between CB and VB. Hence, reduce in recombination of photogenerated charge carrier as compare with TiO_2 itself. Momeni and Ghayeb reported the photocurrent density and hydrogen generated by ZnO-TiO_2 nanotubes as 1.24 mA/cm^2 and 11 μL/cm^{2}h respectively (Momeni & Ghayeb, 2015). Transition metal oxide also upsurge in the interests of synthesizing nanocomposite. One of the candidate is the Chromium III oxide (Cr_2O_3). Through chemical bath deposition, Cr_2O_3 was deposited onto TiO_2 nanotubes. From the performance of this nanocomposite, they reported of photocurrent density of >150 μA/cm^2 at 0.2 V (vs. Ag/AgCl) as compare to bare TiO_2 with only <8 μA/cm^2 that they synthesized. The hydrogen generation performance recorded is 10.67 μL/cm^{2}h where is 12.8 times higher compare to its bare TiO_2 (Momeni & Ghayeb, 2016).

There are many studies by incorporating in nonmetallic element such as N and H with TiO_2 to enhance its absorption ability of visible light. Chen and his research members has reported on the synthesizing hydrogen treated TiO_2 nanotubes. Comparatively, hydrogen treated TiO_2 nanotubes exhibited higher photocurrent density (~6 mA/cm^2) and photoconversion efficiency (2.96 %) as compared with as-grown TiO_2 nanotubes which is 10 times lower its efficiency (Chen *et al.*, 2013). Besides, nitrogen doped anodic TiO_2 nanotubes in PEC water splitting also been reported by the team of Park et al. Nitrogen was introduced to combine with the 2p states of oxygen in TiO_2 increase the VB band

hence reduce the band gap energy. As anodized TiO_2 nanotube array was brought to hydrothermally treated in mixed gases of NH_3/Ar for 3 hours at 773K. Two modes (UV and visible spectrum) has been tested on the performance of water splitting reaction. The hydrogen generated rate after UV light irradiation was recorded as 40 μmol/h and 38.6 μmol/h with respect to N-TiO_2 and TiO_2 nanotubes. Under visible light illumination, the hydrogen evolution rate of N-doped TiO_2 nanotubes was ~4.3 μmol/h where TiO_2 nanotubes is ~1.5 μmol/h (Park *et al.*, 2011). From the result, N doped TiO_2 nanotubes shows the better performance in hydrogen generation compared with pure TiO_2 nanotubes.

Table 2.3 Summary of the works reported on the different element decorated TiO_2 photocatalys

Materials	Method	Finding	Citation
Transferred TiO_2 nanotubes arrays on a TCO substrate	Immersed in 33 wt% H_2O_2 solution to separate TiO_2 nanotubes layer.	- Rapid flame reduce (>1000 °C) anatase TiO_2 by generating O^{2-} vacancies and Ti^{3+}. - Chemical reduction of TiO_2 nanostructure in $TiCl_3$ successfully introduce O^{2-} vacancies. - Highest photocurrent density reported was ~2.0mA/cm^2.	(Cho *et al.*, 2015)
Au	Seed-growth method.	- Photocurrent density of Au-TiO_2 and TiO_2 recorded at 0V are 1.49 and 0.82 mA/cm^2.	(Pu *et al.*, 2013)
	Chemical bath deposition	- Au nanorod decorated TiO_2 exhibited three times higher under visible light illumination than bare TiO_2.	(Pu *et al.*, 2013)
	Photocatalytic reduction method	- Highest photocurrent density obtained as ~150 μA cm^{-2} when under illumination of visible light.	(Zhang *et al.*, 2012b)
Ag	Microwave-assisted chemical reduction	- Best hydrogen generation in the medium contain of ethanol (10 vt%) and H_2O under solar illumination is 1.34 μmol/cm^2h.	(Wu *et al.*, 2013)
ZnO	Chemical bath deposition	- High electron mobility of ZnO improve the process of electron transfer between CB and VB. - Photocurrent density and hydrogen generated by ZnO-TiO_2 nanotubes as 1.24 mA/cm^2 and 11 μL/cm^2h respectively.	(Momeni & Ghayeb, 2015)
Cr_2O_3	Chemical bath deposition	- Photocurrent density of >150 μA/cm^2 at 0.2 V (vs. Ag/AgCl) as compare to bare TiO_2 with only <8 μA/cm^2 that they synthesized.	(Momeni & Ghayeb, 2016)
H	Heat treatment	- Hydrogen treated TiO_2 nanotubes exhibited higher photocurrent density (~6 mA/cm^2) and photoconversion efficiency (2.96 %).	(Chen *et al.*, 2013)

N	Hydrothermal	- Nitrogen was introduced to combine with the 2p states of oxygen in TiO_2 increase the VB band hence reduce the band gap energy.
		- Hydrogen generation rate:
		  - UV light irradiation - 40 μmol/h and 38.6 μmol/h with respect to N-TiO_2 and TiO_2 nanotubes.
		  - Visible light illumination- N doped TiO_2 nanotubes was ~4.3 μmol/h where TiO_2 nanotubes is ~1.5 μmol/h.
			(Park *et al.*, 2011)

2.10 CdSe-loaded TiO_2 Nanotubes Film

Over the past few years, hybrid CdSe-TiO_2 photocatalyst has gained much attention and has been intensively studied because of the unique features of resultant binary oxide photocatalyst which include increase in the photocatalytic activity by controling the energy levels of the semiconductor pair. Among the vast number of different low band gap semiconductor, CdSe is one of the most capable candidates to be coupled with TiO_2 photocatalyst for the enhancement in water splitting application. In fact, CdSe is one of the most popular II-VI semiconductor materials used to sensitize wide band gap semiconductors due to its wider absorption range (below 730 nm). Buhler *et al* (Buehler *et al.*, 1984) reported that CdS is also one of the promising wide band gap semiconductors sensitizer where its absorption range is below the wavelength of approximately 550 nm and has a flat band potential of 0.66 V (pH 7). However, the E_g of CdS is still relatively large (2.5 eV) and is not stable in aqueous solution under irradiation (anodic dissolution) (Babu *et al.*, 2015). A small band gap of CdSe with the conduction band edge higher than that of TiO_2 and has large extinction coefficient strongly absorb visible light which is more beneficial in sensitizing TiO_2 nanotubes. The photogenerated electrons in the small band gap CdSe can be easily evoked to the conduction band of the TiO_2 when the light wavelength of evoking light is less than or equal to 730 nm and thereby, contribute to increased solar energy conversion (Meng *et al.*, 2013; Wang *et al.*, 2016). The band gap narrowing effects will improve visible light absorption, increasing light harvesting efficiency and provide sites that slow down the recombination of charge carriers can be expected. Figure 2.6 shows the schematic diagram of the separation of generated electrons and holes on the interface of CdSe- TiO_2 semiconductor. Deposition of CdSe on TiO_2 nanotubes is thermally stable, has large cross section absorptions, and does not easily photodegrade. CdSe forms a type II band alignment with TiO_2. As a result, any photoexcited electrons in the CdSe doping can be injected into TiO_2 and subsequently

collected by an electrode or used to initiate a photocatalytic reaction. This type of heterostructure material can make use of visible or near-IR photons as well as facilitate charge separation to prevent recombination (Wang *et al.*, 2009).

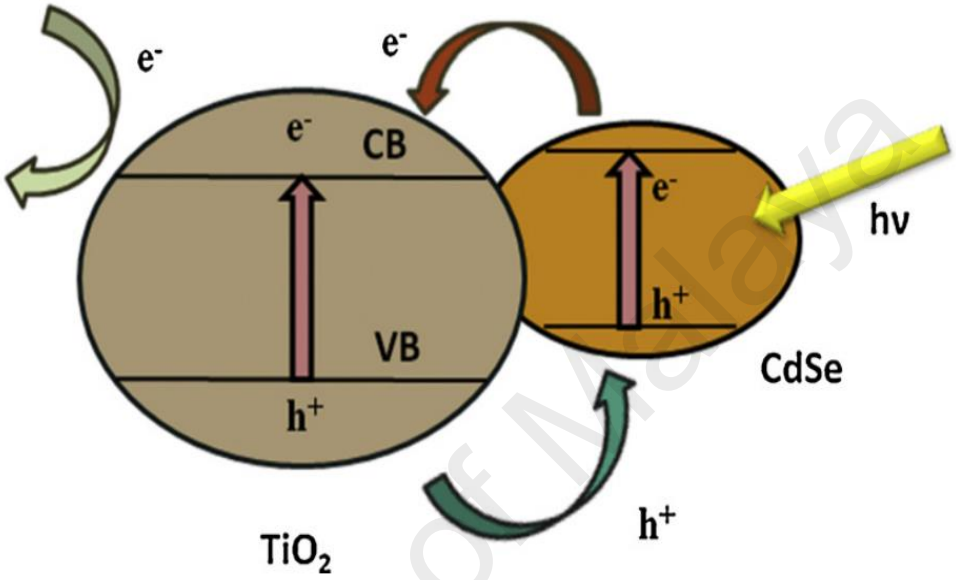

Figure 2.6: Schematic diagram of the charge-transfer process after being excited by light on the interface of CdSe-TiO_2 semiconductor. [CB and VB refer to the energy levels of the conduction and valence bands, respectively, for the CdSe and TiO_2] (Gan *et al.*, 2012)

2.11 Preparation of CdSe-loadedTiO_2 Nanotubes Film

Recently, various synthesis methods to form active and efficient CdSe-loaded TiO_2 photocatalyst have been explored. The incorporation of the CdSe species can control the physiochemical properties of TiO_2 photocatalyst. To date, there are several synthesis methods that can be utilized to produce hybrid CdSe-loaded TiO_2 photocatalyst either in particle, thin film, or nanostuctured form. The techniques are vacuum evaporation (Padiyan *et al.*, 2003; Ramaiah *et al.*, 2001), electrochemical deposition (Lv *et al.*, 2015), sol-gel (Armelao *et al.*, 2009), spray pyrolysis (HyukáIm & HyeokáPark, 2010), successive ionic layer adsorption and reaction method (SILAR) (González-Pedro *et al.*,

2013; Lee *et al.*, 2009), radio-frequency (RF) sputtering (Fernandes *et al.*, 2016; Fernandes *et al.*, 2014), chemical vapour deposition (Afzaal *et al.*, 2003), chemical bath deposition (CBD) technique (Chouhan *et al.*, 2011; Esparza *et al.*, 2015; Rodenas *et al.*, 2013) and etc. Some techniques are economic and simple but some require sophisticated instruments and costly precursors. In the next section, three main CdSe-TiO_2 nanotubes preparation methods (chemical bath deposition, successive ionic layer adsorption and reaction, electrochemical deposition) was briefly introduced.

2.11.1 Chemical bath deposition

Chemical bath deposition (CBD) is one of the chemosynthesis methods for sensitizing wide band gap semiconductor by growing directly on the surface of the TiO_2 nanotube arrays. It is an inexpensive, simple and convenient method with added advantages such as reproducibility, minimum material wastage, no need of handling poisonous gases, no requirement of sophisticated instruments, and well suitable for economical way of large area deposition at relatively low temperatures (Dhanam *et al.*, 2008; Pawar *et al.*, 2013). The CBD is working based on the the principle of ion-by-ion condensation in a solution state similar to the atom-by-atom deposition in a vacuum process (More *et al.*, 2003).

The CBD technique has been used extensively for years to prepare thin films of chalcogenide semiconductors, such as CdS, for its application as a window layer material in solar cell fabrication (Gopakumar *et al.*, 2010). Studies of depositing CdSe onto TiO_2 nanotube arrays through CBD by facilitating the growth parameters which included pH value, concentration of Cd^{2+} and Se^{2-} ions, deposition temperature, time and addition of different additives in bath resulted into different types of crystal structures, such as, amorphous, cubic, a mixture of cubic and hexagonal (Pawar *et al.*, 2013; Wang *et al.*, 2010; Yu *et al.*, 2012). Robel *et al.* reported on the use of bifunctional surface modifiers (SH-R-COOH) to sensitize CdSe QDs onto mesoscopic TiO_2 films, which was employed

as a photoanode in a photoelectrochemical cell (Robel *et al.*, 2006). Besides, Zhang *et al.* demostrated the introduction of CdSe by CBD into the TiO_2 nanotube films to enhance the photocathodic protection of stainless steel (Zhang *et al.*, 2012a).

The basic principle underlying the deposition of CdSe have been discussed by Chopra and Das (Chopra & Das, 1983). It is based on the slow release of Cd^{2+} and Se^{2+} ions from its complex in a basic aqueous bath. Subsequently, it condenses through an ion-by-ion basis onto the TiO_2 nanotubes substrates that are vertically mounted in the reaction bath (Dhanam *et al.*, 2008). Dissociation of Cd^{2+} and Se^{2-} ions from its complex either allow the CdSe nanocrystals to deposit gradually on TiO_2 nanotubes or aggregate into larger undesired particles, while it can be manipulated by controlling the parameters. The precipitation of metal chalcogenides in CBD occurs only when the ionic product exceeds the solubility product (K_{sp}) of metal chalcogenides. The solubility product of CdSe is very low. Therefore, even very low concentration of Cd^{2+} and Se^{2-} ions is sufficient to yield the solid phase (Gopakumar *et al.*, 2010; Pawar *et al.*, 2013).

Basically, source of Cadmium is prepared from its salts or oxide to form a complex by slowly adding alkaline (i.e. ammonium solution) under agitation until a clear solution was obtained. The steps of formation of precursor of Cd complex ions are as below:

$$Cd(CH_3COO)_2 + 2NH_4OH \rightarrow Cd(OH)_2 + 2NH_4(CH_3COO) \quad \text{(Equation 2.7)}$$

$$Cd(OH)_2 + 4NH_4OH \leftrightarrow Cd(NH_3)_4^{2+} + 2(OH^-) + 4H_2O \quad \text{(Equation 2.8)}$$

$$Cd(NH_3)_2^{4+} \leftrightarrow Cd^{2+} + 4NH_3 \quad \text{(Equation 2.9)}$$

Meanwhile, freshly prepared sodium selenosulphate (Na_2SeSO_3) solution acts as the source of Se^{2+} ions. It can be prepared through heating of Se metal or its oxide with sodium sulphite under reflux. The reduction of Na_2SeSO_3 to elemental Se in CBD process is shown through the following reaction in the aqueous ammoniacal medium.

$Na_2SeSO_3 + 2OH^- \rightarrow Na_2SO_4 + H_2O + Se^{2+}$ (Equation 2.10)

Hence, the overall chemical reaction is as below:

$Cd(NH_3)_2^{4+} + Na_2SeSO_3 + 2OH^- \rightarrow CdSe + 2NH_3 + Na_2SO_4 + H_2O$ (Equation 2.11)

2.11.2 Successive ionic layer adsorption and reaction (SILAR)

Successive ionic layer adsorption and reaction (SILAR) is one of the popular methods of depositing the metal chalcogenide semiconductor layer on the metal oxide films, such as TiO_2 nanostructures-based photoelectrochemical (PEC) cells in order to harvest the visible sunlight, and to enhance the conversion efficiency (Becker *et al.*, 2014; Luo *et al.*, 2012). Nicolau was the first scientist who demonstrated the use of SILAR to grow ZnS and CdS films in 1984 (Nicolau, 1985). Since then, the SILAR process is used to deposit various inorganic semiconductor, particularly, the metal sulfides. In 2009, Lee *et al.* have successfully prepared CdSe QD through SILAR process (Lee *et al.*, 2009). In the SILAR process, semiconductor CdSe is deposited onto substrates surface, where the substrate is dipped in sequence into precursor solutions of the reactants. Ions of the reactants are first segregated into two precursor solutions, then, they interact with the surface of the substrate through absorption in the first dip (e.g. Cd^{2+}) and rinse with solvent before react with ions of the opposite charge in the second dip (e.g. Se^{2-}). This is to facilitate its reaction with the surface-bound Cd^{2+} to yield CdSe at Cd^{2+} adsorption sites. The process is repeated until the desired thickness is obtained (Becker *et al.*, 2014; Zhou *et al.*, 2013). SILAR cycles is typically defined as below:

$Cd^{2+} \rightarrow$ ethanol rinse $\rightarrow Se^{2-} \rightarrow$ ethanol rinse = 1 SILAR cycle

Different from CBD, SILAR involves sophisticated procedures. This includes the preparation of each cationic and anionic precursor solutions, as well as closely monitoring of the dipping duration and sequences. Repetition of the process is required to obtain the

desired layer thickness of the doping and further, it leads to toxic waste generation where excess unbound Cd^{2+} ions were removed from the rinsing step. On the other hand, CBD is one pot reaction with minimal waste and repetition is not required.

2.11.3 Electrochemical deposition

Electrochemical deposition is a method with the aim of tuning the response of wide band gap semiconductor in visible region. By applying this method, optimum amount of CdSe nanocrystals can be deposited intra- and inter-tubular space of the TiO_2 nanotubes that forms three-dimensional (3D) multijunction structure (Xue *et al.,* 2013). Electrochemical deposition is performed in a three-electrode system. As the prepared TiO_2 nanotube arrays serves as working electrode, inert electrode, such as graphite or Pt rod, will serve as counter electrode while saturated calomel electrode (SCE) or Ag/AgCl electrode will work as the reference electrode. Zhang *et al.* reported the fabrication of CdSe/TiO_2 nanotube arrays heterogeneous structure through electrochemical deposition (Zhang *et al.*, 2014). Wang *et al.* also reported the successfully modified bare as anodized TiO_2 nanotubes with CdSe nanocrystals as the photoanode for driving the photoelectrocatalytic (PEC) generation of hydrogen and simultaneous degradation of organic pollutants in a PEC system (Wang *et al.*, 2016). However, electrochemical deposition has limited application in coating of TiO_2 nanotubes substrate. High cost and accurate instruments, for example, computerized potentiostat are required for the deposition to prudently control the reaction parameters. The coverage of sweeping potential, potential sweeping rate and accuracy of the deposition potential as well as the time affects the growth of CdSe nanocrystal on the surface of nanotubes. The changes in the pH value of electrolyte by the current density results in the amount of CdSe deposited (Xue *et al.*, 2014).

CHAPTER 3: METHODOLOGY

3.1 Introduction

This chapter provides the detail methodology to synthesize the hybrid CdSe-loaded TiO_2 nanotube arrays and characterization methods for their multifunctional application under solar irradiation. General information and some properties of raw materials and chemicals used in this study are encompassed in the first section. Subsequently, the experiment design and experimental procedures to attain hybrid CdSe-loaded TiO_2 nanotube arrays are elaborated in second section. This includes all the controlling processing parameters on the formation of high-aspect ratio anodic TiO_2 nanotubes via anodization method and further hybridization by chemical bath deposition technique. Then, third part of the chapter's outline is the characterization on morphological, chemical, structural, optical, electronic and electrochemical properties of the synthesized hybrid TiO_2 nanotubes arrays. Various characterization techniques include Field Emission Scanning Electron Microscopy (FESEM), Energy-dispersive X-ray Spectroscopy (EDX), X- ray diffraction (XRD), Raman Spectroscopy, Photoluminescence Spectroscopy (PL), UV-vis Diffuse Reflectance Spectroscopy (UV-vis DRS) and X-ray Photoelectron Spectroscopy (XPS). This part also covers a brief explanation on the characterization equipments, operating principles and sample preparation. The final part of the Chapter 3 devotes to the procedures involved in the solar-induced PEC water splitting performance test by utilizing the newly exploited hybrid TiO_2 nanotubes. The overview of the research methodology is presented in Figure 3.1.

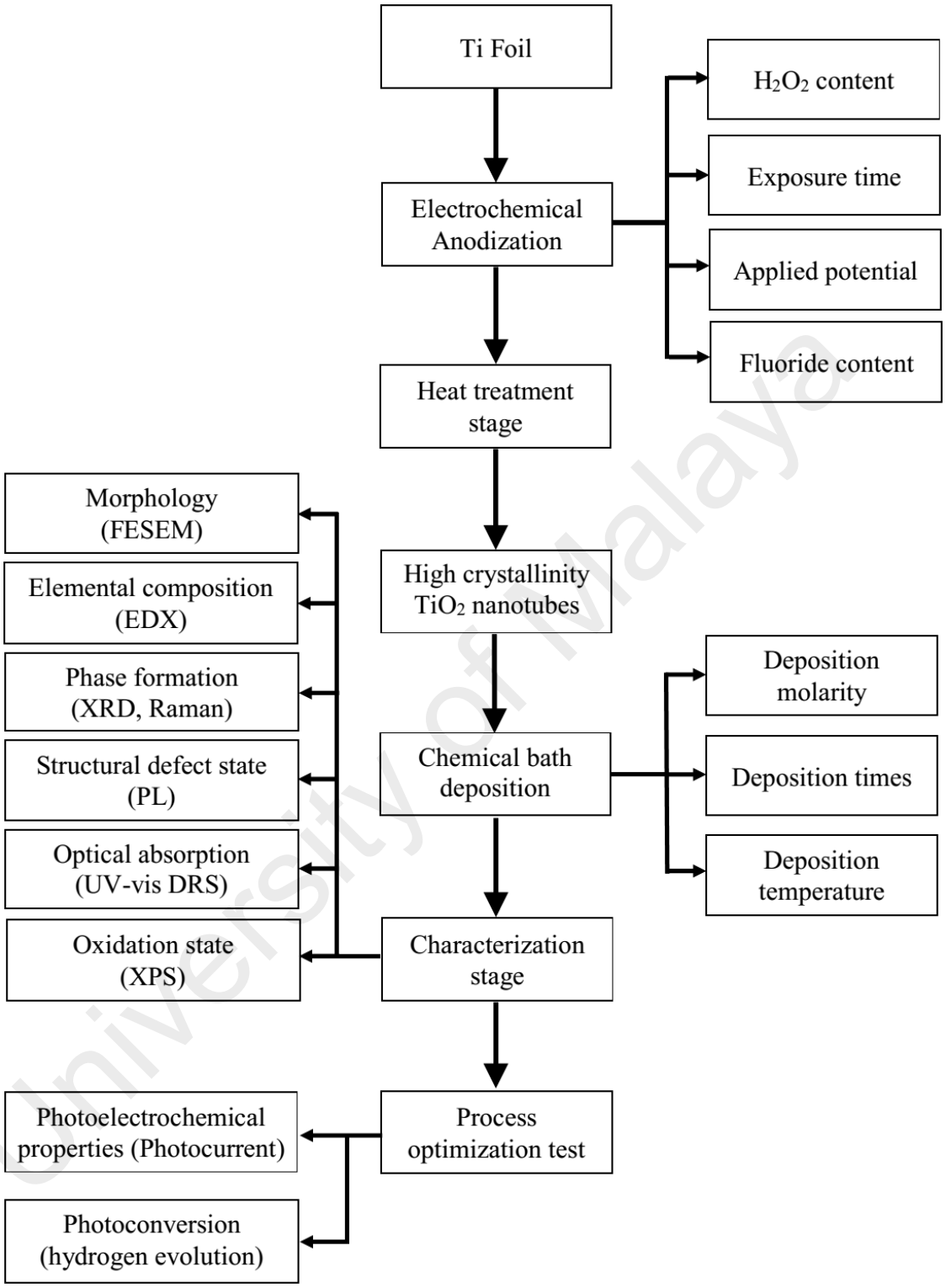

Figure 3.1: Overview of the research methodology

3.2 Materials Synthesis

3.2.1 Raw Materials

The materials and chemicals used in synthesizing pure TiO_2 nanotubes are Ti foil, ethylene glycol, hydrogen peroxide (H_2O_2), ammonium fluoride (NH_4F), and acetone. Meanwhile, to produce CdSe-TiO_2 nanotubes via CBD technique, cadmium acetate dihydrate ($Cd(CH_3COO)_2$), selenium metal powder, ammonium hydroxide (NH_4OH) and sodium sulphite (Na_2SO_3) were used as precursors. Potassium hydroxide (KOH) is an alkaline inorganic compound, which was used as an electrolyte in the PEC cell. The general information and some properties of the raw materials and chemicals used in this research are detailed in Table 3.1.

Table 3.1: Raw materials and chemicals used for the synthesis of CdSe-loaded TiO_2 nanotube arrays

Material	Function	Manufacturer	Properties
Titanium foil (Ti)	Substrate	Sigma Aldrich	Purity: 99.7% Thickness: 0.127 mm Density: 4.5 g/cm^3 Melting point: 1660 °C
Ethylene glycol	Electrolyte	Friendemann Schmidt	Molecular formula: $C_2H_6O_2$ Purity: 99 % Molar mass: 62.068 g/mol Viscosity: 1.61 x 10^{-2} Pa.s
Ammonium fluoride	Electrolyte	Merck	Chemical formula: NH_4F Purity: 98 % Molar mass: 37.0367 g/mol Melting point: Decompose at elevated temperature (100 °C)
Hydrogen peroxide	Oxidizing agent	Friendemann Schmidt	Chemical formula: H_2O_2 Purity: 30 % H_2O_2 and 70 % H_2O Molar mass: 34.0147 g/mol

Table 3.1: Raw materials and chemicals used for the synthesis of CdSe-loaded TiO_2 nanotube arrays, continued

Material	Function	Manufacturer	Properties
Acetone	Cleaning agent	Friendemann Schmidt	Chemical formula: $CO(CH_3)_2$ Molar mass: 58.08 g/mol Density: 0.79 g/cm^3
Cadmium acetate dihydrate	CdSe precursor	Merck	Chemical formula: $(CH_3COO)_2Cd \bullet 2\ H_2O$ Purity: 99 % Molar mass: 266.52 g/mol Melting point: 256 °C
Selenium metal powder,	CdSe precursor	Merck	Purity: 99.0 % Molar mass: 78.96 g/mol Density: 1.27 g/cm^3 Melting point: 217 °C
Ammonium hydroxide	CdSe precursor	Merck	Chemical formula: $CO(CH_3)_2$ Purity: 28 % Molar mass: 58.08 g/mol Density: 0.90 g/cm^3
Sodium sulphite	CdSe precursor	Merck	Chemical formula: Na_2SO_3 Purity: 97 % Molar mass: 126.04 g/mol Melting point: 500 °C

3.3 Sample Preparation

3.3.1 Foil preparation

To ensure better architecture of nanotubes growth, cleanliness and purity of initial Ti foil is very important. Hence, any form of contaminations such as finger prints, oil, grease and debris must be removed prior to anodization process. Ti foil (99.7 % purity) with thickness of 0.127 mm from Sigma Aldrich was used as substrate in this experimental work. Ti foil was cut into desired dimension (50 mm × 10 mm) then degreased by sonication in acetone for 30 min using Thermo-6D Ultrasonic Cleaner (40 kHz, 180 W). Ti foil was then rinsed in deionized water and dried in ambient temperature.

3.3.2 Electrolyte preparation

Electrolyte composition plays an important role in potentiostatic anodization. Structural morphology of the resulting nanostructure formed is either in compact nanotubular or porous structure and highly depend on its composition. In this present study, ethylene glycol used as electrolyte with dissolved NH_4F salt and H_2O_2. Prior to anodization, both NH_4F and H_2O_2 were added into the ethylene glycol electrolyte and the mixture of solution was stirred for 30 min by magnetic agitation. The purpose was to dissolve NH_4F and H_2O_2 into the ethylene glycol homogeneously.

3.3.3 Anodization procedure

To perform anodization, Ti foil was connected to the positive terminal of DC power supply (CBS Scientific EPS-200X) as anode in two-electrode configuration. Platinum rod, which acted as the counter electrode was connected to the negative terminal, which acted as the cathode. Subsequently, both the Ti foil and platinum rod exposed into prepared ethylene glycol electrolyte. The distance of two electrodes fixed was fixed ~20 mm (Figure 3.2). The anodization was carried out through manually switched on and off to monitoring the exposure time at desired potential. A smooth transfer of bubbles supplied from the bottom of anodization tanker was helped to homogenize the electrolyte and maintained a uniform current during anodization process. The configuration of the electrochemical anodization cell is shown in Figure 3.2.

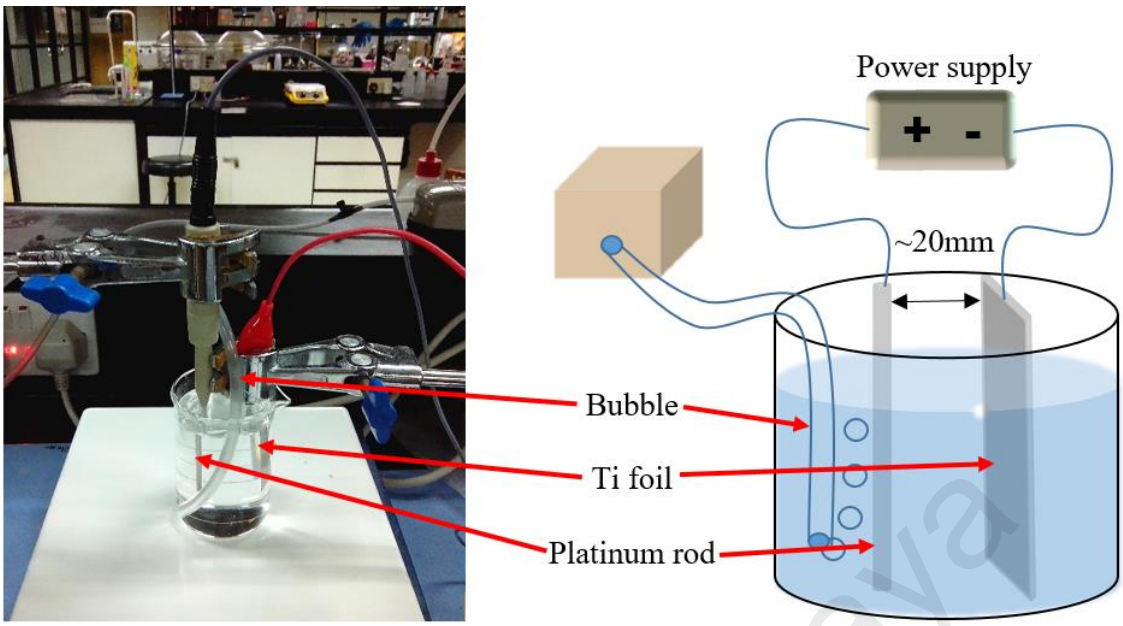

Figure 3.2: Electrochemical anodization cell experiment set-up

3.3.4 Cleaning TiO_2 nanotubes

Upon finishing anodization, the as-anodized TiO_2 foil was cleaned with deionized water and subsequently immersed into acetone to sonication (Thermo-6D Ultrasonic Cleaner, 40 kHz, 180W) for 1 min. It functions to remove the remaining electrolyte on the nanotubes layer and eliminate the debris and precipitation layers on top of the nanotubes.

3.3.5 Heat treatment process

Heat treatment or annealing process is where the materials are heated up to a suitable temperature and cools down to convert innate amorphous structure to crystalline structure. As compare with amorphous structure, crystalline structure formed produce changes in its properties such as strength, hardness, and phase composition. In this research, anatase crystalline phase is the most desirable structure which obtained by annealing at 400°C for 4 hours in air atmosphere. Based on literature, it is sufficient to fully transform from amorphous TiO_2 into anatase crystalline phase (Fernandes *et al.*,

2014). This is important because anatase is well known more efficient in PEC water splitting hydrogen generation (Luttrell *et al.*, 2014; Sreekantan *et al.*, 2009).

Heat treatment process involves three stages which are heating, soaking and cooling. Both heating and cooling rate used in this project were fixed at 5 °C/min whilst soaking time was 4 hours. All the samples were placed upright in an alumina boat before heat treated in the furnace. The example of the heating profile is presented in Figure 3.3.

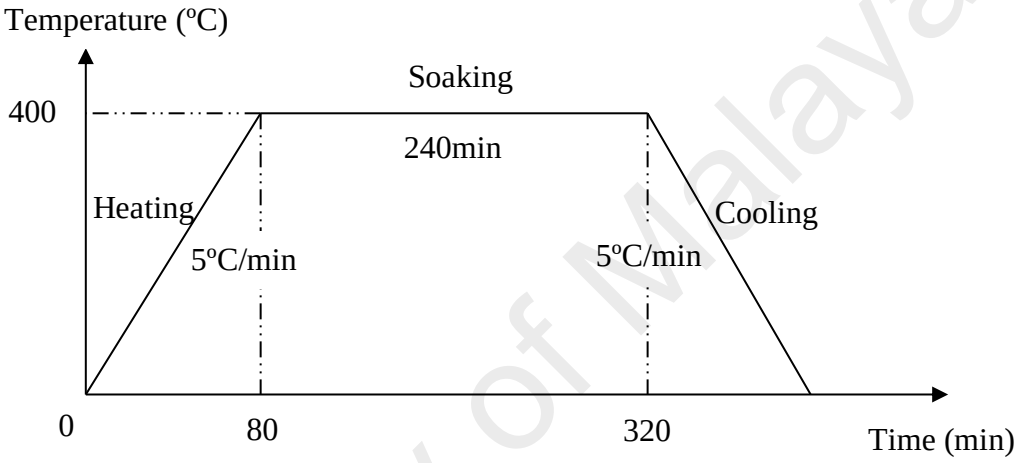

Figure 3.3: Annealing profile of anodized Ti foil

3.3.6 Preparation of CdSe-TiO_2 nanotubes by chemical bath deposition

CdSe-TiO_2 nanotubes were synthesized through CBD technique. Two steps were employed to assemble CdSe onto the substrate. First is the preparation of sodium selenosulphate (Na_2SeSO_3) and $Cd(NH_3)_4^{2+}$ solution, precursors of Se and Cd. Second is the deposition of CdSe onto as annealed pure TiO_2 nanotubes. .

In the preparation of Na_2SeSO_3 solution, sodium sulphite (Na_2SO_3, 5 g) and selenium metal powder (0.8 g) were added in 100ml distilled water then heated under reflux at 90 °C for 3 hours. An apparent of black colour Se sedimentation was formed in the solution at the beginning and was then slowly digested to form Na_2SeSO_3 compound accompanied by the formation of a clear solution. It gives the complete conversion of Se into Na_2SeSO_3.

The temperature of the solution was then brought down to room temperature and used directly for the synthesis.

Cadmiun precursor was prepared by dissolving 2.7 g cadmium acetate dehydrate $Cd(CH_3COO)_2 \bullet 2H_2O$ in 50 ml deionized water. Concentrated ammonia solution (30%) was added to the mixture slowly under magnetic stirring agitation. Initially, the solution became milky and turbid due to the formation of $Cd(OH)_2$. Further addition of excess concentrated ammonia solution dissolved the turbidity and made the solution clear and transparent.

Both freshly prepared Cd and Se precursors were mixed and homogenized by stirring for 10 min. Meanwhile, ammonia was used to adjust the pH of the solution between 12 and 12.5. This was to prevent the reverse reaction of $Cd(NH_3)_4^{2+}$ to form stable cadmium hydroxide $Cd(OH)_2$. As annealed anatase TiO_2 nanotubes was bathed in the bath solution inclined vertically at 20° to the wall of beaker. The substrate doped with CdSe was removed after desired exposure time and was rinsed in deionized water and dried in air. This study aims to optimize the molarity of electrolyte, reaction time and reaction temperature of TiO_2 nanotubes in CdSe solution to enhance the PEC water splitting performance.

3.4 Characterization Techniques

The properties of the synthesized samples were characterized via various characterization techniques. These techniques that comprehend properties such as morphological studies by Field Emission Scanning Electron Microscopy (FESEM), elemental composition analysis by Energy-dispersive X-ray Spectroscopy (EDX), phase structure analysis by X- ray diffraction (XRD) and Raman Spectroscopy, carrier recombination analysis by Photoluminescence Spectroscopy (PL), optical properties analysis by UV-vis Diffuse Reflectance Spectroscopy (UV-vis DRS) and also chemical

state analysis by X-ray Photoelectron Spectroscopy (XPS). Brief explanation on all the characterization method, basic principles and sample preparation of such analytical equipment describes in this section.

3.4.1 Field Emission Scanning Electron Microscope

Field emission scanning electron microscopy (FESEM) is a type of electron microscope which able to provide morphological and elemental information at the magnification from 10 times until 150,000 times with limited depth of field. Basically, a focused electron beam is generated and passes through a vacuum column focus onto the specimen's surface. Accelerated electrons in an FESEM carry significant amounts of kinetic energy and this energy is dissipated as a variety of signals produced by electron-sample interactions when the incident electrons are decelerated in the solid sample. These signals include secondary electrons, backscattered electrons (BSE), Electron backscatter diffraction (EBSD that are used to determine crystal structures and orientations of minerals), photons (characteristic X-rays that are used for elemental analysis and continuum X-rays), visible light (cathodoluminescence) and heat. Secondary electrons and backscattered electrons are commonly used for imaging samples: secondary electrons are the most valuable for showing morphology and topography on samples and backscattered electrons are the most valuable for illustrating contrasts in composition in multiphase. FESEM analysis is considered to be a "non-destructive", so it is possible to analyze the same materials repeatedly. Any kind of solid material can be studied by using FESEM. For the materials which are electrically conductive may be examined directly while for the nonconductive materials, a thin conductive coating is required to prevent electrical charging of the specimen. FESEM is a very popular surface examination method due to its capability of obtaining the three-dimensional-like images of the surface of the samples. In this research, CdSe-loaded TiO_2 nanotubes samples were cut into desired size (5 mm x 5 mm) and placed on a conductive carbon tape. It has been observed

using a JEOL JSM 7600-F field emission scanning electron microscope operated at 5 kV and 10 kV and magnifications of 30, 50 and 100 kX were typically used for detailed characterization.

Energy-dispersive X-ray spectroscopy (EDX) is known as an elemental composition analysis used with field emission scanning electron microscopy. It has the same concept as FESEM by detecting the x-rays emitted from the sample during an electron beam bombardment to characterize the elemental composition of the analyzed volume. Features or phases as small as 1 μm or less can be analyzed. The sample preparation is same with SEM analysis, where non-conductive materials need to be coated with gold palladium layer. Analysis of compositions of elements in the annealed CdSe-loaded TiO_2 nanotubes samples were determined by EDX.

3.4.2 X-ray Diffraction

For phase structure and compositional analysis, the samples were characterized by powder X-ray diffraction (XRD) using Bruker AXS D8 Advance (Germany). XRD analysis was conducted using a Cu target (Nickel filter), Kα radiation ($\lambda = 0.1546$ nm) to determine the crystalline phase of the sample at scanning rate over angle, θ in the range 10 - 90°. Values for intensity and diffraction angle, 2θ, were recorded and a graph was plotted from these data values. X-ray diffraction (XRD) is one of the most common methods used to determine the crystal structure of materials by using the principle of Bragg's Law. The degree and intensity of the diffracted ray is detected by a diffractometer with radiation counter. Once a monochromatic beam of X-rays is directed at a sample which is a crystalline material, either the reflection or diffraction of the X-rays at various angles with respect to the primary beam can be observed. Then, the X-ray constructively interferes will determine the intensity of the reflected X-ray. For constructive interference, it is defined as the path between rays from two subsequent crystal planes is

equal to a whole number of the X-ray wavelength. Hence, it comes with the Bragg's Law equation: $n\lambda = 2d \sin \theta$, where n represents the order of diffraction, λ represents the wavelength of the X-ray beam, θ represents the angle of incidence of the X-ray and d represents the distance between each set of atomic planes of the crystal lattice. The X-ray patterns of a crystalline substance can be analogous as a "finger-print" due to the unique and different diffraction pattern for each crystalline material. Therefore, the unknown compound can be identified with comparing the interplanar spacings and intensities of its XRD patterns to the reference patterns of Joint Committee on Powder Diffraction Standards in the powder infraction file (PDF).

3.4.3 Raman Spectroscopy

Raman spectroscopy is a spectroscopic technique used to study sample phase by the vibrational, rotational and other low frequency transitions. Monochromatic laser beam either in the visible, near infrared or near ultraviolet range irradiated on the sample results in the energy of the laser photons being shifted up or down. This shift is due to interaction of beams with the vibrational energy levels of the molecules in the specimen. The majority of the scattering radiation at the wavelength corresponding to the laser line (Rayleigh scattering or elastic scattering) is filtered out. Inelastic scattering or raman scattering gives information about the with molecular vibrations energy level provided fingerprint by which molecules can be identified. Raman spectrum is generated by plotting the intensity of the raman scattering versus frequency indicating the energy levels of different functional group vibrations. In this research, the crystal structures of the specimens were identified by using a Raman spectrometer (Renishaw inVia, United Kingdom) over the range of 100 cm^{-1} to 1000 cm^{-1}, at an excitation wavelength of 532 nm generated by an Ar ion laser.

3.4.4 Photoluminescence Spectroscopy

Photoluminescence spectroscopy is a non-destructive and non-contact method for observing the electronic structure and recombination mechanism of materials. In essence, it is similar as Raman spectroscopy which initiate by photoexcitation, an ultraviolet or visible photon irradiate onto a material. The substrate absorbs photons further excite electrons from the equilibrium states to excitation states and emit photons as it relaxes and release energy and returns back to equilibrium states. The emission of photons through this process is known as photoluminescence, PL. The emitted photon energy (photoluminescence) relates to the transition energy level between equilibrium states and excites states. In semiconductors, these two electron states (valance and conduction bands) involved in the photoluminescence whereas the transition energy is known as band gap energy. Dissipation of electron energy to equilibrium stated is known as recombination. The quantity of PL emitted from a material is directly related to the relative amount of recombination rates. Recombination rates are typically associated with level of photoexcitation, impurities surface defects and temperature. Thus, analysis of photoluminescence can qualitatively monitor changes in material quality as a function of growth and processing conditions and help understand the underlying physics of the recombination mechanism. In this research, recombination in the samples was characterized using monochromatic beam with 325 nm wavelength at room temperature. The photoluminescence were recorded in the range of 350 nm to 750 nm.

3.4.5 UV-vis Diffuse Reflectance Spectroscopy

UV-vis diffuse reflectance spectroscopy or ultraviolet-visible spectrophotometry refers to absorption spectroscopy or reflectance spectroscopy in the ultraviolet-visible spectral region. It was developed to identify the absorption and reflectance of sample in liquid, solid thin film or powder form by measuring relative change of transmittance or reflectance of light. A solution has essentially to transmit certain range of wavelengths of

light, which depend on dissolved components that have (allowed) electronic transitions over that energy range. When the energy levels of the component lies within the wavelength of light, it may absorb the light energy to move electrons from the filled energy level (valence band) into this empty level (conduction band), which causes a relative decrease in the amount of light at that particular energy. Hence, relative change in light transmission or increase in light absorbance will be recorded.

By the same line of reasoning, a solid sample with high surface roughness, the effective reflection is not specular and conversely we cannot measure the transmitted intensity (it is too low). Therefore, for powders or thin films of high surface roughness, we use DRS where apart from recording reflectance, we can also measure absorbance of the sample collecting all the diffuses reflected beams (from the sample surface) using a semispherical collector. This will give a DRS spectrum which shows the interaction of the samples with light of various wavelengths. It is then possible to compute the energy band gap value of the materials based on the spectrum.

In this study, the optical properties of the CdSe-loaded TiO_2 nanotubes was characterized using a Shimadzu UV-2700 UV-vis Spectrophotometer and DRS measurements were done in wavelength range of 240 to 800 nm using an integrating sphere.

3.4.6 X-ray Photoelectron Spectroscopy

X-ray Photoelectron Spectroscopy (XPS) also known as Electron Spectroscopy for Chemical Analysis (ESCA) is a quantitative spectroscopic technique. It is applied to a broad range of materials that measures the elemental composition, empirical formula, chemical state and electronic state with analysis depth 10 nm or less of any solid surface. XPS is typically accomplished by exciting a samples surface by utilizing mono-energetic x-rays while simultaneously measure both the kinetic energy and number of

photoelectrons to be escaped from the sample surface. An electron energy analyzer is used to measure the energy of the escaped photoelectrons. From the binding energy and intensity of a photoelectron peak, the elemental identity, chemical state, and quantity of a detected element can be determined. In this study, the investigation of chemical and oxidation states of CdSe-loaded TiO_2 nanotubes was determined on a PHI Quantera II scanning X-ray microprobe using an Al cathode ($h\nu$ = 1486.8 eV) with 100 microns spot size and 280 eV pass energy. The core level spectra of Ti 2p, O 1s, C 1s, Cd 3d and Se 3d were subsequently recorded through high resolution narrow scans.

3.5 PEC water splitting cell testing

The PEC properties of the samples were characterized using a three electrodes PEC cell under solar irradiation. Specimen was served as the working electrode, platinum rod served as the counter electrode and Ag/AgCl in saturated KCl served as the reference electrode. These electrodes consequently dipped in electrolyte used for PEC cell consisted of 1M KOH aqueous solution. All three electrodes were connected to the potentiostat (Autolab PGSTAT 204, Netherlands) by using a control software NOVA for photoelectrochemical measurements. The current range is fixed from 10 mA to 10 nA. All CdSe loaded TiO_2 nanotubes samples and the best morphology with the highest aspect ratio pure TiO_2 nanotubes sample were characterized through linear sweep potential as PEC performance. A 150W Xenon lamp (Zolix LSP-X150, China) was used as the light source, with intensity 100 mW/cm^2 light beam was focused on the immersed portion of working electrode. Graphically illustration of the photocurrent (mA^{-1}) versus applied bias potential (V) was generated over the -1.0 V to 1.0 V range at scan rate of 5 mV/s under dark and illumination. Among all hybrid CdSe-loaded TiO_2 nanotubes samples, the best PEC performance and the best pure TiO_2 nanotubes used in hydrogen evolution measurement. The H_2 evolution measurement was subsequently performed under a bias potential 0.6 V for 1 hour. The H_2 gas generated at platinum rod was collected with a

reverted burette by using the water displacement technique. As the H_2 gas is produced in counter electrode in PEC water splitting cell, it will bubble up into inverted burette. The volume of gas is determined by reading the gas level on the side of burette. The overall photoconversion efficiency (η) is used to define the highest energy output that able to be generated from a product from energy supplies in the form of light (Grimes *et al.*, 2007). Hydrogen generation rate and photoconversion efficiency, η (conversion efficiency from light energy to the chemical energy) (Zhang *et al.*, 2012b) was calculated based on the Equation 3.1 and 3.2 below.

$$\text{Hydrogen generation rate} = \frac{\text{Volume of hydrogen gas generated (mL)}}{\text{Area of sample (cm}^2\text{)} \times \text{Time (h)}} \quad \text{(Equation 3.1)}$$

$$(\eta) = \frac{\text{Total power output} - \text{Electrical power output}}{\text{Light power input}} \times 100\%$$

$$= \frac{jp\,(E°rev - |Eapp|)}{I_o} \times 100\% \quad \text{(Equation 3.2)}$$

where j_p stand for photocurrent density (mA/cm^2), both $j_pE^\circ_{rev}$ and $jp\,|E_{app}|$ are total power output and electrical power input respectively. I_o is the incident light power density (mW/cm^2), E°_{rev} is the standard reversible potential (1.23 V/SHE) and $E_{app} = E_{mean} - E_{aoc}$. E_{mean} is the working electrode potential (versus Ag/AgCl electrode) under illumination and E_{aoc} is the open-circuit potential (versus Ag/AgCl electrode) of the working electrode.

Figure 3.4 shows the schematic diagram of the experimental set up for PEC performance and H_2 generation.

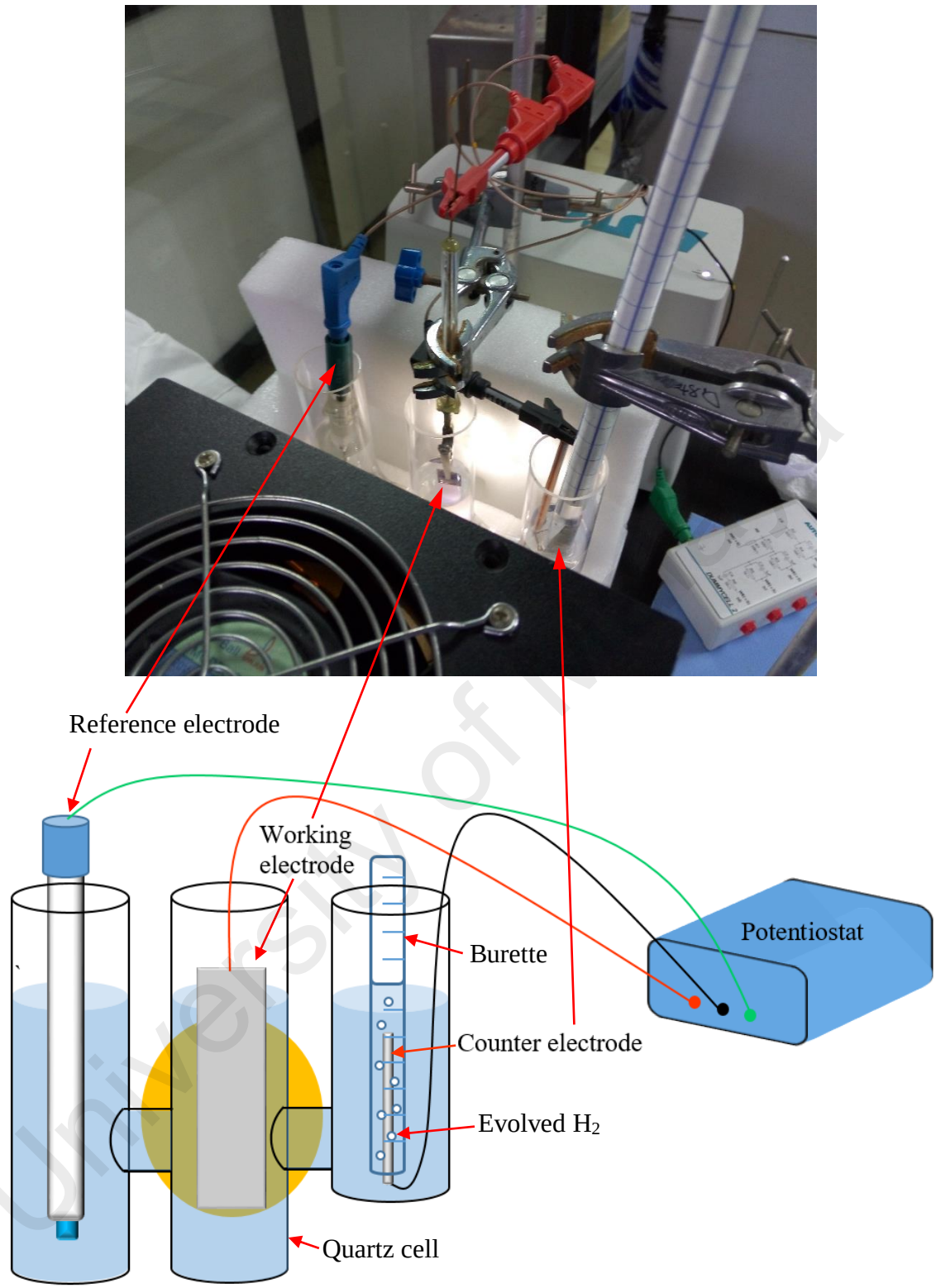

Figure 3.4: Experimental set-up of H_2 generation by the PEC water splitting process

CHAPTER 4: RESULT AND DISCUSSION

4.1 Introduction

Chapter 4 includes the experimental results obtained from the experiments conducted as well as the discussion of all analysis. There are two sections in this chapter. The first section presents the information regarding the formation of high aspect ratio bundle-free TiO_2 nanotubes in ethylene glycol electrolyte consisting H_2O_2 and NH_4F via electrochemical anodization. The influences on the surface morphology, aspect ratio and phase structure of the pure TiO_2 nanotubes with respect to anodization voltage, anodization duration, NH_4F and H_2O_2 content in the ethylene glycol electrolyte were evaluated in detail.

The second section of this chapter discussed the incorporation of CdSe on TiO_2 nanotubes via CBD technique. A comprehensive study was conducted to optimize several deposition parameters (deposition molarity, reaction time and temperature) in order to obtain the desired CdSe-TiO_2 nanotubes structure with the best PEC water splitting performance under solar illumination. In the present study, the amount of H_2 generated by CdSe-TiO_2 nanotubes was also compared with the pure TiO_2 nanotubes. Based on our study, it was found that hybrid CdSe-TiO_2 nanotubes showed better hydrogen generation compared to pure TiO_2 nanotubes because the coupling of CdSe and TiO_2 can control the recombination of the photogenerated change carriers and increase charge separation of TiO_2 during illumination.

4.2 Formation of TiO_2 nanotubes via electrochemical anodization

Electrochemical anodization method was used to produce the highly ordered bundle-free TiO_2 nanotubes array films. The influence of H_2O_2 addition, anodization time, anodization potential and fluoride content into the ethylene glycol electrolyte towards surface morphology of oxide layer were evaluated in detail.

4.2.1 Effect of H_2O_2 in the electrolyte on the anodic oxide formed

In order to synthesis highly ordered TiO_2 nanotubes, we demonstrated the effect of H_2O_2 in the anodization electrolyte which acted as oxygen provider to supply sufficient O^{2-} ions to accelerate the anodic oxidation. Figure 4.1 and Table 4.1 illustrates the results obtained for the dimensional of anodic TiO_2 oxide layers by incorporating different content of H_2O_2. Different top surface morphologies of Ti foil anodized with different wt % of H_2O_2 and the inset of oxide's cross sectional view were presented in Figure 4.1. The average diameter, length and wall thickness, aspect ratio (AR) and geometric surface area factor (G) of anodic Ti nanotubes formed were summarized accordingly in Table 4.1. Both formulations and calculations for aspect ratio and geometric surface area factor are as followed (Lee *et al.*, 2015):

$$AR = L/ (D + 2w)$$

$$G = [4\pi L (D + w)]/ [(\sqrt{3}) (D + 2w)^2] + 1$$

where L = nanotube length in nm; D = pore size diameter; w = wall thickness.

As shown in the images in Figure 4.1, the appearance of anodic oxides on Ti foils was dependent on the wt % of H_2O_2 in the fluorinated electrolyte. For the sample anodized in 1 wt% H_2O_2, nanotubes with the length of 800 nm were obtained. This nanotube arrays was found bundled at the top layer of the nanotubes and cause pores blockages. When the content of H_2O_2 was 2 wt%, an incomplete nanotubes structure was formed. Nanotubular layer was slightly increased to 1.1 µm. Using 3 wt% of H_2O_2, the diameter of the nanotubes became larger with an approximately 50 nm and length of 1.9 µm. The over layer that covered the nanotubes was minimized and random interconnected pits started to grow when 3 wt% of H_2O_2 was added into the electrolyte. With further increased of H_2O_2 content to 4 wt%, the diameter of the nanotubes became larger at 64 nm and length of 2.3 µm. At the H_2O_2 content of 5 wt%, the nanotubes formed were circular, with an

average diameter of 76 nm and length was increased to 5.6 µm. The pH of this electrolyte was about 6.5. However, further increased of H_2O_2 content to 10 wt% produced a negative effect on the self-ordering of the anodic oxide. The nanotubular structure disappeared whereby the anodic oxide was composed of irregular porous layers with thickness of ~0.8 µm, as shown in Figure 4.1 (f).

In order to get high aspect ratio of nanotubes array, H_2O_2 which is known as a powerful oxidant was added to act as the oxygen provider. At ambient conditions, H_2O_2 is unstable and will decompose to HO_2^- and H^+ ions (Equation 4.1) which then further react to form •OH and HO_2• radicals (Equation 4.1 to 4.3). These radicals increased the oxidation rate of the anodization process (Equation 4.4 and 4.5). Field-assisted dissolution, and chemical dissolution reactions were improved by •OH and HO_2• radicals during the anodization process. Hence, growth of strong and bundle-free nanotubes on Ti substrate was observed with the increase of the H_2O_2 content in electrolyte (Grimes & Mor, 2009).

In an anodization process, O^{2-} ions first migrated towards Ti induced growth of passivation layer with high electric field across the thin layer. This high electric field then further induces electric field dissolution and formed random pits accompanied with breakdown of the passivation layer. The formation of random pits through electric field dissolution on the oxide surface was assisted by the polarization of Ti-O bond. F^- ions in the electrolyte perform as etchant and react with those random pits and grow into pores via the formation of $[TiF_6]^{2-}$ complex ions (Equation 4.6) (Grimes & Mor, 2009). Nonetheless, there is an optimum amount of H_2O_2 which lead to high growth rate of self-ordering nanotubular structure. Further increase content of H_2O_2 would be detrimental. Excessive H_2O_2 will give rise to form high H^+ ions in the electrolyte and pH of the electrolyte also reduced to 6.2 (Equation 4.1). Furthermore, it led to high chemical dissolution rate and diminished the nanotubular structure as depicted in Equation 4.6.

Thus, 5 wt% H_2O_2 was found to be the optimum for the formation of circular nanotubes with lengths approximately 5.6 µm.

$H_2O_2 \rightarrow HO_2^- + H^+$ (Equation 4.1)

$H_2O_2 + e^- \rightarrow \bullet OH + OH^-$ (Equation 4.2)

$H_2O_2 + \bullet OH \rightarrow H_2O + HO_2\bullet$ (Equation 4.3)

$Ti \rightarrow Ti^{4+} + 4e^-$ (Equation 4.4)

$Ti^{4+} + 2H_2O \rightarrow TiO_2 + 4H^+$ (Equation 4.5)

$TiO_2 + 6F^- + 4H^+ \rightarrow [TiF_6]^{2-} + 2H_2O$ (Equation 4.6)

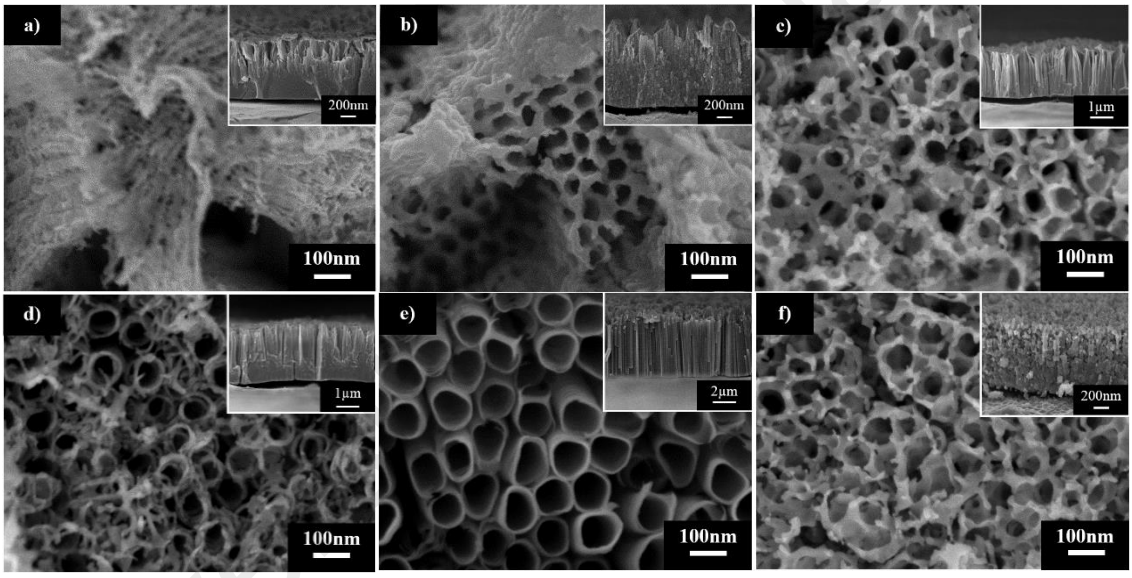

Figure 4.1: FESEM images of TiO_2 nanostructures obtained with varying H_2O_2 content: (a) 1 wt%, (b) 2 wt%, (c) 3 wt%, (d) 4 wt%, (e) 5 wt% and (f) 10 wt%. Insets are the side views of the samples

Table 4.1: Pore diameter, length, wall thickness, aspect ratio, and geometric surface area factor of TiO_2 nanotubes synthesized in electrolyte with different H_2O_2 content

H_2O_2 content (wt %)	Diameter (nm)	Length (μm)	Wall thickness (nm)	Aspect Ratio, AR	Geometric surface area factor, G (m^2g^{-1})
1	-	0.8±0.1	-	-	-
2	-	1.1±0.1	-	-	-
3	50±2.3	1.9±0.1	20±1.4	21.1	120.13
4	64±2.6	2.3±0.2	13±1.3	25.5	159.63
5	76±2.4	5.6±0.1	10±0.9	58.3	380.13
10	57±1.4	0.8±0.1	23±1.8	7.8	44.77

4.2.2 Effect of anodization time

In this part of experiment, electrochemical anodization was performed in ethylene glycol containing 5 wt% of H_2O_2 and 0.3 wt% NH_4F at 40 V for different durations from 10 to 120 min. Figure 4.2 shows the FESEM images for samples anodized at different times. At the anodization time of 10 min, nanotubular structure was visible but was not well-defined with thickness of 1.2 μm as shown in Figure 4.2 (a). It is a well-known fact that random small oxide pits were formed on Ti surface due to breakdown of the passivation layer with the presence of chemical dissolution and field-assisted dissolution reactions at local point of high energy. After 20 min of anodization, it could be noticed that those random pits undergo further oxidation and localized dissolution to form interconnected pores structure. Nanotubes with approximately 46 nm in diameter and 2.0 μm in thickness were formed [Figure 4.2 (b)]. Increasing anodization time to 30 and 40 min, the anodic oxide layer was composed of nanotubular structures could be observed with increasing average diameter up to 50 and 56 nm, respectively as exhibited in Figure 4.2 (c) & (d). The average length of the synthesized nanotubular structure was found to be increased significantly with 3.2 um and 4.1 μm for 30 min and 40 min of anodization respectively. Anodization for 50 min resulted in bigger and longer uniform nanotubes (diameter: 74 nm; length: 5.1 μm), as shown in Figure 4.2 (e). As shown in Figure 4.2(f),

an anodic oxide layer was formed after applying 60 min of anodization. The anodic oxide layer was composed of nanotubular structures with round and isolated nanotubular structure. The average diameter and length are 77 nm and 5.8 μm respectively. Further prolong the anodization duration to 120 min resulted in the reduction of the formation rate for nanotubular structure with tube length of approximately 7.3 μm and average pore size of 84 nm respectively.

Based on the obtained results, it can be concluded that high growth rate of anodic nanotubular within 60 min of anodization time could be achieved. The main reason is attributed to the presence of sufficient powerful oxidant of H_2O_2 within the electrolyte. As explained in the previous section, higher growth rate of TiO_2 nanotubes in ethylene glycol containing H_2O_2 were caused by the pronounced dissolution at the bottom of the nanotubes in the presence of •OH and HO_2• radicals. These radicals increased the deepening rate of the pores and thus formed high AR and G nanotubes within 60 min anodization time. After 60 min of anodization process, it could be understood that most of the unstable H_2O_2 has been decomposed to form short-lived oxidizing hydroxyl radical and consumed in the early anodization process. Hence, the growth rate of nanotube array was decreased (Santos *et al.*, 2009). The average diameter, length, wall thickness, aspect ratio (AR), and geometric surface area factor (G) of the nanotubes anodized with varying anodization duration are summarized in Table 4.2.

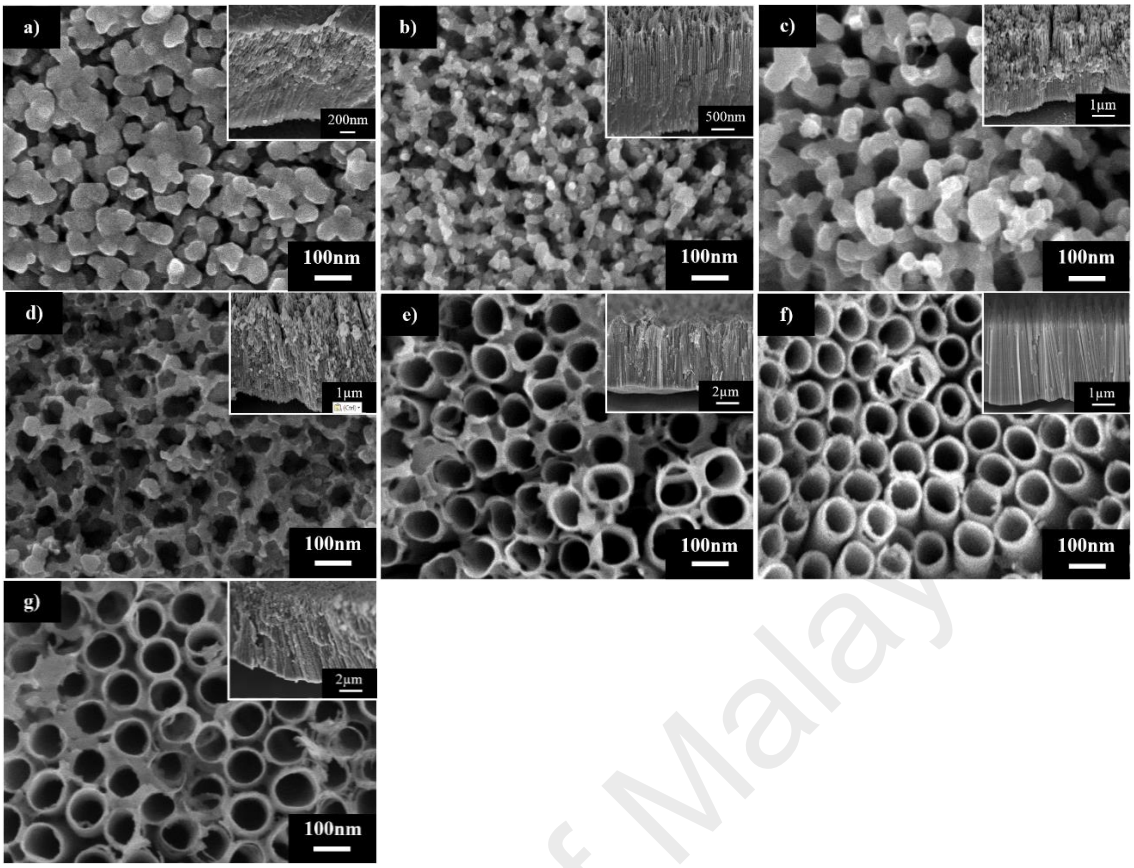

Figure 4.2: FESEM images of TiO_2 nanostructures obtained with varying anodization duration: (a) 10 min, (b) 20 min, (c) 30 min, (d) 40 min, (e) 50 min, (f) 60min and (g) 120min. Insets are the side views of the samples

Table 4.2: Pore diameter, length, wall thickness, aspect ratio, and geometric surface area factor of TiO_2 nanotubes synthesized with varying anodization duration in ethylene glycol containing 5 wt% H_2O_2

Anodization duration (min)	Diameter (nm)	Length (µm)	Wall thickness (nm)	Aspect Ratio, AR	Geometric surface area factor, G (m^2g^{-1})
10	-	1.2±0.1	-	-	-
20	46±2.6	2.0±0.1	25±1.5	20.8	112.79
30	50±2.3	3.2±0.1	20±1.8	35.5	201.64
40	56±2.1	4.1±0.2	19±1.4	43.6	253.49
50	74±1.6	5.1±0.1	14±1.2	50.0	313.97
60	77±1.4	5.8±0.2	10±0.9	59.7	390.09
120	83±2.7	7.3±0.1	10±1.3	70.9	465.28

4.2.3 Effect of anodization voltage

It is a well-known fact that anodization voltage controls field-assisted oxidation and field-assisted dissolution during anodization process and, thus, varies the diameter and the length of the nanotubular structure. Continuing from the previous part of the experiment, anodization time and amount of H_2O_2 added into the electrolyte were fixed at an optimum value. All the samples were anodized in fluorinated ethylene glycol composed of 5 wt% H_2O_2 for 60 min. The voltage was varied from 10 V to 60 V. Figure 4.3 clearly shows that the applied voltage affects the geometric features of the nanotubes on the Ti foils based on the illustrative top view and cross-sectional view FESEM image.

As seen in Figure 4.3(a), nanotubes with the smallest diameter ~ 13 nm and the shortest length of approximately 500 nm were successfully produced at lower voltage of 10 V. With further increased in the anodization voltages to 20 V, the diameter of the nanotubes array shows ~ 24 nm and the length was ~ 800 nm [Figure 4.3(b)]. Ti foil anodized at 30 V shows increased nanotubes diameter and length up to ~ 55 nm and 2.5 µm respectively. Interestingly, it was found that when Ti foil was anodized at 40 V, the largest geometric surface area factor (389.11 G (m^2g^{-1})) and aspect ratio (60.4) nanotubes arrays with ~ 74 nm in diameter and 5.8 µm in length [Figure 4.3(d)] was observed. Ti anodized at higher voltages of 50 V produced nanotube arrays with an average diameter of 84 nm length of ~ 6 µm as exhibited in Figure 4.3(e). However, at higher anodization voltage of 60 V, both the diameter and length of the nanotubes array were reduced to ~ 54 nm and 3 µm, respectively.

This diminution phenomenon might be caused by imbalance of field-assisted dissolution and field-assisted oxidation reactions on the anodic oxide layer at the beginning electrochemical anodization stage. Meanwhile, high chemical dissolution rate occurred simultaneously and eventually, etching of the top surface of TiO_2 nanotubes via

the formation of fluoride complex ions [Equation 4.6]. Furthermore, it could be understood that high anodization voltage provide higher driving force of both etchants H^+ ions and F^- ions to accelerate chemical dissolution rate of Ti and TiO_2 [Equation 4.6] (Kim *et al.*, 2014). It was well-established that the influence of applied voltage on the diameter and length of nanotubes is related to the number of the pits formed at the early stage of anodization process. Therefore, the use of high voltage causes severe electric field dissolution and forms more pits during the early stage of anodization. Based on the results obtained, more pits formed and further etched to form larger pores when higher voltage applied. As for these pores become dominant, it was resulting the tubular nanoarchitecture on the anodic oxide layer (Sopha *et al.*, 2015).

At lower potential, short nanotubes were formed on Ti foil due to insufficient electric field dissolution occurs during electrochemical anodization stage. Further increased in the anodization voltage increased the nanotube length. This might be attributed to the high driving force for ionic transport through the barrier layer at the bottom of the pore. Hence, results in faster movement of the Ti/TiO_2 interface into the Ti metal. The length of nanotubes will further increase until the rate of chemicals dissolution of nanotubes equals with field assisted dissolution and oxidation (Yasuda *et al.*, 2007). As for this study, formation of TiO_2 nanotubes with the AR and G of 60.4 and 389.11 G (m^2g^{-1}) were achieved in the electrolyte composing of 5 wt% H_2O_2 by applying voltage of 40 V for 1 h. These compositions were selected because it favoured the formation of well-aligned and highly ordered TiO_2 nanotubes.

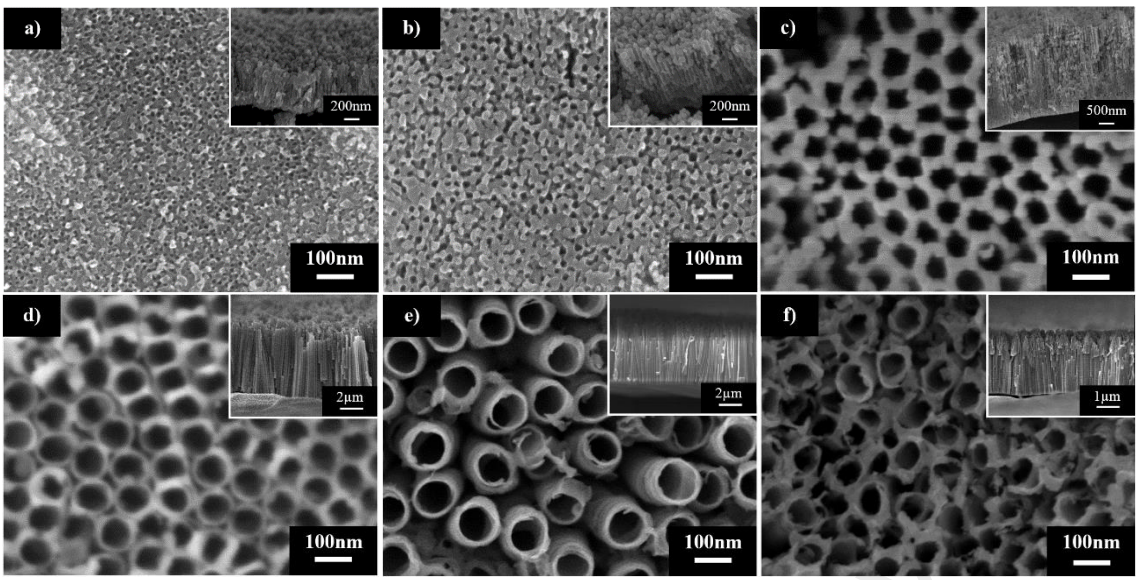

Figure 4.3: FESEM images of TiO_2 nanotubes obtained for different anodization voltage at: (a) 10 V; (b) 20 V; (c) 30 V; (d) 40 V; (e) 50V and (f) 60V. Insets are the side views of the samples

Table 4.3: Pore diameter, length, wall thickness, aspect ratio, and geometric surface area factor of TiO_2 nanotubes synthesized with varying anodization voltage in ethylene glycol containing 5 wt% H_2O_2 for 60 min

Anodization voltage (V)	Diameter (nm)	Length (μm)	Wall thickness (nm)	Aspect Ratio, AR	Geometric surface area factor, G (m^2g^{-1})
10	13±3.6	0.5±0.1	9±1.0	16.1	84.05
20	24±2.9	0.8±0.1	14±0.9	15.4	82.57
30	55±3.7	2.5±0.1	30±1.2	21.7	117.58
40	74±1.7	5.8±0.2	11±1.5	60.4	389.11
50	84±2.1	6.0±0.2	10±1.4	57.7	379.32
60	54±2.7	3.0±0.1	17±2.3	34.1	200.56

4.2.4 Effect of Fluoride Ion Content

Fluoride ion content is known to play a crucial role in the formation of anodic TiO_2 nanotubes array via electrochemical anodization. Therefore, in this part of experiment, different amount of NH_4F in ethylene glycol containing 5 wt% H_2O_2 was investigated. The content of NH_4F was varied from 0.1 to 0.5 wt%. All samples were anodized at optimizing processing parameters (60 min at 40 V) based on the results obtained from previous part of experiment. As shown in Figure 4.4(a), thin compact TiO_2 oxide layer

was formed on the surface of Ti foil with 0.1 wt% NH_4F added. This result inferred that insufficient F^- ionic species to trigger the chemical dissolution reaction for pits formation on the anodic oxide layer during this electrochemical anodization. Further increased in the amount of NH_4F up to 0.2 wt%, the FESEM micrograph showed irregular nanoporous structure layer formed on Ti foil. The irregular nanoporous structure layer was formed with an average diameter and length of 49 nm and 600 nm, respectively [Figure 4.4(b)]. It was caused by the incomplete chemical dissolutions at the interface between Ti and the electrolyte. For the 0.3 wt% NH_4F content, a hollow cylindrical oxide was successfully obtained with an average diameter of 78 nm and length 5.5 µm [Figure 4.4(c)]. This result indicated that the amount of F^- ions were sufficient to increase the chemical dissolution and led to further acidification to develop a nanotubular structure. When the content of NH_4F was further increased to 0.4 wt%, resultant anodic oxide layer showed destructive effect. The nanotubes became shorter (1.2 µm) with an average diameter of 73 nm [Figure 4.4(d)]. Continual increased of NH_4F content to 0.5 wt% generated smaller pits. Shorter nanotubular structure was also formed with an approximately 700 nm in length [Figure 4.4(e)]. The reduction in length might be attributed to the excessive chemical etching on the surface of the nanotubes during the chemical dissolution. As the pH of the electrolyte became more acidic with increasing NH_4F, etching on the surface of the nanotube structure also occurred (Ismail *et al.*, 2011).

Thus, the optimum fluoride ions content for the formation of well-aligned nanotubes was identified to be 0.3 wt% and was then further enhanced by 5 wt% of H_2O_2 and 60 min of anodization with the potential 40V. The average diameter, length, wall thickness, aspect ratio (AR), and geometric surface area factor (G) of the nanotubes anodized with varying fluoride ion content are summarized in Table 4.4.

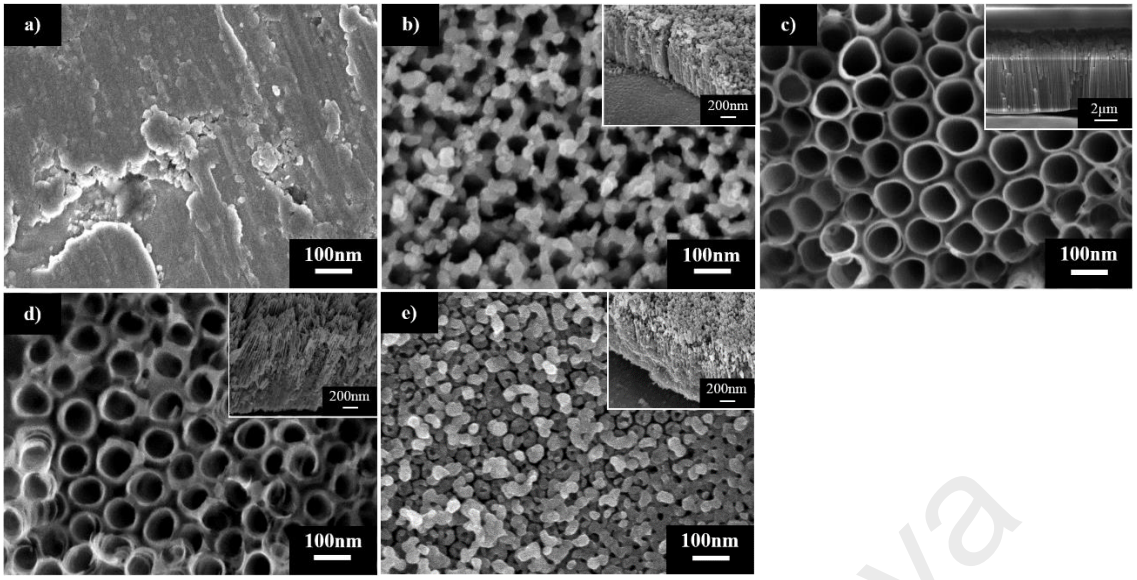

Figure 4.4: FESEM images of TiO_2 nanostructures obtained with varying fluoride ion content: (a) 0.1 wt%, (b) 0.2 wt%, (c) 0.3 wt%, (d) 0.4 wt% and (e) 0.5 wt%. Insets are the side views of the samples

Table 4.4: Pore's diameter, length, wall thickness, aspect ratio, and geometric surface area factor of TiO_2 nanotubes synthesized in electrolyte with 5 wt% H_2O_2 and varying fluoride ion content at 40 V for 60 min

Fluoride ion content (wt %)	Diameter (nm)	Length (μm)	Wall thickness (nm)	Aspect Ratio, AR	Geometric surface area factor, G (m^2g^{-1})
0.1	-	-	-	-	-
0.2	49±1.6	0.6±0.1	21±2.8	6.6	37.80
0.3	78±2.7	5.5±0.2	10±0.7	56.1	366.63
0.4	73±2.4	1.2±0.1	17±1.9	11.2	64.88
0.5	-	0.7±0.1	-	-	-

4.2.5 Phase Structure Analysis by XRD

XRD analysis was conducted to determine the compound and crystal phase transition of the un-annealed and annealed TiO_2 nanotubes sample prior to anodization in ethylene glycol containing 5 wt% H_2O_2, 0.3 wt% NH_4F for 60 min at 40 V. It is a well-known fact that the as-anodized TiO_2 nanotubes layer were amorphous in nature (Luttrell *et al.*, 2014). The heat treatment process has significant effects on the morphological of TiO_2 nanotubes. In the present study, heat treatment of 400 ˚C was selected due to the promotion of the crystallization of Ti anatase phase from the amorphous phase (Fernandes

et al., 2014). Figure 4.5 exhibits the XRD patterns of un-annealed and annealed TiO_2 nanotube arrays at 400 ˚C. It was found that the presence of both anatase phase and Ti metal within the TiO_2 nanotubes array film after annealing at 400 °C in air atmosphere. The presence of anatase phase was detected with its diffraction peaks allocated at 25.37°, 38.67º, 48.21º, 54.10º, 55.26º, 62.66º and 68.74º are corresponding to (101), (112), (200), (105), (211), (204) and (116) crystal planes respectively [JCPDS No 21-1272]. Besides, diffraction peaks of Ti substrate were observed on both XRD spectrum at 35.1°, 38.4°, 40.2° and 53.0°, which correspond to the crystal planes of (100), (002), (101) and (102), respectively. Surface tension was induced while drying after rinse as anodized sample where these tension further cause of the oxide layer to crack or separate apart. From the crack, Ti metal substrate was reviewed further contributed to the Ti diffraction peaks. Stable Ti metal was remained as Ti metal itself after underwent annealing without further react with oxygen to form TiO_2. Hence Ti peaks were observed in the annealed sample. Based on the literatures, 400 °C is sufficient to convert amorphous to anatase phase of TiO_2, which exhibited thermodynamically stable and higher surface stability for photoelectrochemical activity (Fernandes *et al.*, 2014; Sreekantan *et al.*, 2009). From the result, it shows success in producing high crystallinity of anatase phase of TiO_2 nanotubes array through electrochemical anodization and subjected to heat treatment stage at 400 °C.

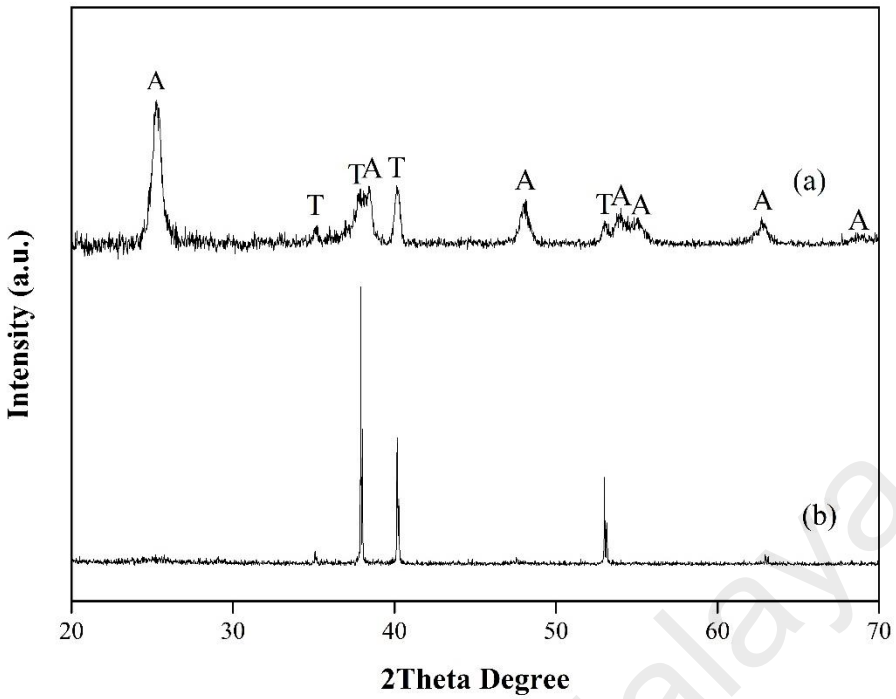

Figure 4.5: XRD pattern of (a) TiO_2 nanotubes annealed at 400˚C in air atmosphere and (b) un-annealed TiO_2 nanotubes sample formed in ethylene glycol with 0.3 wt% NH_4F and 5wt% H_2O_2 at 40 V for 60 min [T=Titanium; A=Anatase]

4.3 Incorporation of CdSe onto TiO_2 Nanotubes

Based on aforementioned discussion, highly ordered TiO_2 nanotubes was successfully synthesized via electrochemical anodization of Ti foil in ethylene glycol electrolyte composed of 0.3 wt% NH_4F and 5 wt% H_2O_2 at 40V for 60 min then subsequently annealed at 400 °C to form anatase phase of TiO_2 nanotubes film. Hence, in the following studies, highly ordered TiO_2 nanotubes film was synthesized in above-mentioned conditions to investigate the influence of CdSe on the TiO_2 nanotubes. The aim of this section is to improve the solar illumination absorption and further reduce the recombination loss of charge carriers.

By following the experimental procedure in Chapter 3, deposition of the CdSe took place in a bath solution containing of both Se^{2-} and Cd^{2+} precursor. When the ionic product (IP) of Cd^{2+} and Se^{2-} ions exceeds the solubility product (SP) of CdSe (i.e., IP ≥

SP (10-33)), CdSe deposition took place on the TiO_2 nanotubes substrate as stated in the following steps:

Sodium selenosulphate (Na_2SeSO_3) hydrolyzes in solution to give Se^{2-} ions,

$$Na_2SeSO_3 + OH^- \rightarrow Na_2SO_4 + HSe^- \quad \text{(Equation 4.7)}$$

$$HSe^- + OH^- \rightarrow H_2O + Se^{2-} \quad \text{(Equation 4.8)}$$

Ammonia solution was added in Cd salt solution to form the complex cadmium tetraammine ion $[Cd(NH_3)_4^{2+}]$:

$$Cd^{2+} + 4NH_3 \rightarrow Cd(NH_3)_4^{2+} \quad \text{(Equation 4.9)}$$

Then $Cd(NH_3)_4^{2+}$ reacts with hydrolyzed Se^{2-} ion to form CdSe:

$$Cd(NH_3)_4^{2+} + Se^{2-} \rightarrow CdSe + 4NH_3 \quad \text{(Equation 4.10)}$$

In the present study, CdSe-TiO_2 nanotubes were fabricated using CBD. This study aims to determine the optimum CBD parameters in order to achieve the desired CdSe-TiO_2 nanotubes for the highly efficient PEC water splitting performance. Three important parameters including molarity of electrolyte, reaction time and reaction temperature were studied and investigated in detail.

4.3.1 Effect of molarity of CdSe bath solution

Highly ordered TiO_2 nanotubes array film produced at optimum conditions as discussed in previous section were prepared for CBD studies. In this study, both Cd and Se precursor's molarity were varies from 1 to 15 mM with the soaking time of 1 h.

4.3.1.1 Morphological and Elemental Analysis by FESEM-EDX

The effect of precursor's molarity on the morphology of the highly-ordered TiO_2 nanotubes is discussed in this section. FESEM micrographs of TiO_2 nanotube surfaces after soaking at different precursor's molarity for 1 h were shown in Figure 4.6 and the EDX analysis was summarized in Table 4.5. As shown in the Figure 4.6 (a), sample bathed in 1 mM deposition molarity revealed similar appearance to the pure TiO_2 nanotubes due to the low concentration of Cd and Se species in the bath solution (Pawar *et al.*, 2013) (the ionic product of Cd^{2+} and Se^{2-} ions not exceeds the solubility product (SP) of CdSe). The EDX result of 1 mM deposition molarity shows the presence of 0.35 and 0.27 at% average Cd and Se content. Further increased in the precursor molarity to 3 mM, the average at% of Cd and Se in the sample increased to 0.68 and 0.56, respectively. From Figure 4.6 (b), irregular nanoclusters were formed on the pore entrance of nanotubes and increased the tube thickness to ~22.5nm. However, as the molarity of the precursor solution increased to 5 mm, it was noticed that the resultant TiO_2 nanotube arrays were extensively covered by aggregated CdSe nanocluster with approximately 1.19 at % of Cd content and 1.06 at% of Se content, respectively [Figure 4.6 (c)]. At the deposition molarity of 10 mM, some sphere structure with an average diameter of 170 nm was observed as seen in Figure 4.6(d). It was found that the nanotubes pores at the entrance were completely clogged with the CdSe sphere and negatively affected the self-organized nanotubes. A higher Cd and Se content (~2.41 and 2.24 at%) was also obtained from EDX analysis. This is indicating that the incorporation of Cd and Se species becomes prominent with the increasing of deposition molarity. At the highest deposition molarity of 15 mM, bigger sphere with the size approximately of 245 nm formed on or nearly to the pore entrance of the nanotubes [Figure 4.6 (e)]. The average Cd and Se at% content in this sample was further increased to approximately 4.14 and 3.86 at% respectively.

In the bath solution with the deposition molarity of Cd and Se precursors more than 5 mM, it contained higher ionic product (Cd and Se ions) than solubility product (CdSe solid phase). Therefore, it leads to rapid formation of ion-by-ion condensation of the Cd^{2+} and Se^{2-} or by adsorption of colloidal particles from the solution onto the TiO_2 nanotubes (Lokhande *et al.*, 2005; VanderHyde *et al.*, 2015). The average elemental compositions of the pure TiO_2 and CdSe loaded TiO_2 nanotubes with different deposition molarity based on the EDX spectra are summarized in Table 4.5.

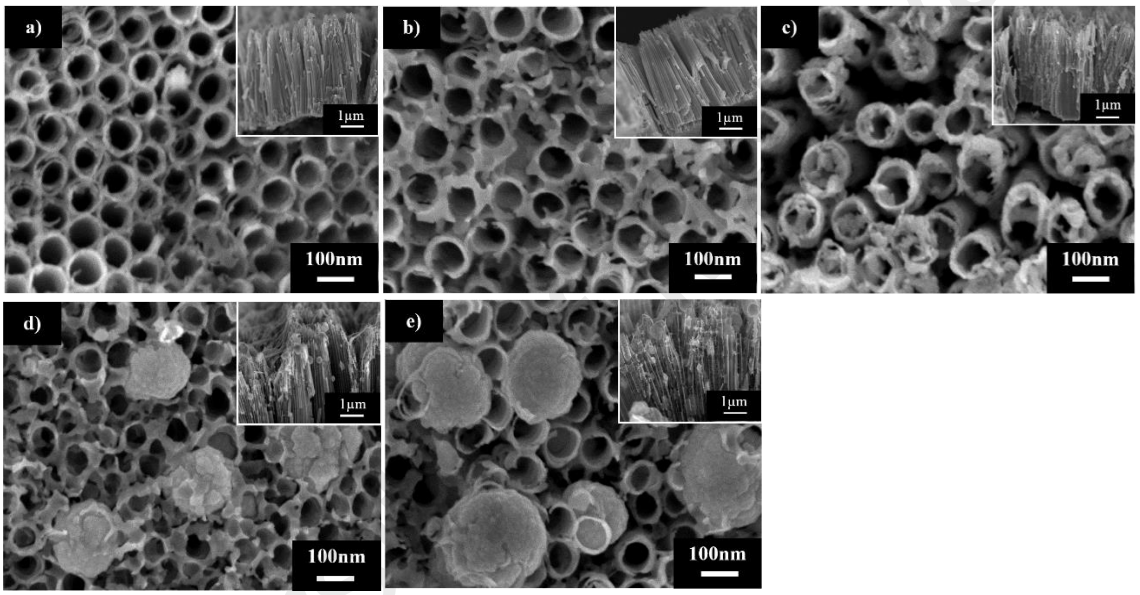

Figure 4.6: FESEM images of pure TiO_2 nanotubes soaked in (a) 1, (b) 3, (c) 5, (d) 10 and (e) 15 mM CdSe solution for 1 h. Insets are the side view of the samples

Table 4.5: Average at% of pure and CdSe loaded TiO_2 nanotubes produced at different molarities of CdSe solution obtained from EDX analysis

Molarity of CdSe (mM)	Atomic percentage (at%)			
	Ti	O	Cd	Se
0.0	38.46	61.54	-	-
1	38.22	61.15	0.35	0.27
3	38.93	59.82	0.69	0.56
5	39.97	57.78	1.19	1.06
10	40.04	55.31	2.41	2.24
15	35.79	56.20	4.14	3.86

4.3.1.2 Phase Structure Analysis by XRD

XRD analysis was used to determine the crystallographic structure and the changes in the phase structure of the CdSe loaded TiO_2 nanotubes soaked in different deposition molarities of Cd and Se content solution. Based on the study above, heat treatment of anodic pure TiO_2 nanotubes at 400 °C could transform the amorphous structure into the crystalline anatase phase. Therefore, in the current study, anatase TiO_2 phase was formed by annealing the anodized pure TiO_2 nanotubes at 400 °C in an air atmosphere. The XRD patterns of the pure TiO_2 and CdSe loaded TiO_2 nanotubes as a function of deposition molarity are shown in Figure 4.7. Obvious diffraction peaks from the XRD pattern attributed to the anatase phase. The diffraction peaks at 25.37°, 38.67°, 48.21°, 54.10°, 55.26°, 62.66° and 68.74° are corresponding to (101), (112), (200), (105), (211), (204) and (116) crystal planes of the anatase phase respectively [JCPDS No 21-1272]. Besides the peaks coming from anatase phase, there also diffraction peaks from Ti substrate at 35.1°,38.4°,40.2° and 53.0°, which correspond to the crystal planes of (100), (002), (101) and (102) respectively [JCPDS No 44-1294]. All the X-ray diffraction peaks are indexed to anatase phase TiO_2 and Ti metal itself indicating the incorporation of CdSe does not change the lattice structure of TiO_2 (Wang *et al.*, 2014). Moreover, small characteristic diffraction peak of cubic zinc blended phase CdSe at 49.7° appeared in the sample soaked in 10 and 15mM respective to crystal plane of (311) [JCPDS No 19-0191]. In addition, there was also an obvious increased of the diffraction peak at 25° was observed at the deposition molarity of 15 mM. This is due to overlapping of the peak of (111) plane (25.35°) of cubic phase CdSe and the peak of (101) planes of anatase TiO_2. No obvious CdSe phase was observed in the XRD patterns for the lower content CdSe (< 2 at% from EDX analysis). A possible explanation might be attributed to the insensitive of XRD analysis to detect very low content element within TiO_2 nanotubes (Leghari *et al.*, 2011; Wang *et al.*, 2014).

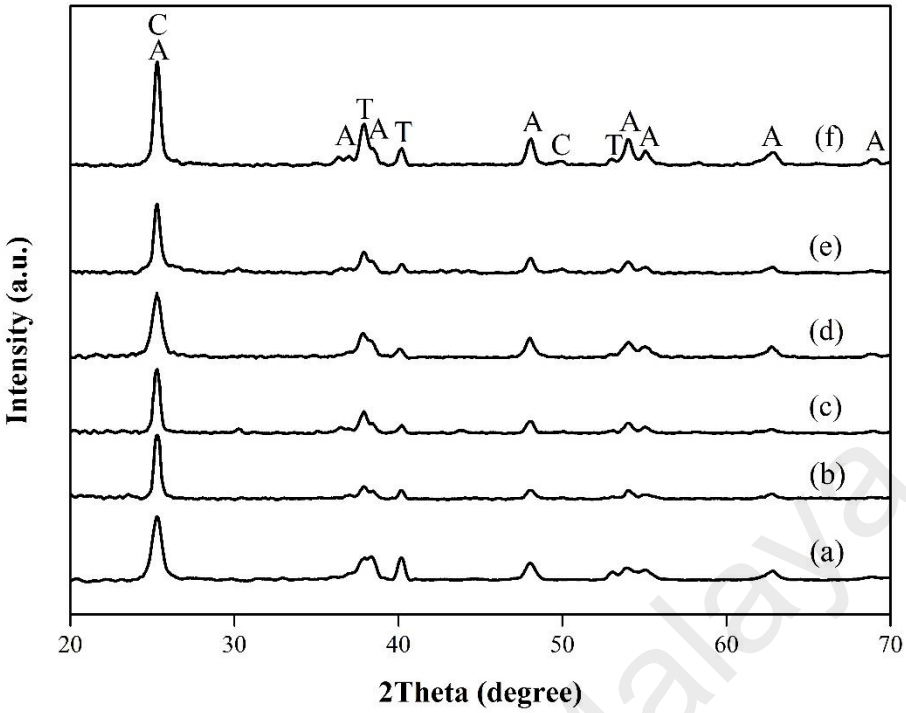

Figure 4.7: XRD diffraction patterns of (a) pure TiO_2 and CdSe loaded TiO_2 nanotubes soaked in b) 1, (c) 3, (d) 5, (e) 10, and (f) 15 mM of CdSe precursor solution for 1 h. [A = anatase, T = Ti metal, C = CdSe]

4.3.1.3 Chemical Structure Analysis by Raman Spectroscopy

Raman analysis was conducted to enhance the confirmation of the existent of cubic CdSe phase on hybrid CdSe-TiO_2 nanotubes shown in Figure 4.8. CdSe deposition molarities were fixed form 1 to 15 mM for 1 h. The resultant Raman spectra of each samples are presented in Figure 4.8. The major characteristic peaks at 144, 394, 515, 636 cm^{-1} were detected from the Raman spectrums are assigned as E_g, B_{1g}, A_{1g}, and E_g four modes. They corresponded well with the bonding vibration of anatase phase of TiO_2 and were also consistent with XRD results. In this case, E_g peak is mainly contributed by symmetric stretching vibration of O−Ti−O in TiO_2, the B_{1g} peak is caused by symmetric bending vibration of O−Ti−O, and the A_{1g} peak is caused by antisymmetric bending vibration of O−Ti−O (Bhirud *et al.*, 2015; Tian *et al.*, 2012). However, the intensity of the Raman peaks decreased with increased precursor solution molarities, which indicates increased in cubic CdSe content. As a matter of fact, an ambiguous peak at 206 cm^{-1}

which could be detected from the Raman spectra corresponded to the first order for CdSe longitudinal optical phonon (LO) (Todescato *et al.*, 2013). It becomes more obvious with the samples subjected to higher precursor solution molarity of 5, 10 and 15 mM.

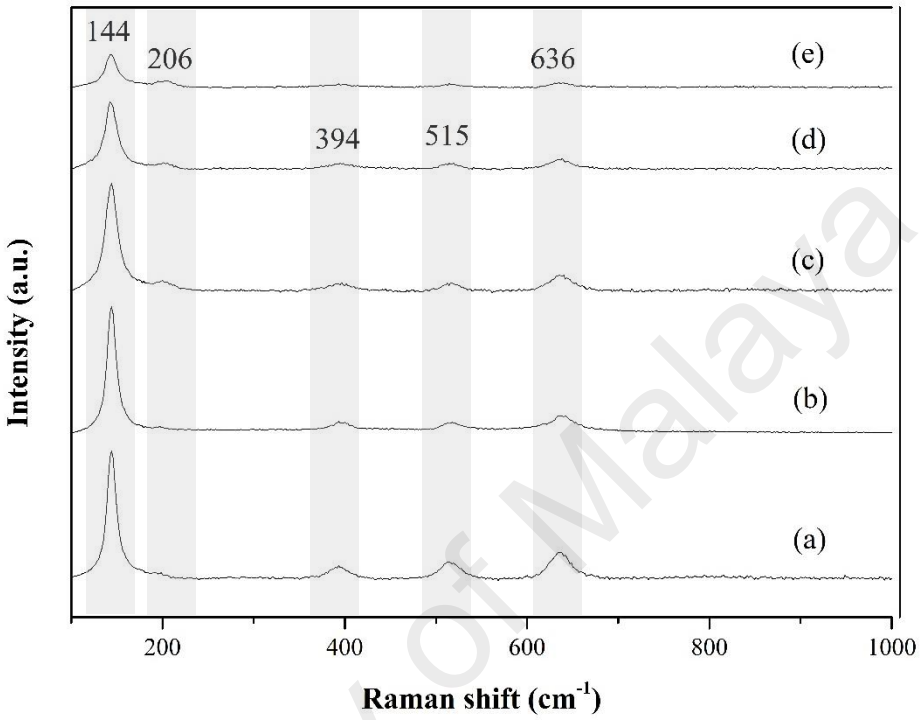

Figure 4.8: Raman spectrum of CdSe loaded TiO_2 nanotubes deposited in b) 1, (c) 3, (d) 5, (e) 10, and (f) 15 mM of CdSe precursor solution for 1 h

4.3.1.4 PEC water splitting performance evaluation

Linear sweep potential was used to measure photocurrent density, j_p under an applied potential. j_p-V characteristic curves for the CdSe-TiO_2 nanotubes synthesized in different CdSe deposition molarities are plotted in Figure 4.9. All samples exhibited insignificant j_p which was lower than 10 μA/cm^2 in dark condition. On the other hand, the j_p was increased under solar light illumination. A maximum j_p of 2.50 mA/cm^2 was obtained for TiO_2 nanotubes deposited with 5 mM CdSe precursor for 1 h. It was relatively higher as compared to the pure TiO_2 nanotubes itself with the j_p as 1.45 mA/cm^2. These results are in line with literature, which suggested that the presence of optimum CdSe species onto TiO_2 nanotubes could improve their character of large extinction coefficient in absorbing

the visible light from solar. In this case, more electrons could be injected into the conduction band of TiO_2. Thereby, those photo-induced electrons transported rapidly from the TiO_2 nanotube walls to the Ti substrate for high photocurrent generation. (Li *et al.*, 2014b). As the precursor solution molarity was increased up to 15 mM, the j_p relatively decreased, and reached a minimum j_p of 1.27 mA/cm^2. This decrease might be ascribed to the higher amount of CdSe species loaded on TiO_2 nanotubes, which acted as recombination centers and resulted in a low quantum yield. As presented in previous section, the excess CdSe species deposited on the nanotube wall surfaces clogged on the open pore of the nanotubes [as shown in Figure 5.6 (d & e)]. Thus, increased the surface barrier and eventually formed recombination centers for charge carriers. Therefore, fine-tuning the CdSe content within the TiO_2 nanotubes is important to develop an efficient visible light-driven photocatalyst.

Based on literature, size and distribution of doping have significant influence on the PEC performance. These aggregated CdSe spheres definitely decrease the surface area of TiO_2 nanotubes consequently reduce sample's photoresponse under light illumination (Su *et al.*, 2014). Large CdSe spheres also might serve as recombination centers of the photogenerated holes and electrons by preventing injection of electrons into the TiO_2 nanotubes network as effectively as smaller sized CdSe nanoparticles (Yang *et al.*, 2010a).

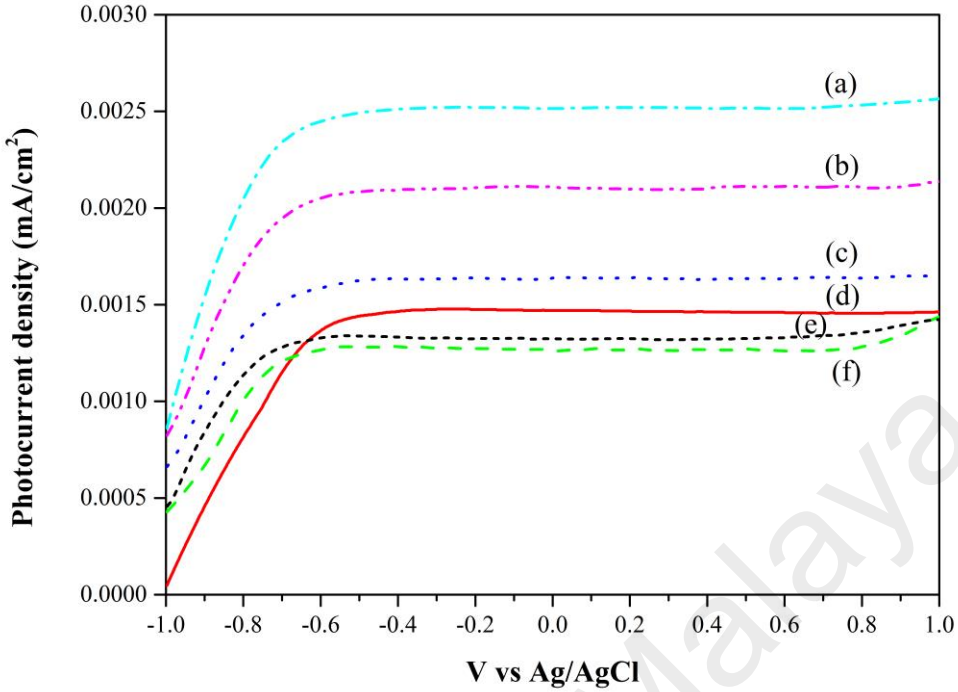

Figure 4.9: The j_p-V characteristic curves of CdSe-TiO_2 nanotubes soaked with different molarities of CdSe precursor: (a) 5 mM, (b) 3 mM, (c) 1 mM, (d) pure TiO_2 nanotubes, (e) 10 mM, and (f) 15 mM

4.3.2 Effect of soaking time in CdSe bath solution

In the present study, soaking duration for pure TiO_2 nanotubes film into CdSe bath solution is essential in determining the generation rate of the Cd complex and Se anions. In fact, CdSe bath solution could be obtained homogeneously by combining those Cd complex and Se anions into clusters. In this manner, those clusters might aggregate into desired nano-sized particle under an optimum duration. Therefore, optimization of the soaking duration during the chemical bath process for CdSe-TiO_2 nanotubes film is crucial in improving the PEC water splitting performance.

4.3.2.1 Morphological and Elemental Analysis by FESEM-EDX

FESEM micrograph in Figure 4.10 represents the effect of soaking duration from 30 min to 10 h on the annealed self-organized TiO_2 nanotubes. Figure 4.10 (a) shows that the morphology of the nanotubes soaked for 30 min is almost similar to that of pure TiO_2

nanotubes with clear opening without any aggregated CdSe nanoparticle on the surface of nanotubes. Generally, the formation of CdSe precipitate from a solution involves the steps of nucleation and particle growth. Both of the processes take place between the reactions of slowly released metal ions and chalcogen ions in aqueous solution. There is some minimum number of both ions required in order to produce a stable phase called as nucleus. Nucleus form in solution will either undergo decomposition reverse to ionic form or in contact of particles and combine to grow up to a certain size of precipitate (Lokhande *et al.*, 2005). This is called the concept of nucleation in solution. In the time of 30 min, it was insufficient for the nucleation process to form significant precipitate. As determined through EDX analysis, the average content of both Cd and Se for 30 min soaking duration are 0.46 and 0.39 at% respectively. At the soaking duration of 3 h [Figure 4.10 (b)], CdSe clusters formed and surrounds the pores entrance and thus results in the narrowing of nanotubes diameter to 50 nm. Besides, some CdSe spheres clogged on the pore entrance were observed and content of Cd and Se were approximately 2.85 and 2.69 at%. Further increased in soaking duration to 5 and 10 h, most of the nanotubes were covered by the precipitate and CdSe spheres were formed with the size of 230 nm and 300 nm respectively. The EDX result shows both the content of Cd and Se increase with the duration. At 5 h of soaking duration, average content of Cd and Se are 5.04 and 4.82 at% respectively. For 10 h soaking duration, the average elemental composition of Cd and Se are 8.89 and 8.25 at% respectively. These results indicate time dependent formation of CdSe precipitate on CdSe – TiO_2 nanotubes. The average elemental compositions of the pure TiO_2 and CdSe loaded TiO_2 nanotubes at different soaking time based on the EDX spectra are summarized in Table 4.6.

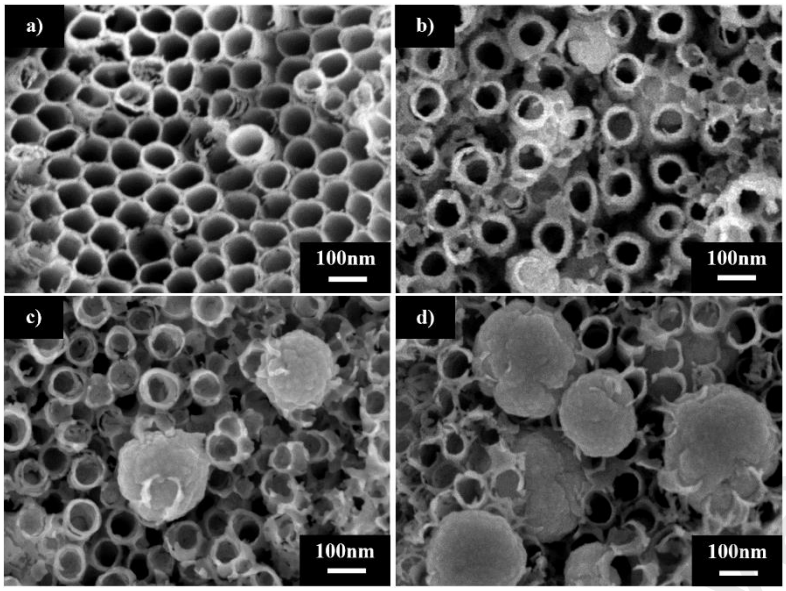

Figure 4.10: FESEM images of CdSe loaded TiO_2 nanotubes soaked for (a) 30 min, (b) 3, (c) 5, and (d) 10 h in 5 mM CdSe solution

Table 4.6: Average at% of CdSe loaded TiO_2 nanotubes soaked in 5mM CdSe solution at different soaking times obtained by EDX analysis

Soaking Time (h)	Atomic percentage (at%)			
	Ti	O	Cd	Se
0.5	37.92	61.23	0.46	0.39
3	37.98	56.48	2.85	2.69
5	34.18	55.96	5.04	4.82
10	32.79	50.07	8.89	8.25

4.3.2.2 Phase Structure Analysis by XRD

XRD measurements were conducted to determine the crystal plane of hybrid CdSe loaded TiO_2 nanotubes soaked for different durations in 5 mM Cd and Se precursor solution. The XRD spectra were shown in Figure 4.11. It shows similar result as our previous studies. Intense peaks from the XRD pattern at 25.37°, 38.67°, 48.21°, 54.10°, 55.26°, 62.66° and 68.74° are corresponding to (101), (112), (200), (105), (211), (204) and (116) crystal planes of anatase phase of TiO_2 [JCPDS No 21-1272]. Ti substrate found with the diffraction peaks at 35.1°,38.4°,40.2° and 53.0°, which correspond to the crystal planes of (100), (002), (101) and (102) respectively [JCPDS No 44-1294]. Highest peak is contributed by overlapping the peak of anatase crystal plane (101) and (111) plane of

cubic CdSe [JCPDS No 19-0191]. Increasing in the peak intensity was observed with increased of soaking duration from 3 h to 10 h at 25° indicating increased in crystallinity at the crystal plane (111) of cubic CdSe. Besides, a small weak characteristic diffraction peak of (311) planes of cubic zinc blended phase CdSe at 49.7° also appeared in the sample for 3, 5 and 10 h of soaking duration. The peak intensity was more obvious with the soaking duration, and indicates the abundancy of the CdSe crystal plane equivalent as the EDX analysis. From the XRD pattern, the sample soaked for 30 min shows no obvious cubic zinc-blended CdSe peaks due to lower content of CdSe (< 2 at% from EDX analysis). This is due to little amount of CdSe which gives insufficient response to detect by XRD analysis (Leghari *et al.*, 2011).

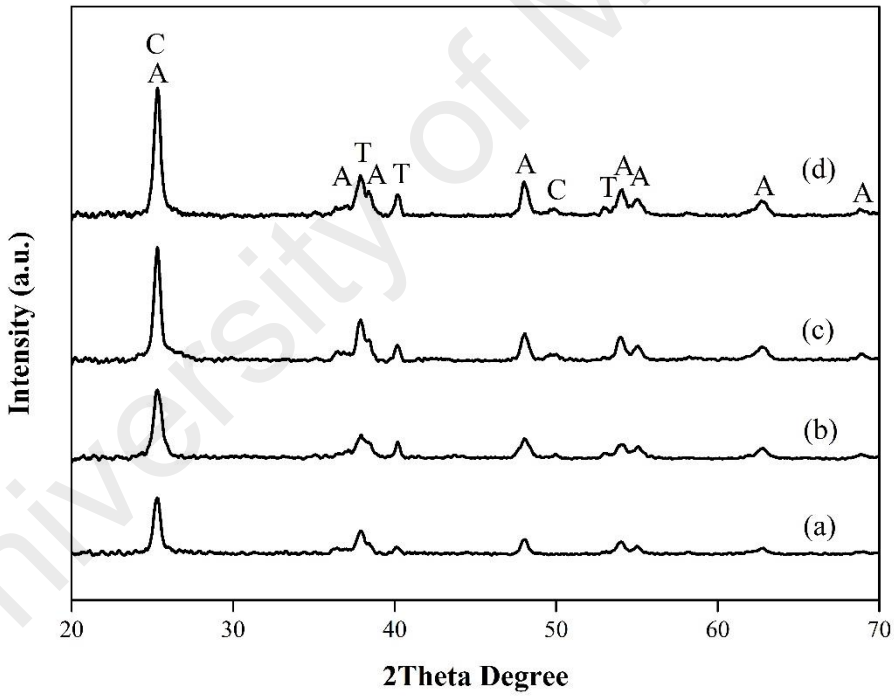

Figure 4.11: XRD diffraction patterns of CdSe loaded TiO2 nanotubes soaked for (a) 30 min, (b) 3, (c) 5 and (d) 10 h in 5 mM CdSe solution [A = anatase, T = Ti metal, C = CdSe]

4.3.2.3 Chemical Structure Analysis by Raman Spectroscopy

Raman measurements were conducted to validate the crystal structure of the samples synthesized with different deposition durations. The Raman results are shown in Figure 4.12. Four bands at 144, 394, 515 and 636 cm^{-1} were attributed to the E_g, B_{1g}, A_{1g}, and E_g vibration modes of anatase phase TiO_2 respectively (Bhirud *et al.*, 2015; Tian *et al.*, 2012). A gradual decreased in the intensity of the four anatase bands was observed with increased deposition duration. It was due to the increase of the CdSe content as shown in EDX analysis (Table 6) as solid phase precipitate covered on the surface of TiO_2 nanotubes substrate. Hence, this gradually reduces the signal received in the Raman analysis. Furthermore, a Raman band at 206 cm^{-1} corresponds to the first order cubic CdSe longitudinal optical phonon (LO) was observed at the raman spectra of the deposition duration 3, 5 and 10 h. This further confirmed the presence of cubic CdSe phase in XRD measurement with the trend shown by EDX elemental analysis discussed above.

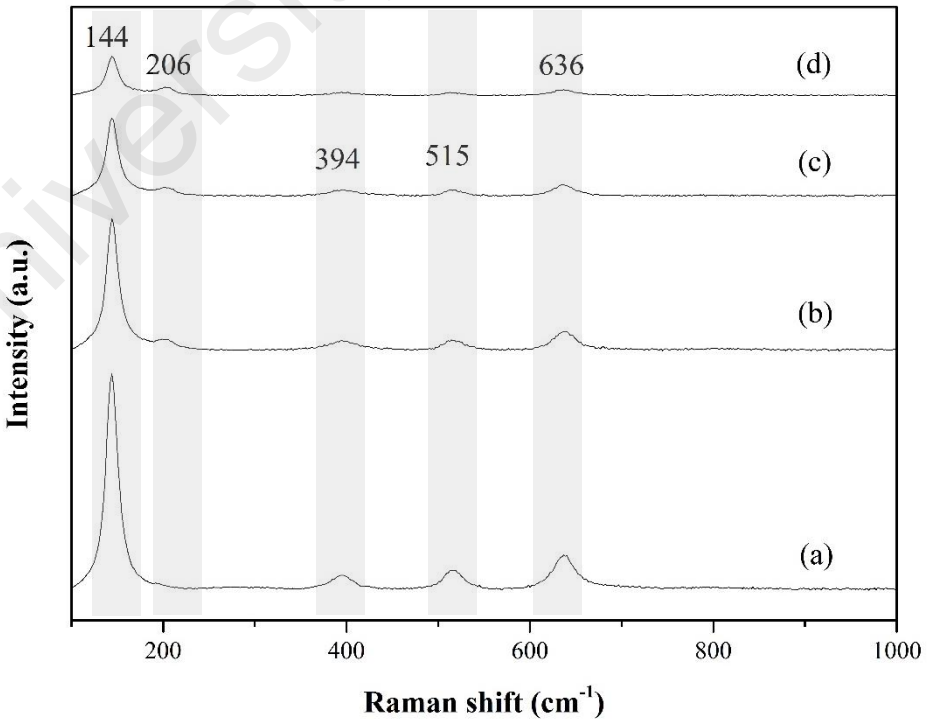

Figure 4.12: Raman spectrum of CdSe loaded TiO_2 nanotubes soaked for (a) 30 min, (b) 3, (c) 5, and (d) 10 h in 5 mM CdSe solution

4.3.2.4 PEC water splitting performance evaluation

A j_p-V characteristic plot for the different deposition durations of the CdSe-TiO_2 nanotubes in 5 mM CdSe precursor is shown in Figure 4.13. All samples showed approximately 0 mA in dark condition whereas photocurrent responses were observed with solar illumination for the whole set of samples. A maximum j_p of 1.58 mA/cm^2 was observed in the CdSe-TiO_2 nanotubes subjected to 30 min soaking time in precursor solution, which was slightly higher compared with that of the pure TiO_2 nanotubes (1.45 mA/cm^2). The CdSe-TiO_2 nanotubes subjected to 3, 5, and 10 h soaking times exhibited decreased j_p of approximately 1.22, 0.79 and 0.35 mA/cm^2, respectively. These results clearly demonstrate the significant effects of different soaking duration on the TiO_2 nanotubes towards to the PEC performances. The observed changes in the surface morphology and structure of Cdse-TiO_2 nanostructure led to essential variations in the electrochemically active surface area. At the soaking durations 3, 5 and 10 h, over accumulation of CdSe cluster by forming spherical structure cause deceased in the electrochemical active surface area, and further hindered transferring of photo-induced charge carriers (Su *et al.*, 2014; Yang *et al.*, 2010a).

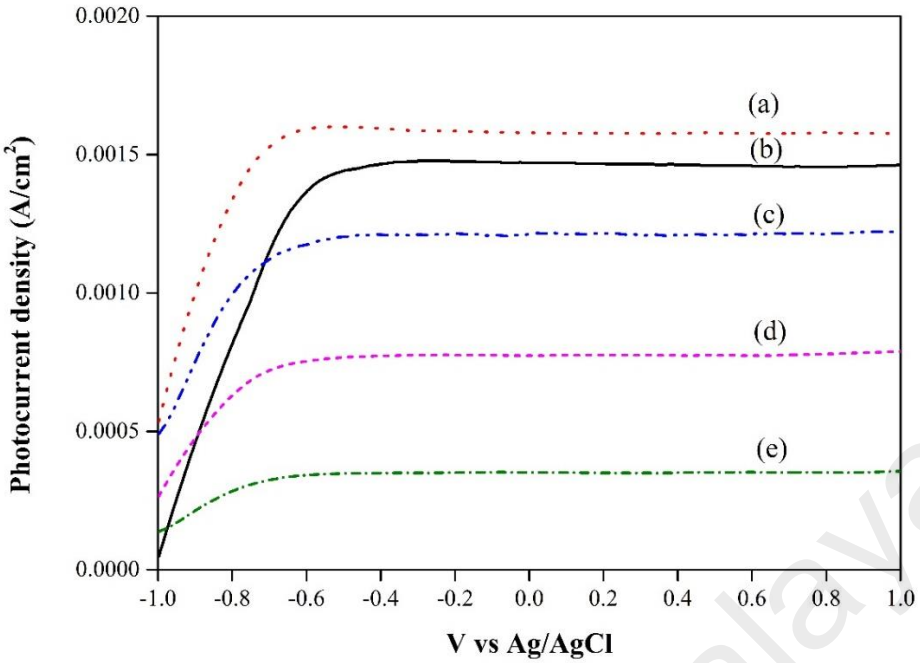

Figure 4.13: The j_P-V characteristic curves of CdSe-TiO_2 nanotubes soaked at different duration of CdSe precursor: (a) 30 min, (b) pure TiO_2 nanotubes, (c) 3 h, (d) 5 h and (e) 10 h

4.3.3 Effect of deposition temperature

Deposition temperature plays an important role in manipulating the thermal dislocation of the Cd complex and Se anion by control the rate of release of selenium ions from sodium selenosulphate leads to growth of cluster. Hence, CBD of CdSe onto TiO_2 nanotubes substrate was performed in bath solution with 5 mM of Cd and Se precursor for 1 hour.

4.3.3.1 Morphological and Elemental Analysis by FESEM-EDX

FESEM was employed to investigate the surface morphology of high aspect ratio annealed TiO_2 nanotubes deposited at different deposition temperature for 1 h in 5mM of CdSe precursor solution. EDX was also used to determinet the content of each element in atomic percentage. Figure 4.14 (a) shows the FESEM image of the sample deposited at 20 °C. It gives a similar morphology with un-doped sample [Figure 4.1 (e)]. However, as

the deposition temperature increased to 40 °C, significant precipitate coagulated at the wall of the nanotubes was observed and also some CdSe sphere clogged the pore entrance [Figure 4.14(b)]. Additional negative effects was observed at the nanotubular structure when the deposition temperature was further increased to 50 °C and 60 °C shown in Figure 4.14 (c) and (d). Bigger CdSe precipitate clogged the pore entrance with the average diameter of 145nm and 220nm at the bath of 50 °C and 60 °C respectively. The content of CdSe in the sample increases with the deposition temperature (Table 4.7). The larger CdSe precipitates were obtained with increased temperature of the chemical bath and were due to the phenomenon of coalescencence. Hence, the higher bath temperature results to bigger particles (Deshpande *et al.*, 2013; Hatam & Ghobadi, 2016). The average elemental compositions of the pure TiO_2 and CdSe loaded TiO_2 nanotubes at different deposition temperature based on the EDX spectra are summarized in Table 4.7.

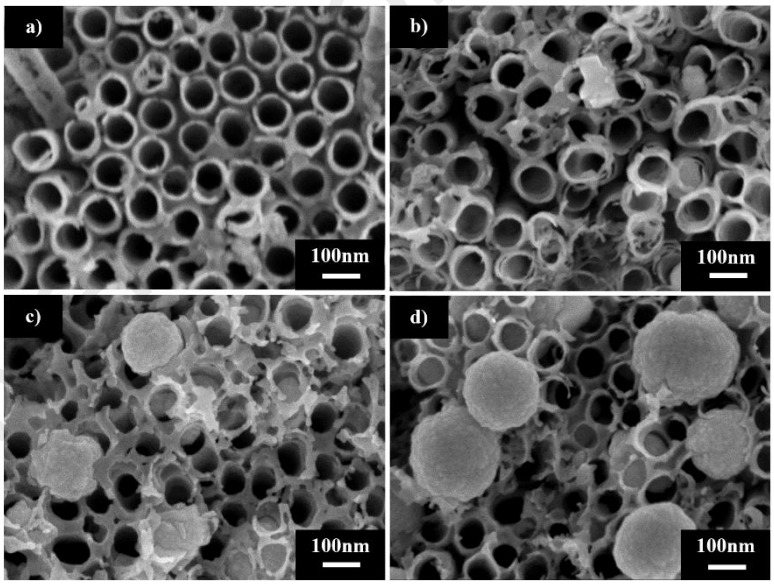

Figure 4.14: FESEM images of pure TiO_2 nanotubes soaked at temperature (a) 20 °C, (b) 40 °C, (c) 50 °C, and (d) 60 °C in 5 mM CdSe solution

Table 4.7: Average at% of CdSe loaded TiO_2 nanotubes soaked in 5mM CdSe solution at different temperature obtained by EDX analysis

Temperature (°C)	Atomic percentage (at%)			
	Ti	O	Cd	Se
20	40.77	58.45	0.41	0.37
40	39.62	56.66	1.90	1.82
50	38.16	55.84	3.03	2.97
60	36.27	51.83	6.04	5.86

4.3.3.2 Phase Structure Analysis by XRD

The crystal structure phases of hybrid CdSe loaded TiO_2 nanotubes at different deposition temperatures have been identified using XRD measurement. Literature review shows that CdSe can be either hexagonal (wurzite) [JCPDS No 8-459], cubic (zinc-blende) [JCPDS No 19-0191] or sometimes mixture of both structure (Deshpande *et al.*, 2013; Zhao *et al.*, 2013). The CdSe precipitate deposited on TiO_2 nanotubes were in the pure cubic phase with the zinc-blended type of structure according to the XRD analysis shown in Figure 4.15. The highest intensity reflection peak was observed and composed of two crystal planes which are (111) from cubic CdSe and (101) from anatase TiO_2. Both of the peaks appearing at $2\theta = 25.37°$ and 25.35° respectively according to the standard data of JCPDS. Besides, there was a small diffraction peaks of CdSe can be vaguely observed at 49.7° respect to the crystal plane (311). But beyond that, other peaks at 38.67°, 48.21°, 54.10°, 55.26°, 62.66° and 68.74° are corresponding to (112), (200), (105), (211), (204) and (116) crystal planes of anatase phase of TiO_2 [JCPDS No 21-1272]. Ti substrate found with the diffraction peaks at 35.1°,38.4°,40.2° and 53.0°, which correspond to the crystal planes of (100), (002), (101) and (102) respectively [JCPDS No 44-1294].

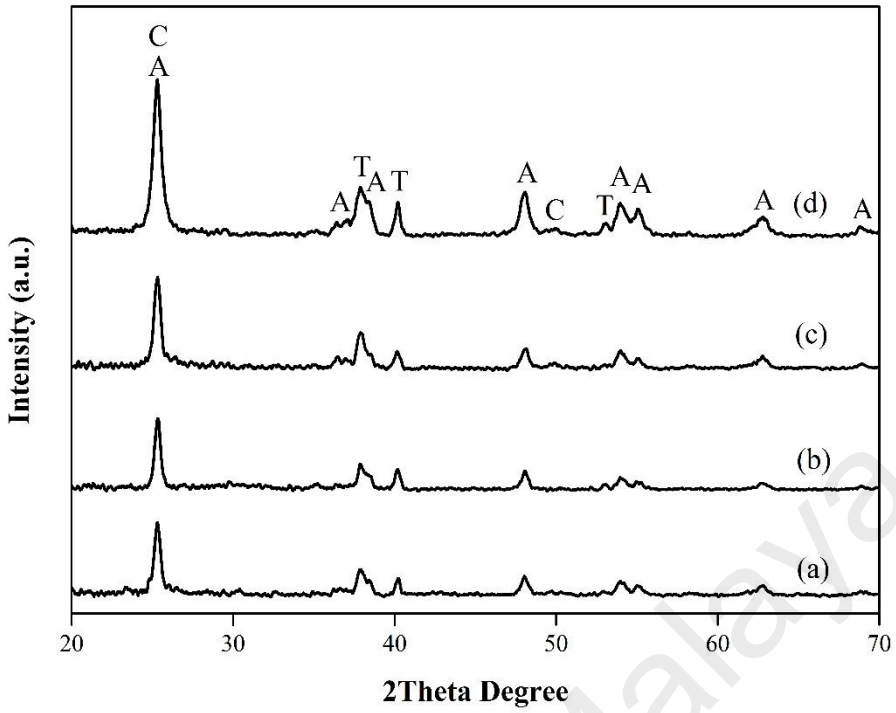

Figure 4.15: XRD diffraction patterns of CdSe loaded TiO_2 nanotubes soaked at temperature (a) 20 °C, (b) 40 °C, (c) 50 °C, and (d) 60 °C in 5 mM CdSe bath solution for 1 h. [A = anatase, T = Ti metal, C = CdSe]

4.3.3.3 Chemical Structure Analysis by Raman Spectroscopy

The Raman spectra in Figure 4.16 represent CdSe-TiO_2 nanotubes deposited from the temperature of 20 °C to 60 °C. A total of five Raman bands were observed. Characteristic bands of anatase phase of TiO_2 assigned as E_g, B_{1g}, A_{1g}, and E_g are the four modes corresponding to the bands at 144, 394, 515 and 636 cm^{-1} respectively. Characteristic band of Cubic CdSe [first order cubic CdSe longitudinal optical phonon (LO)] was found at 206 cm^{-1} in the Raman spectrum with the samples undergo deposition at 40 °C or above. Sign of gradually increase in the band intensity at 206 cm^{-1} with the increase of deposition temperature can be explain by more cubic CdSe precipitate formed quantitatively. It was equivalent with the results shown in XRD and EDX analysis discussed above.

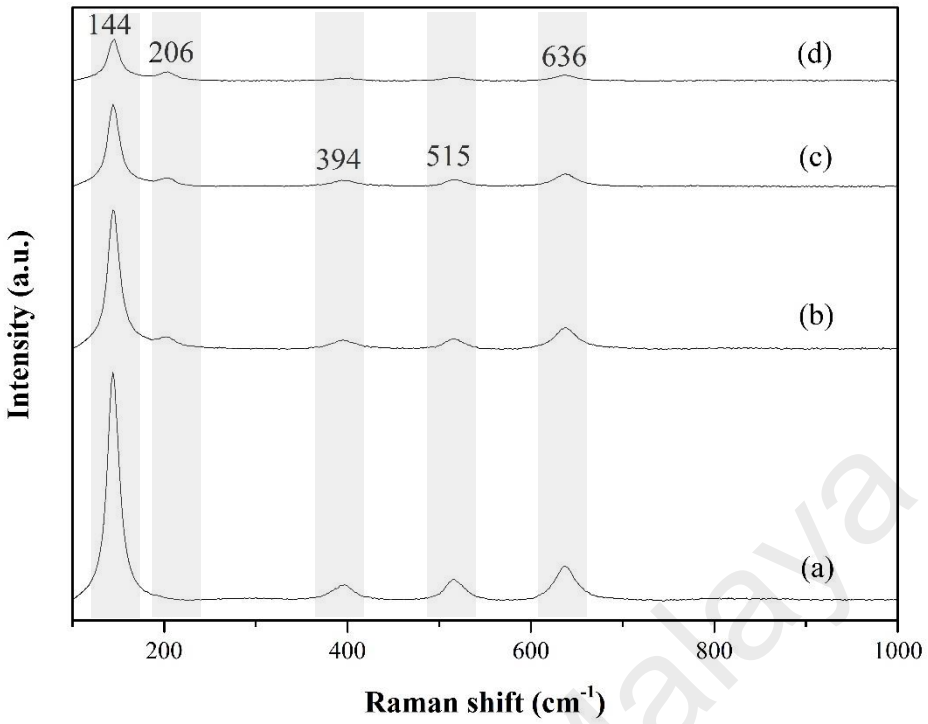

Figure 4.16: Raman spectrum of CdSe loaded TiO_2 nanotubes soaked at temperature (a) 20 °C, (b) 40 °C, (c) 50 °C, and (d) 60 °C in 5 mM CdSe solution for 1 h

4.3.3.4 PEC water splitting performance evaluation

In this part of the experiment, CdSe-TiO_2 nanotubes synthesized in 5 mM CdSe precursor solution at different deposit temperature for 1h were used as photoelectrode in three electrode PEC water splitting evaluation. The corresponding experimental results were presented in Figure 4.17. A maximum j_p of 1.63 mA/cm^2 was observed in the CdSe-TiO_2 nanotubes subjected to 20 °C soaking temperature in CdSe solution, which was relatively higher compared with that of the pure TiO_2 nanotubes (1.45 mA/cm^2). The CdSe-TiO_2 nanotubes which were subjected to 40 °C, 50 °C, and 60 °C soaking condition exhibited decreasing in j_p by approximately 1.13, 0.8, and 0.52 mA/cm^2, respectively. This was due to the extra thermal energy supplied to the system at higher temperature, CdSe nucleus tend to coalesce together and growth into large spherical CdSe particle (150 – 220 nm) clogged at the wall and pores of nanotubes to reduce the high surface energy

(Kale & Lokhande, 2005). The FESEM figure above shows the remarkable change in surface morphology.

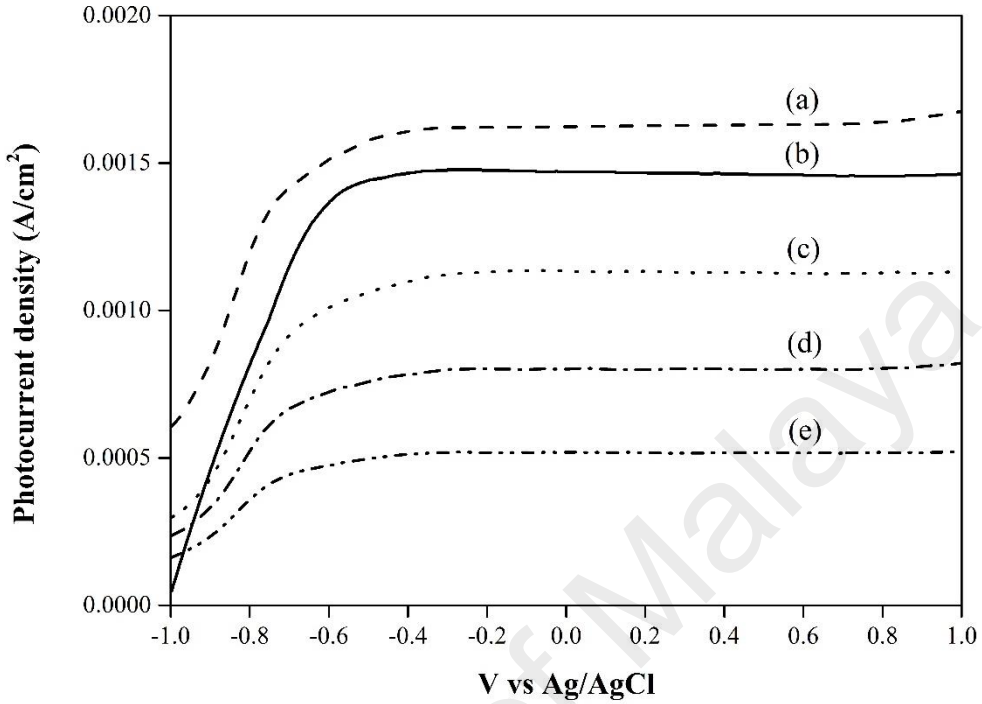

Figure 4.17: The j_P-V characteristic curves of CdSe-TiO_2 nanotubes soaked at different temperature of CdSe precursor: a) 20 °C, (b) pure TiO_2 nanotubes, (c) 40 °C, (d) 50 °C and (e) 60 °C

4.4 Chemical State Analysis by XPS

The Quantitative analysis of the electronic structures and chemical properties of different elements in samples were analyzed by XPS analysis. The best sample based on performance of photocurrent density of CdSe-loaded TiO_2 nanotubes and pure annealed TiO_2 nanotubes was selected for the XPS analysis. The survey spectrum (Figure 4.18) indicates the presence of C, Ti, O, Cd, and Se peaks within the best PEC performance CdSe-TiO_2 sample. This also indicates that the CdSe was successfully loaded onto the nanotubes. The XPS results also further confirmed the EDX elemental identification analysis. Figure 4.19 to 4.23 shows the narrow scan for each element.

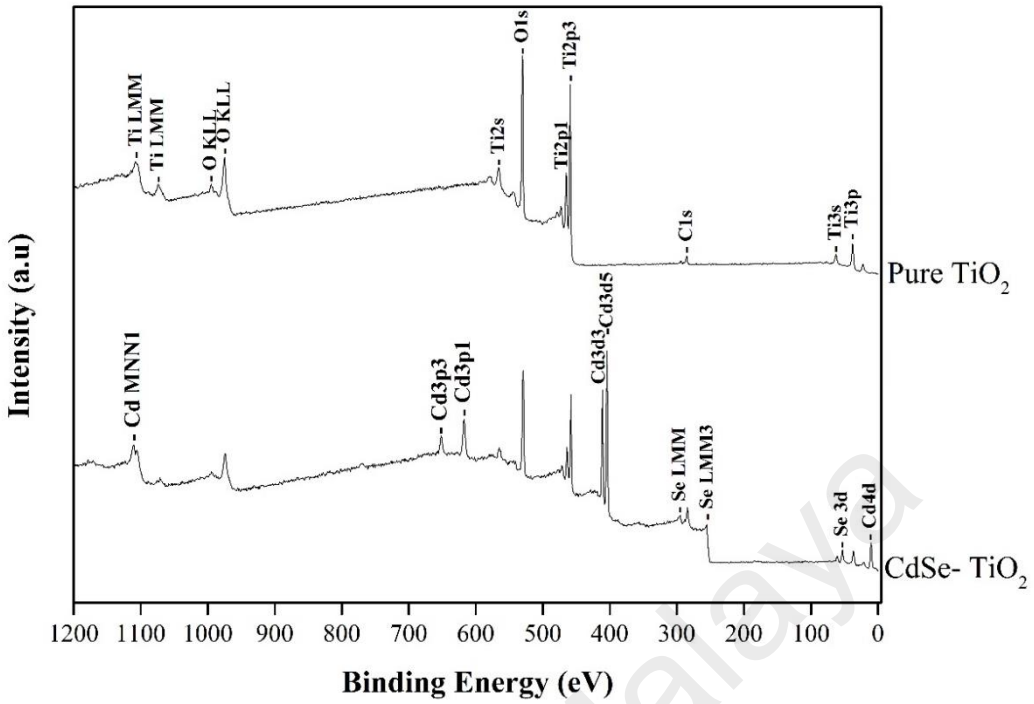

Figure 4.18: XPS survey spectra of CdSe–TiO_2 nanotube and undoped pure TiO_2 nanotubes

As shown in Figure 4.19, Ti 2p XPS spectrum of both samples shows the same two distinct peaks located at the binding energy (BE) of 458.5 and 464.5 eV. Both of the two peaks were associated with the energy of Ti $2p_{3/2}$ and Ti $2p_{1/2}$, respectively. It was in good agreement with Ti in the form of Ti^{4+} oxidation state (Asahi & Morikawa, 2007). It also proved that the loading of CdSe was less likely to affect the Ti chemical state of the modified TiO_2 nanotube arrays.

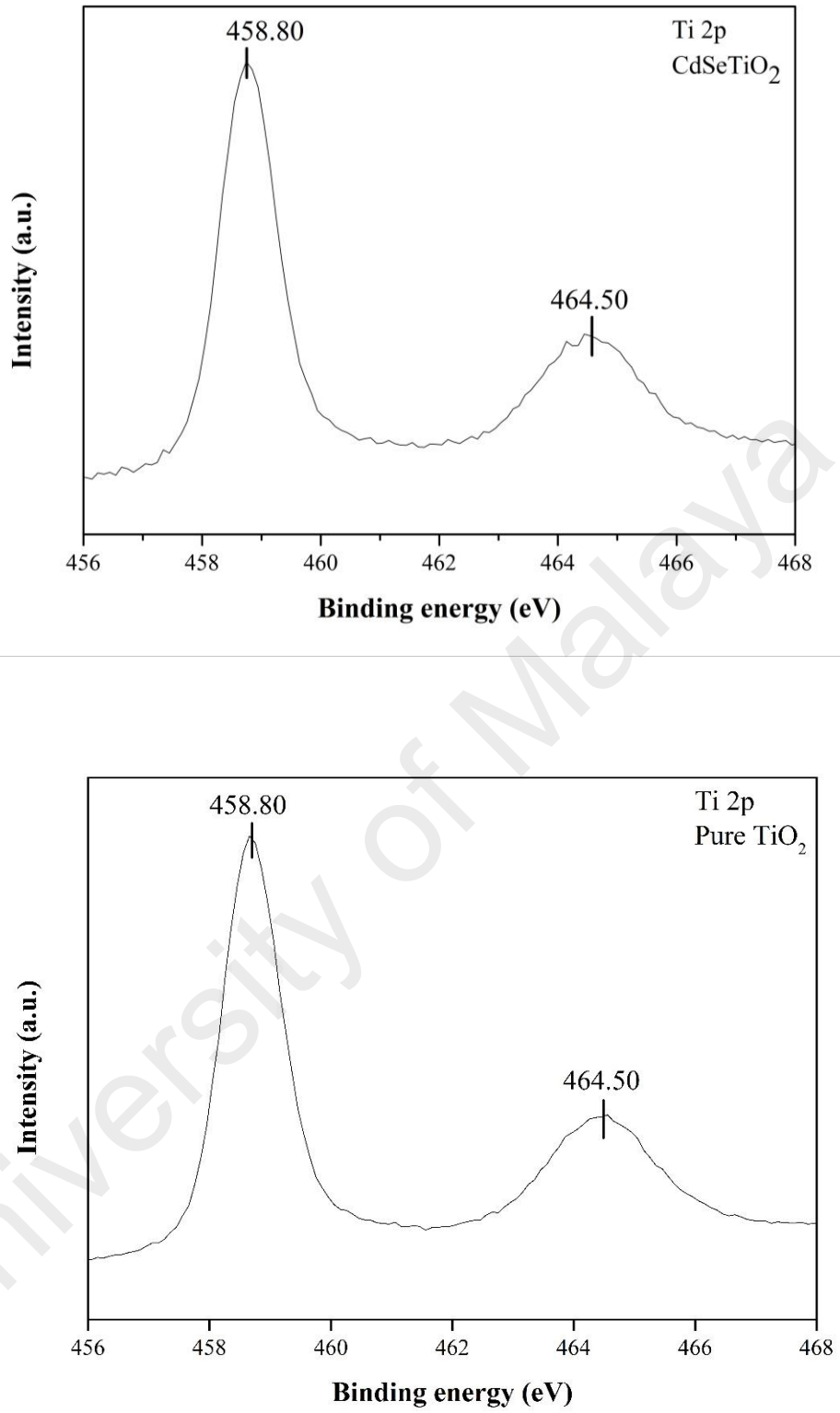

Figure 4.19: XPS spectra of Ti 2p

Furthermore, the O 1s XPS spectrum of modified CdSe-TiO_2 nanotubes and pure TiO_2 nanotube arrays was illustrated in Figure 4.20. From the figure, peak with the binding energy of 529.90 eV and 530.10 eV corresponding to the O 1s core levels of O^{2-} of TiO_2 crystal structure. Another form of oxygen that absorbed on the surface of TiO_2 surface (-OH) gives the small peak with the binding energy 530.97 eV and 531.68 eV. A positive shift of 0.2 eV and 0.71 eV compared to that at 529.90 eV and 530.97 eV of the pure TiO_2 nanotubes after loading CdSe nanoparticles. Such a positive shift of the O1s binding energy of in the hybrid CdSe-TiO_2 nanotubes confirmed the formation of a strong combination force between Cd from CdSe and the TiO_2 on the surface of TiO_2 nanotube arrays. This strong interaction could be served as the heterojunctions for accelerating electron transfer from CdSe (Wang *et al.*, 2016).

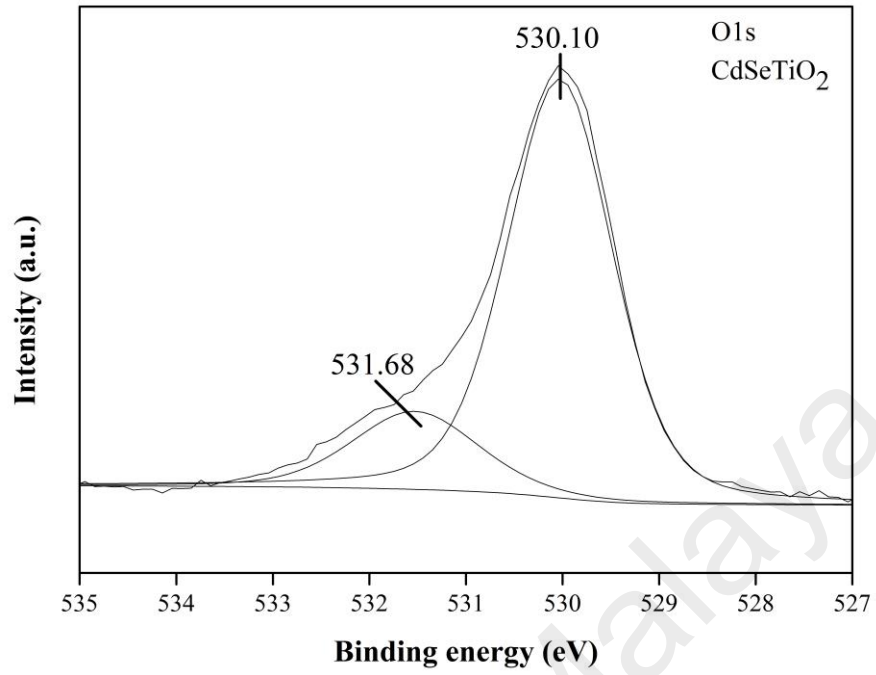

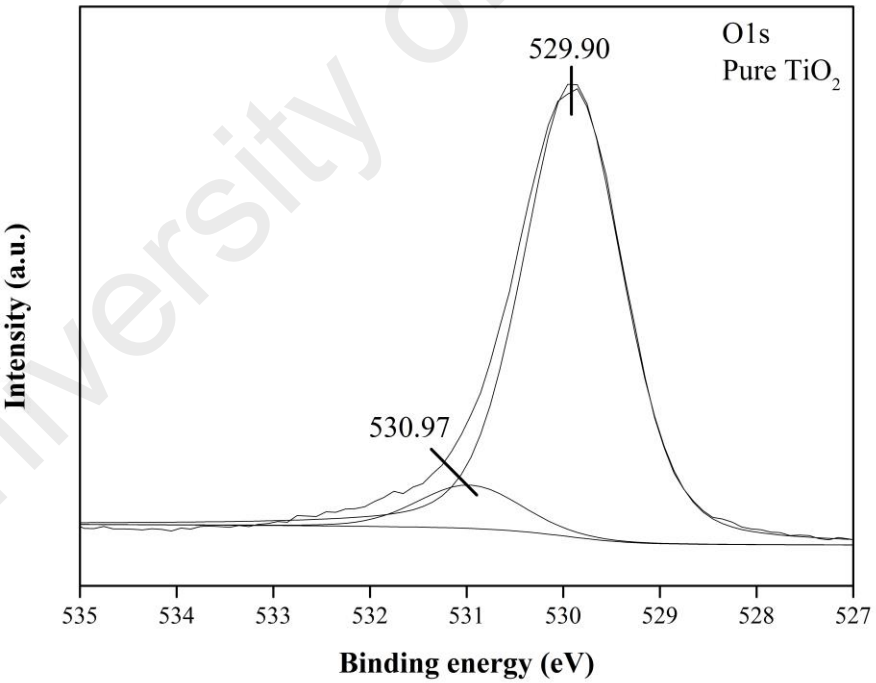

Figure 4.20: XPS spectra of O 1s

In Figure 4.21, one of the C1s peaks located at 284.8 eV was the pollution peak of organic carbon which may be due to the residual carbon from the precursor solution and adventitious hydrocarbon from the XPS instrument itself (Seah, 2001). The peaks at 286.0–289.3 eV indicate that a small amount of carbonate species was present on the surface. It was ascribed to the Ti–C–O bonds of the carbonate species originating from the residual C of the organic ethylene glycol electrolyte and the C atom was diffused into the TiO_2 crystal structure during the annealing process or pyrogenation of EG. Thus, heat treatment plays an important role to form Ti–C–O bonds (Lai & Sreekantan, 2012).

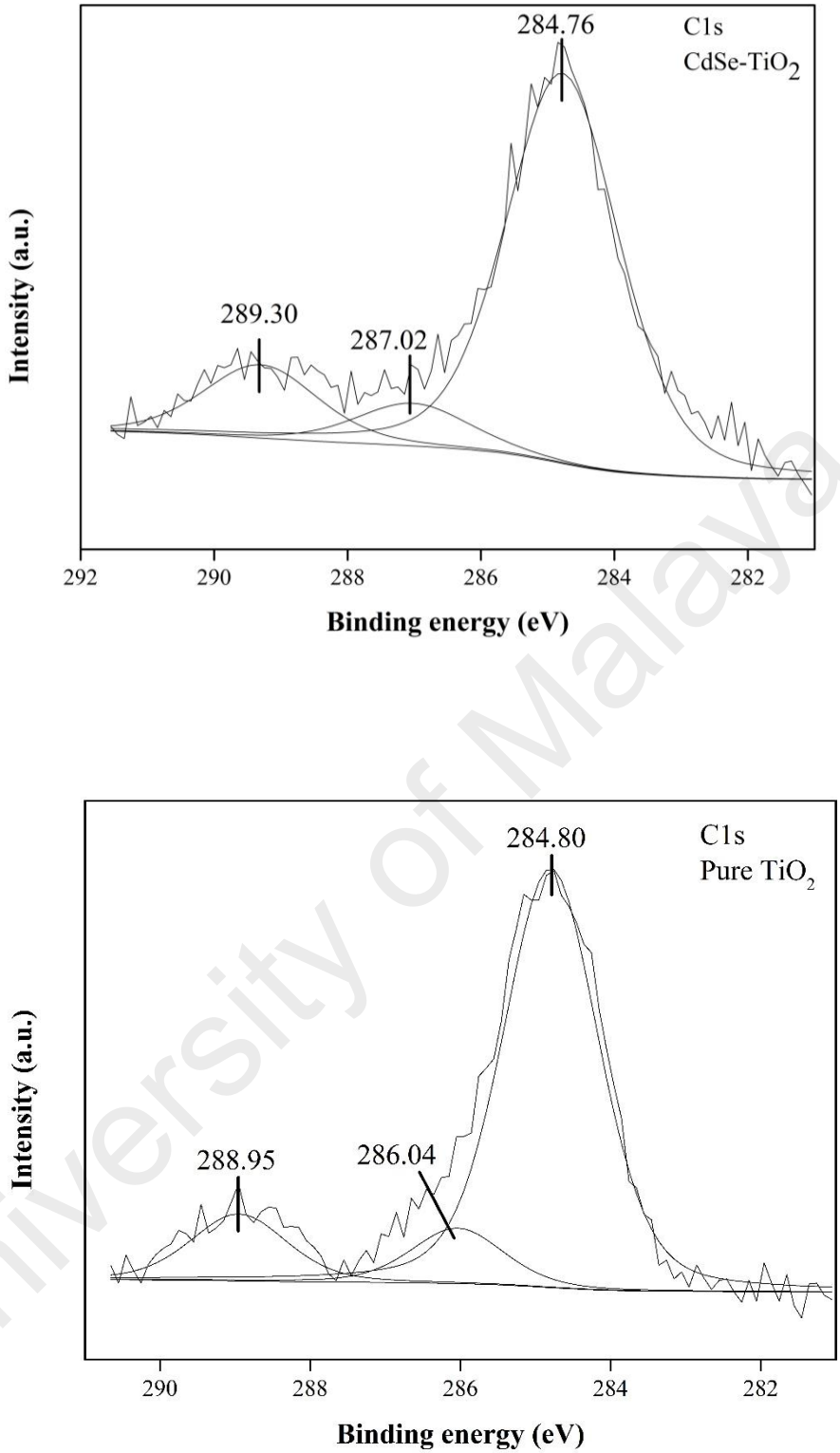

Figure 4.21: XPS spectra of C1s

Two strong characteristic peaks feature of Cd 3d XPS spectra were illustrated in Figure 4.22. Precise analysis on the features of the Cd $3d_{5/2}$ and Cd $3d_{3/2}$ double peaks splits by the spin-orbital coupling was decomposed via Voigt curve fitting function within the Shirley background. The decomposition resulted into a perfect fit of four peaks where two belongs to Cd $3d_{5/2}$ located at 405.13 and 404.59 eV whereas another two corresponds to Cd $3d_{3/2}$ with the binding energy of 411.98 and 411.40 eV. The two peaks were located at the binding energy of 405.13 and 411.98 eV and corresponded to the Cd $3d_{5/2}$ and Cd $3d_{3/2}$ core levels of Cd^{2+}cations of CdSe crystal structure, respectively (Pawar *et al.*, 2013). Additional peaks observed within 405.13 and 411.98 eV with less intensity shows weak shifting in peak positions. Oxidation of Cd in CdSe indicates CdO formation and was reported with a weak shift of Cd $3d_{5/2}$ and Cd $3d_{3/2}$ core levels (Masson *et al.*, 1997; Vargas‐Hernández *et al.*, 2005). Hence, the lower intensity of the peaks at the bonding energy of 404.59 and 411.40 eV verified the existence of a very small amount of CdO in the sample fabricated via CBD technique.

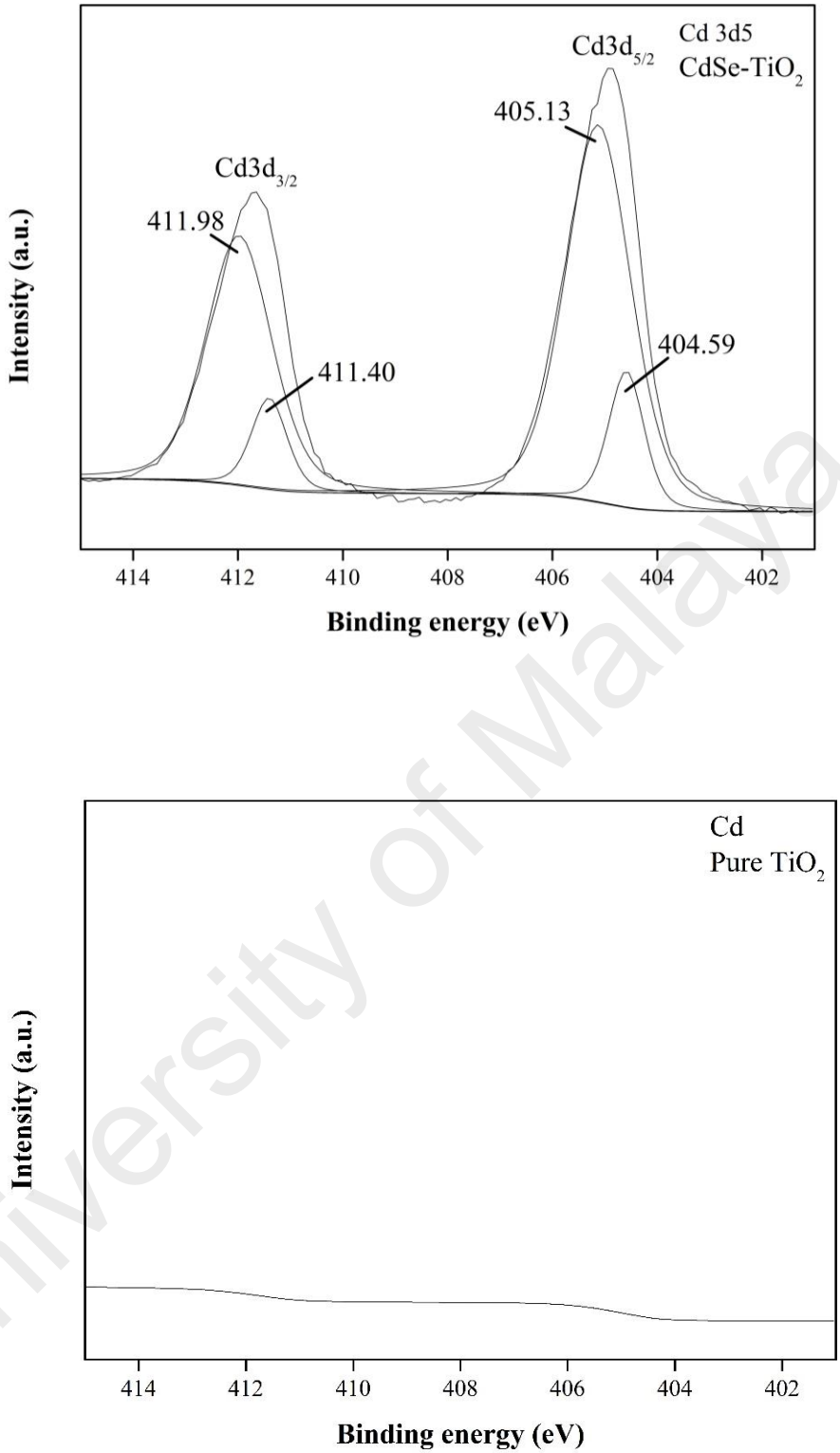

Figure 4.22: XPS spectra of Cd 3d

Similarly, Figure 4.23 shows compound peak feature of the Se (3d) spectra for the CdSe-loaded TiO_2 nanotubes samples, suggesting the presence of element 'Se'. The characteristic peak of Se $3d_{3/2}$ was located at 54.46 eV, indicating that the Se element was in the state of Se^{2-} (Liang *et al.*, 2012; Song *et al.*, 2013). No extra peak was observed in the XPS spectra of Se (3d), which point out no formation of SeO_x during synthesis. This clearly indicates that as-synthesized CdSe-TiO_2 nanotubes consisted of only the elements Se of CdSe, not of its oxides. As shown in both Figure 4.22 and 4.23, pure TiO_2 nanotubes sample did not exhibit any peak of Cd and Se element from the XPS spectra. These results suggested that CdSe nanocrystal were deposited on the wall surface of the TiO_2 nanotubes. Therefore, XPS spectra of CdSe modified TiO_2 nanotubes demonstrate that CdSe has already been incorporated onto TiO_2 nanotubes successfully through CBD technique.

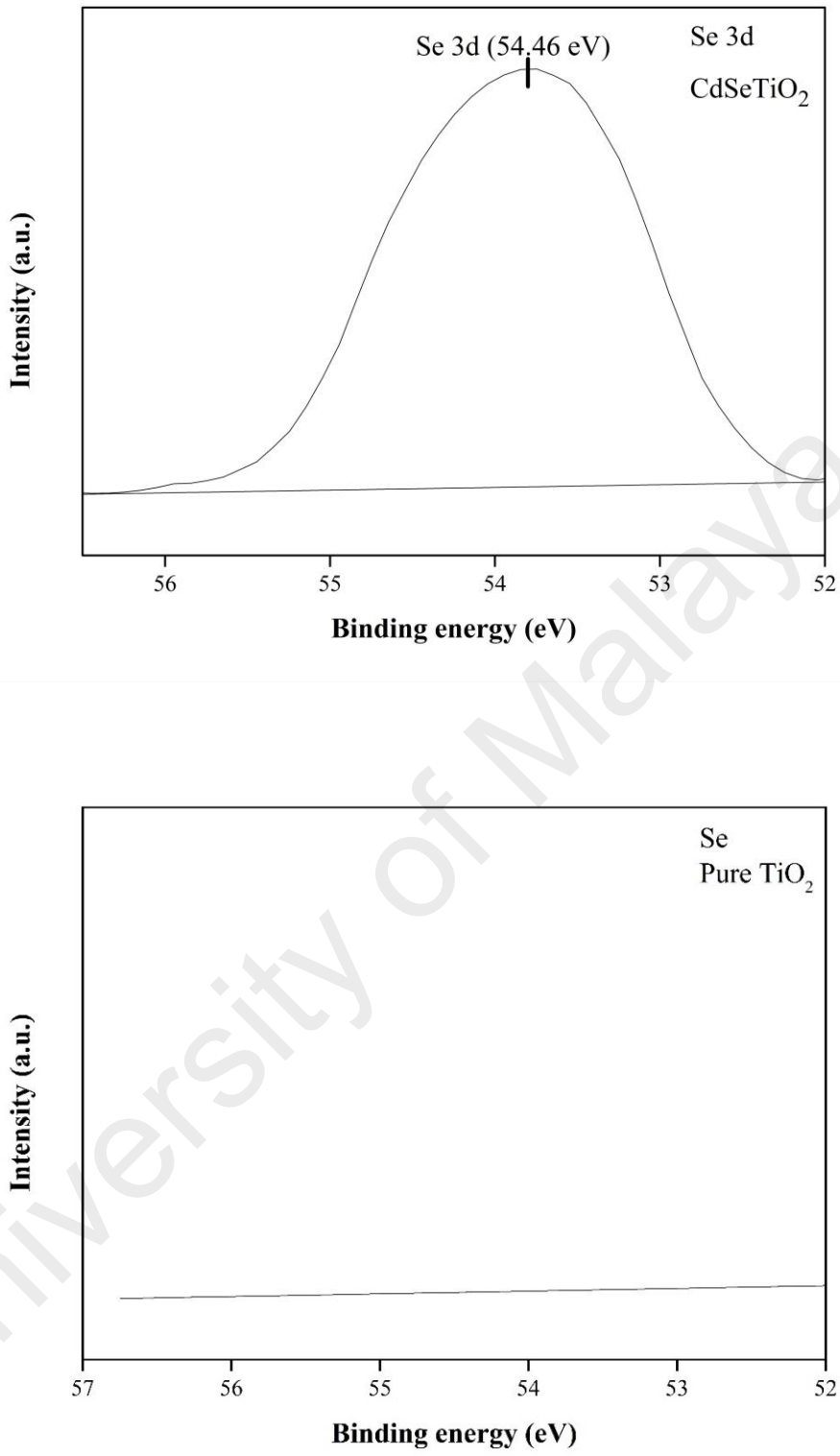

Figure 4.23: XPS spectra of Se 3d

4.5 Optical Properties Analysis by UV-vis DRS

The UV-vis absorption spectra of pure TiO_2 and the best PEC performance CdSe-TiO_2 nanotubes are presented in Figure 4.24. Both the CdSe-loaded TiO_2 nanotubes and pure TiO_2 nanotubes showed excellent absorption performance in the UV range. Furthermore, in the whole UV-vis light region, hybrid CdSe-TiO_2 nanotubes exhibit higher light absorbance than pure TiO_2 nanotubes and showed a red shift in the absorption edges.

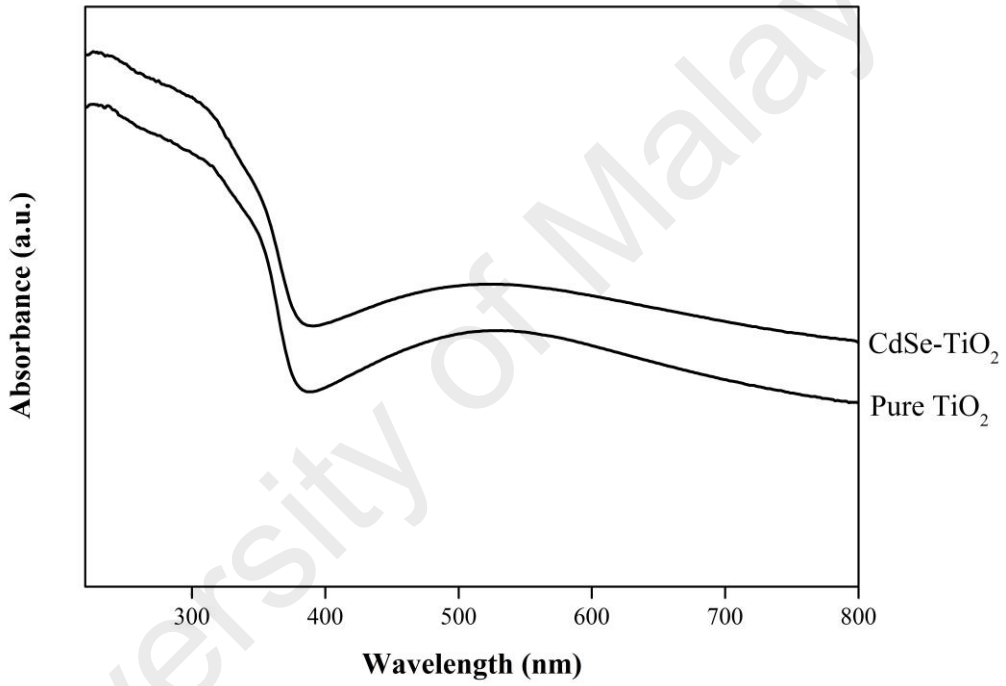

Figure 4.24: Absorption patterns of pure TiO_2 nanotubes and CdSe-loaded TiO_2 nanotubes deposited in 5 mM CdSe precursor solution for 1 h at room temperature

The band gap energy values of coupled CdSe-TiO_2 nanotubes and pure TiO_2 nanotubes were estimated through Kubelka-Munk function of the plot of $(\alpha h\nu)^{1/2}$ versus $h\nu$. As shown in Figures 4.25 (a) and (b), band gap value of pure TiO_2 nanotubes and CdSe-TiO_2 nanotubes were estimated to be 2.74 eV and 2.60 eV respectively. Band gap value of pure TiO_2 nanotubes obtained was significantly lower than typical band gap value of TiO_2 (3.2 eV). This is attributed to the presence of carbon species within the TiO_2 nanotubes which

significantly enhanced the visible light responsiveness of the TiO_2 nanotubes. The band gap energy of TiO_2 was narrowed down by the mixing of the delocalized p state of the carbon species with the 2p orbital of the oxygen species in the valence band of TiO_2 which shifts the valence band edge of TiO_2 upwards (Lai & Sreekantan, 2013). The band energy value of CdSe-TiO_2 nanotubes decreases progressively to 2.60 eV and shows that the deposition of CdSe influences the band energy value of pure TiO_2 nanotubes which leads to enhance light harvesting.

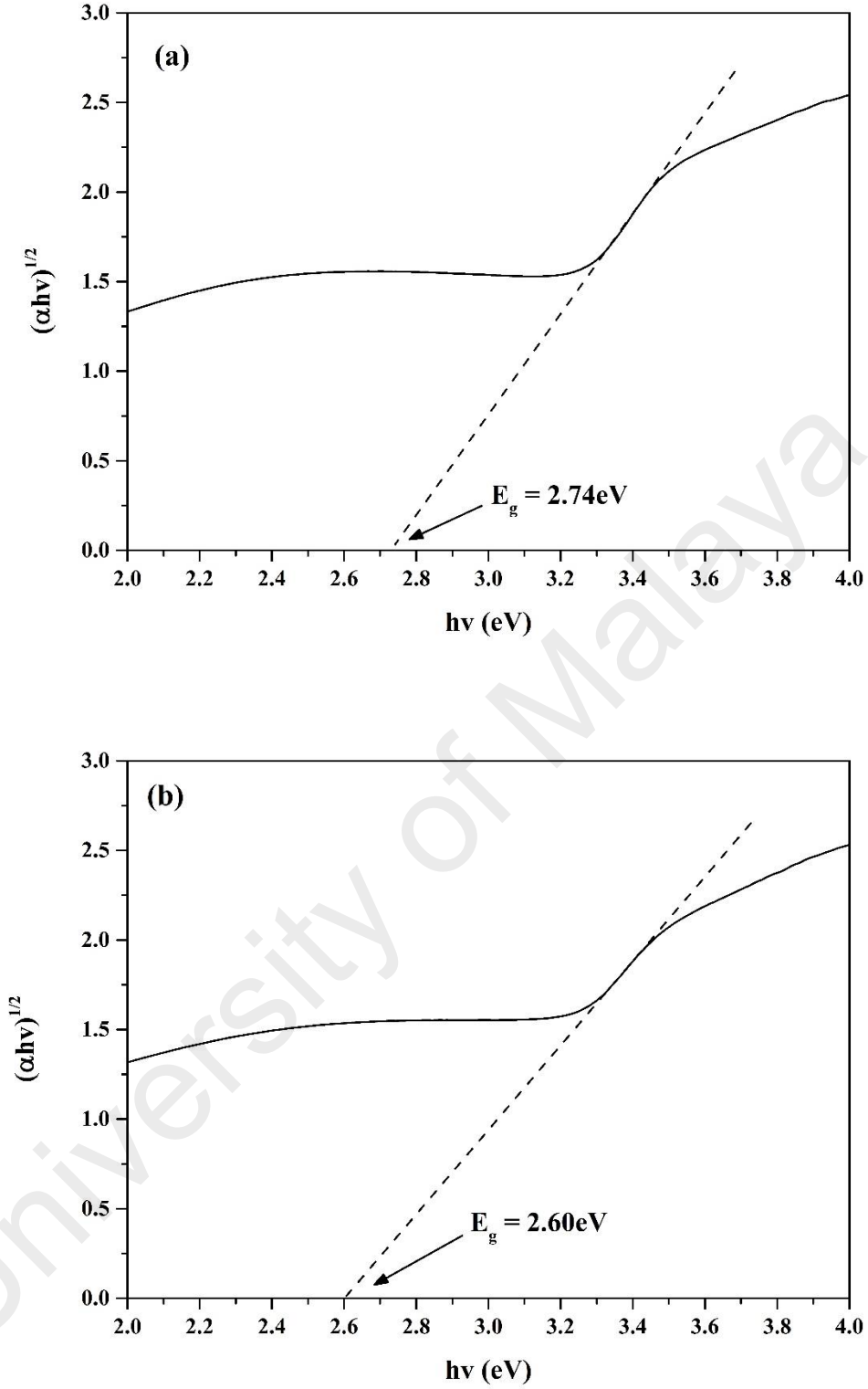

Figure 4.25: Plot of $(\alpha hv)^{1/2}$ versus hν employed to calculate the band gap value of (a) pure TiO_2 nanotubes and (b) CdSe-TiO_2 nanotubes deposited in 5 mM CdSe precursor solution for 1 h at room temperature

4.6 Carrier Recombination Analysis by Photoluminescence Spectroscopy

The photoluminescence, PL emission spectra has been widely used to obtain information on the efficiency of charge carrier, trapping immigration, and transfer (Li *et al.*, 2001). By evaluating through the change in the PL intensity emitted from a material, the recombination of charge carriers can be determined. The recombination, also known as dissipation of energy of electrons in semiconductor to the valence band. Hence, the best CdSe deposited sample was selected for PL analysis and the results were compared with the pure TiO_2 sample to investigate the effect of CdSe doping on the optical properties of the nanotubes.

Figure 4.26 presents the PL spectra of CdSe-loaded TiO_2 nanotubes and pure TiO_2 nanotubes. The higher PL emission intensity corresponds to pure TiO_2 nanotubes whereas CdSe-loaded TiO_2 nanotubes depicted lower PL intensity. Since the PL intensity of a material can be related to the relative amount of recombination rates, we can deduce that the CdSe-loaded TiO_2 nanotubes has lower recombination rate than pure TiO_2 nanotubes (Lopez-Luke *et al.*, 2008). Such a variation in the PL intensity may be due to the existing of CdSe. Thus, this suppressed the recombination of the photogenerated carriers and increased charge separation via its higher conduction band (CB) edge than that of TiO_2. Type II band alignment was formed with TiO_2, allowing effective injection of photogenerated electrons from CdSe to TiO_2 (Su *et al.*, 2014).

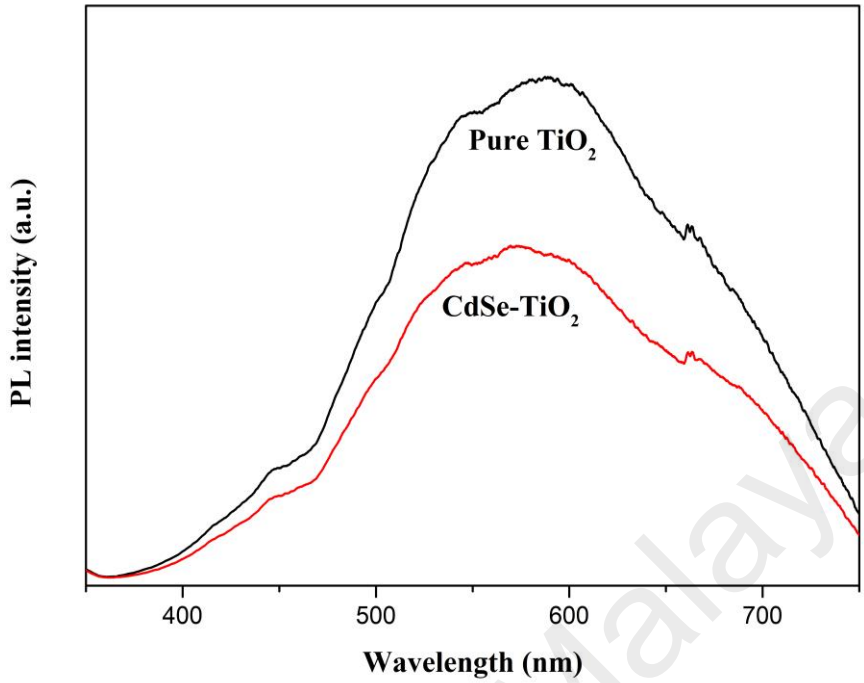

Figure 4.26: PL curve of the best PEC performance CdSe-loaded TiO_2 nanotubes and pure TiO_2 nanotubes

4.7 PEC water splitting performance

The evolution rate of H_2 gas generated from the water-splitting process was evaluated. The H_2 evolution as a function of time is shown in Figure 4.27. H_2 generation rate increased linearly with increasing exposure time. The sample subjected to 1 h of soaking time in 5 mM CdSe precursor achieved a maximum evolution of 9.6 ml, which was relatively higher compared with pure TiO_2 nanotubes (7.1ml). Recorded rate of hydrogen generation for CdSe-loaded TiO_2 and pure TiO_2 (Table 4.8) are 3.2 and 2.78 mL/cm^2h^1 respectively. The photocurrent efficiency, η also has been conducted to estimate the correlation of light absorption quantitatively. Based on the Figure 4.28, the η curve of CdSe-TiO_2 gives the highest η of about 1.9% which compare with η of pure TiO_2 is about 1.11%. Sufficient amount of CdSe nanocluster deposited on the surface of TiO_2 can improve both the light absorption and contact degree with the solution. The excited

electrons from the CdSe can quickly transfer to the TiO_2 nanotubes, reducing the recombination of electrons and holes (Su *et al.*, 2014). Therefore, the binary system of the CdSe-TiO_2 nanotubes exhibited a better charge carrier transfer, thus generating more H_2 gases at Pt electrode. This result was in line with the photocurrent density. The H_2 production completely stopped after the termination of light irradiation. This observation was a clear indication that H_2 is only produced photocatalytically. A constant production rate of H_2 gas was found in the present study.

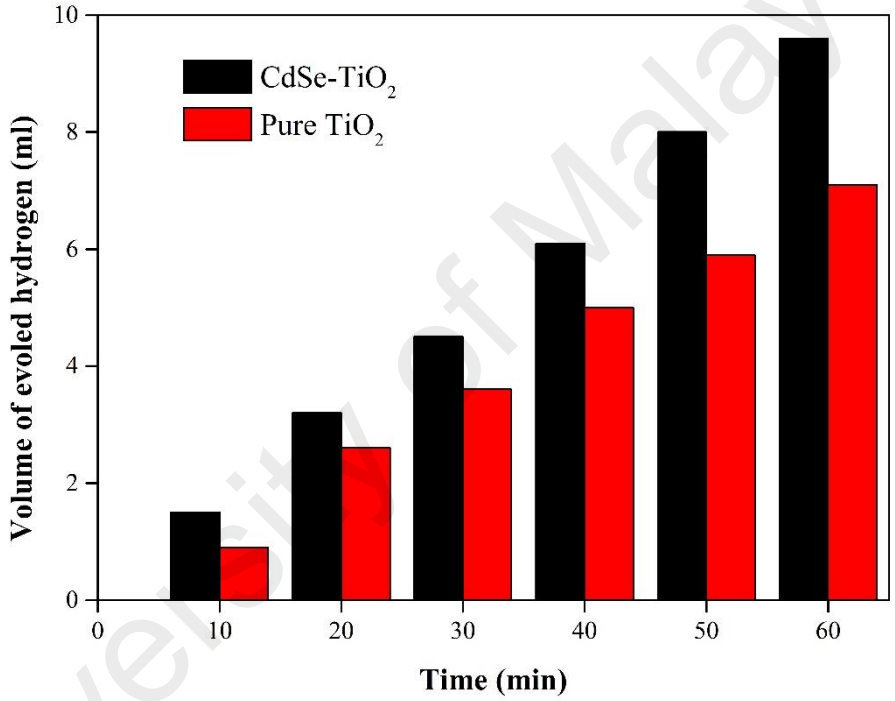

Figure 4.27: H_2 evolution under light illumination of hybrid CdSe-TiO_2 nanotubes and pure TiO_2 nanotubes for 60 min

Table 4.8 Hydrogen generation rate of both CdSe-TiO_2 and pure TiO_2 nanotubes samples

Sample	Rate of hydrogen evolved (mL/cm^2h^1)
Pure TiO_2	3.20
CdSe-TiO_2	2.37

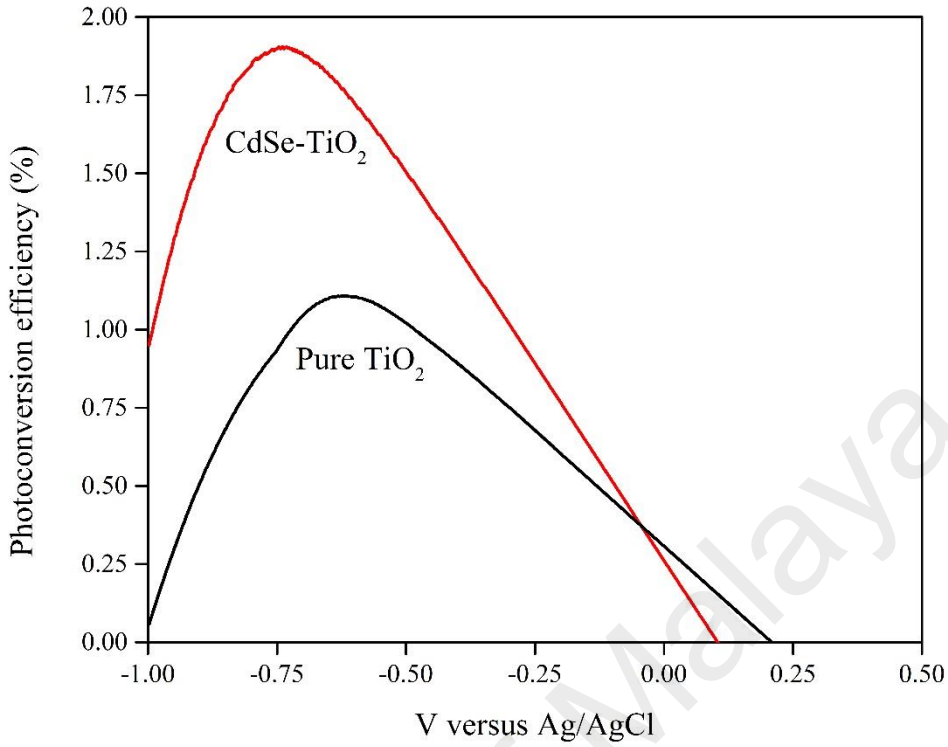

Figure 4.28: The η curves of CdSe-TiO_2 and pure TiO_2 nanotubes in 1M KOH solution under illumination.

CHAPTER 5: CONCLUSION

5.1 Conclusion

This research work was dedicated to fabricate hybrid CdSe-loaded TiO_2 nanotubes for the application of solar-driven PEC water splitting process. In short, the objectives of the experiments were achieved. First, rapid formation of highly ordered CdSe-loaded TiO_2 nanotube arrays film was successfully synthesized through two simple stages, electrochemical anodization and chemical bath deposition techniques. Second, comprehensive study was conducted to study the physical, chemical, and functional properties of hybrid CdSe–loaded TiO_2 nanotubes film as compared to pure TiO_2 nanotubes. Lastly, the photocatalysed water splitting hydrogen generation system under solar illumination was subsequently demonstrated.

In the first stage of research study, the optimized parameters of electrochemical anodization were determined to anodize Ti foil which leads to highly ordered and smooth TiO_2 nanotubes. The conclusions attained from this research work are elaborated as follow:

- Formation of highly ordered TiO_2 nanotube arrays film (aspect ratio of ~60) was achieved by electrochemical anodization technique in ethylene glycol electrolyte containing H_2O_2 and NH_4F at 40 V for 60 min. In the present study, addition of 5 wt% H_2O_2 in the electrolyte functioned as oxygen provider to increase the oxidation rate for growing the nanotubular structure. It was found that high formation rate of anodic nanotubular was within 60 min of electrochemical anodization time. This was due to the presence of the powerful oxidant, H_2O_2 which further decomposed into •OH and HO_2• radicals with pronounced chemical and field-assisted dissolution at the bottom. Meanwhile, 0.3 wt% NH_4F content was found to influence the chemical dissolution rate or etching rate

during electrochemical anodization stage, thus modifying the final morphological of TiO_2 nanotubes film significantly. In addition, as for the optimum applied potential of 40 V, nanotubes with greater length and pore sizes were produced. Thid resulted from the equalization of chemical dissolution rate plus electric field-assisted oxidation and dissolution rate for ionic transport through the barrier layer of TiO_2.

In the second stage, considerable effort has been conducted to further enhanced the transportation of charge carriers and minimize the recombination possess by loading optimum content of CdSe dopants. It is also important to control the deposition molarity, time and temperature during the chemical bath deposition stage. The efficiency of PEC water splitting hydrogen generation using CdSe-loaded TiO_2 nanotubes film was also compared to pure TiO_2 nanotubes film. The conclusions attained in this research work are elaborated as follows:

- Based on the results obtained, pure TiO_2 nanotubes film bathed in a 5 mM CdSe precursor solution extensively covered by approximately 1 at% CdSe exhibited the highest j_p of 2.50 mA/cm^2 among the samples. However, excessive deposition (≥5 mM) was neither negatively affected by the self-organized nanotubes nor decreased in j_p. This condition inferred that higher ionic product (Cd and Se ions) and lower solubility product (CdSe solid phase) will cause the rapid ion-by-ion condensation or adsorption of colloidal particles clogged the opening pore's mouth of TiO_2 nanotubes. Thus, an improvement in the photoresponse was observed when optimum amount (~ 1 at%) of the CdSe was deposited on TiO_2 nanotubes film. Large extinction coefficient of CdSe strongly absorbs visible light, inject electrons into the conduction band of metal oxides further increases in solar energy conversion.

- In the present study, soaking duration played an essential role based on the concept of nucleation in solution, which relies on the rate of release of the Cd and Se ions. The j_p obtained from the sample soaked for 30 min was slightly higher compared with pure TiO_2 nanotubes (1.46 mA/cm^2). In 30 min of deposition duration, it is insufficient for nucleation process to form significant precipitate. Besides that, prolonged soaking duration up to 3 hours or more leads to the accumulation of CdSe cluster which formed spherical structure on the pore entrance deceasing in electrochemical active surface area by hindered transferring of photo-induced charge carriers resulting smaller j_p than pure TiO_2 nanotubes.
- Deposition temperature played an important role in altering the thermal dislocation of the Cd complexes and Se anions through manipulate the release rate of selenium ions from sodium selenosulphate leads to growth of CdSe clusters. At the temperature of 20 °C, similar morphology with pure TiO_2 nanotubes was obtained whereas deposition temperature increased to 40 °C, 50 °C and 60 °C negatively affected the nanotubular structure. Photocurrent response, j_p of 1.63 mA/cm^2 was observed subjected to 20 °C soaking temperature. However, CdSe-TiO_2 nanotubes subjected to 40 °C, 50 °C, and 60 °C soaking condition exhibited decreased j_p. Extra thermal energy has supplied to the system at higher temperature, CdSe nucleus tend to coalesce and reduce the high surface energy.

5.2 Suggestions and Recommendations

In order to further develop the photocatalysis PEC water splitting hydrogen generation technologies, several recommendations for future studies were proposed as follows:

- To optimize the properties of the hybrid nanotubes by investigating the effect of pH to reduce the secondary pollution caused by ammonium solution and precisely control the embedded size of CdSe nanocluster.
- In order to comprehensively understand the charge dynamics within TiO_2 nanotubes and CdSe-TiO_2 nanotubes, detail analysis need to be done by using electrochemical impedance spectroscopy (EIS) and Mott-Schottky analysis.
- Tenary hybrid technology, which is the incorporation of additional types of photocatalyst (e.g., graphene, MoS_2, GaP) into CdSe-TiO_2 nanotubes are believed as a potential approach to further improve the surface charge carriers transfer rate and minimize the recombination rate.

REFERENCES

Afzaal, Mohammmad, Crouch, David, Malik, Mohammad A, Motevalli, Majid, O'Brien, Paul, & Park, Jin-Ho. (2003). Deposition of CdSe thin films using a novel single-source precursor;$[MeCd\{(SePiPr_2)_2N\}]_2$. *Journal of Materials Chemistry, 13*(4), 639-640.

Albu, Sergiu P, Ghicov, Andrei, Aldabergenova, Saule, Drechsel, Peter, LeClere, Darren, Thompson, George E, . . . Schmuki, Patrik. (2008). Formation of double-walled TiO_2 nanotubes and robust anatase membranes. *Advanced Materials, 20*(21), 4135-4139.

Armelao, Lidia, Barreca, Davide, Bottaro, Gregorio, Gasparotto, Alberto, Maccato, Chiara, Tondello, Eugenio, . . . Sada, Cinzia. (2009). Rational design of Ag/TiO_2 nanosystems by a combined RF-sputtering/Sol-Gel approach. *ChemPhysChem, 10*(18), 3249-3259.

Armstrong, Graham, Armstrong, A Robert, Canales, Jesús, & Bruce, Peter G. (2005). Nanotubes with the TiO_2-B structure. *Chemical Communications,* (19), 2454-2456.

Aroutiounian, VM, Arakelyan, VM, & Shahnazaryan, GE. (2005). Metal oxide photoelectrodes for hydrogen generation using solar radiation-driven water splitting. *Solar Energy, 78*(5), 581-592.

Asahi, Ryoji, & Morikawa, Takeshi. (2007). Nitrogen complex species and its chemical nature in TiO_2 for visible-light sensitized photocatalysis. *Chemical Physics, 339*(1), 57-63.

Assefpour-Dezfuly, M, Vlachos, C, & Andrews, EH. (1984). Oxide morphology and adhesive bonding on titanium surfaces. *Journal of Materials Science, 19*(11), 3626-3639.

Attar, A Sadeghzadeh, Ghamsari, M Sasani, Hajiesmaeilbaigi, F, Mirdamadi, Sh, Katagiri, K, & Koumoto, K. (2009). Sol–gel template synthesis and characterization of aligned anatase-TiO_2 nanorod arrays with different diameter. *Materials Chemistry and Physics, 113*(2), 856-860.

Babu, Veluru Jagadeesh, Vempati, Sesha, Uyar, Tamer, & Ramakrishna, Seeram. (2015). Review of one-dimensional and two-dimensional nanostructured materials for hydrogen generation. *Physical Chemistry Chemical Physics, 17*(5), 2960-2986.

Bak, T, Nowotny, J, Rekas, M, Ringer, S, & Sorrell, CC. (2001). Properties of TiO_2 as photoelectrode for hydrogen generation using solar energy. *Ionics, 7*(4-6), 272-274.

Bak, T, Nowotny, J, Rekas, M, & Sorrell, CC. (2002). Photo-electrochemical hydrogen generation from water using solar energy. Materials-related aspects. *International Journal of Hydrogen Energy, 27*(10), 991-1022.

Barreca, Davide, Carraro, Giorgio, Gombac, Valentina, Gasparotto, Alberto, Maccato, Chiara, Fornasiero, Paolo, & Tondello, Eugenio. (2011). Supported metal oxide nanosystems for hydrogen photogeneration: Quo vadis? *Advanced Functional Materials, 21*(14), 2611-2623.

Bavykin, Dmitry V, Parmon, Valentin N, Lapkin, Alexei A, & Walsh, Frank C. (2004). The effect of hydrothermal conditions on the mesoporous structure of TiO_2 nanotubes. *Journal of Materials Chemistry, 14*(22), 3370-3377.

Becker, Matthew A, Radich, James G, Bunker, Bruce A, & Kamat, Prashant V. (2014). How does a SILAR CdSe film grow? Tuning the deposition steps to suppress interfacial charge recombination in solar cells. *The Journal of Physical Chemistry Letters, 5*(9), 1575-1582.

Bhirud, Ashwini P, Sathaye, Shivaram D, Waichal, Rupali P, Ambekar, Jalindar D, Park, Chan-J, & Kale, Bharat B. (2015). In-situ preparation of N-TiO_2/graphene nanocomposite and its enhanced photocatalytic hydrogen production by H_2S splitting under solar light. *Nanoscale, 7*(11), 5023-5034.

Buehler, Niklaus, Meier, Kurt, & Reber, Jean Francois. (1984). Photochemical hydrogen production with cadmium sulfide suspensions. *The Journal of Physical Chemistry, 88*(15), 3261-3268.

Burnside, Shelly, Moser, Jacques-E, Brooks, Keith, Grätzel, Michael, & Cahen, David. (1999). Nanocrystalline mesoporous strontium titanate as photoelectrode material for photosensitized solar devices: increasing photovoltage through flatband potential engineering. *The Journal of Physical Chemistry B, 103*(43), 9328-9332.

Castelli, Ivano E, García-Lastra, Juan María, Hüser, Falco, Thygesen, Kristian S, & Jacobsen, Karsten W. (2013). Stability and bandgaps of layered perovskites for one-and two-photon water splitting. *New Journal of Physics, 15*(10), 105026.

Centi, Gabriele, & Perathoner, Siglinda. (2009). The role of nanostructure in improving the performance of electrodes for energy storage and conversion. *European Journal of Inorganic Chemistry, 2009*(26), 3851-3878.

Chen, Bo, Hou, Junbo, & Lu, Kathy. (2013). Formation mechanism of TiO_2 nanotubes and their applications in photoelectrochemical water splitting and supercapacitors. *Langmuir, 29*(19), 5911-5919.

Chen, Jun Song, Tan, Yi Ling, Li, Chang Ming, Cheah, Yan Ling, Luan, Deyan, Madhavi, Srinivasan, . . . Lou, Xiong Wen. (2010). Constructing hierarchical spheres from large ultrathin anatase TiO_2 nanosheets with nearly 100% exposed (001) facets for fast reversible lithium storage. *Journal of the American Chemical Society, 132*(17), 6124-6130.

Chiu, Sheng-Cheng, & Li, Yuan-Yao. (2009). SiC nanowires in large quantities: Synthesis, band gap characterization, and photoluminescence properties. *Journal of Crystal Growth, 311*(4), 1036-1041.

Cho, In Sun, Choi, Jongmin, Zhang, Kan, Kim, Sung June, Jeong, Myung Jin, Cai, Lili, . . . Park, Jong Hyeok. (2015). Highly efficient solar water splitting from transferred TiO_2 nanotube arrays. *Nano Letters, 15*(9), 5709-5715.

Choi, Jinsub, Wehrspohn, Ralf B, Lee, Jaeyoung, & Gösele, Ulrich. (2004). Anodization of nanoimprinted titanium: a comparison with formation of porous alumina. *Electrochimica Acta, 49*(16), 2645-2652.

Chopra, Kasturi Lal, & Das, Suhit Ranjan. (1983). *Why thin film solar cells?* : Springer.

Chouhan, Neelu, Yeh, Chai Ling, Hu, Shu-Fen, Liu, Ru-Shi, Chang, Wen-Sheng, & Chen, Kuei-Hsien. (2011). Photocatalytic CdSe QDs-decorated ZnO nanotubes: an effective photoelectrode for splitting water. *Chemical Communications, 47*(12), 3493-3495.

Cortright, RD, Davda, RR, & Dumesic, JA. (2002). Hydrogen from catalytic reforming of biomass-derived hydrocarbons in liquid water. *Nature, 418*(6901), 964-967.

Crabtree, George W, & Lewis, Nathan S. (2007). Solar energy conversion. *Physics today, 60*(3), 37-42.

Currao, Antonio. (2007). Photoelectrochemical water splitting. *CHIMIA International Journal for Chemistry, 61*(12), 815-819.

Deshpande, MP, Garg, Nitya, Bhatt, Sandip V, Sakariya, Pallavi, & Chaki, Sunil H. (2013). Characterization of CdSe thin films deposited by chemical bath solutions containing triethanolamine. *Materials Science in Semiconductor Processing, 16*(3), 915-922.

Dhanam, M, Prabhu, Rajeev R, & Manoj, PK. (2008). Investigations on chemical bath deposited cadmium selenide thin films. *Materials Chemistry and Physics, 107*(2), 289-296.

Esparza, Diego, Zarazúa, Isaac, López-Luke, Tzarara, Cerdán-Pasarán, Andrea, Sánchez-Solís, Ana, Torres-Castro, Alejandro, . . . De la Rosa, Elder. (2015). Effect of different sensitization technique on the photoconversion efficiency of CdS quantum dot and CdSe quantum rod sensitized TiO_2 solar cells. *The Journal of Physical Chemistry C, 119*(24), 13394-13403.

Fernandes, Jesum A, Khan, Sherdil, Baum, Fabio, Kohlrausch, Emerson C, dos Santos, José Augusto Lucena, Baptista, Daniel L, . . . Santos, Marcos J Leite. (2016). Synergizing nanocomposites of CdSe/TiO_2 nanotubes for improved photoelectrochemical activity via thermal treatment. *Dalton Transactions*.

Fernandes, Jesum A, Migowski, Pedro, Fabrim, Zacarias, Feil, Adriano F, Rosa, Guilherme, Khan, Sherdil, . . . Santos, Marcos JL. (2014). TiO_2 nanotubes sensitized with CdSe via RF magnetron sputtering for photoelectrochemical applications under visible light irradiation. *Physical Chemistry Chemical Physics, 16*(19), 9148-9153.

Fujishima, A, & Honda, K. (1972). Electrochemical study of spectral sensitization. *Nature, 238*(37), 2.

Fujishima, Akira, Rao, Tata N, & Tryk, Donald A. (2000). Titanium dioxide photocatalysis. *Journal of Photochemistry and Photobiology C: Photochemistry Reviews, 1*(1), 1-21.

Galinska, Anna, & Walendziewski, Jerzy. (2005). Photocatalytic water splitting over Pt-TiO_2 in the presence of sacrificial reagents. *Energy & Fuels, 19*(3), 1143-1147.

Gan, Jiayong, Zhai, Teng, Lu, Xihong, Xie, Shilei, Mao, Yanchao, & Tong, Yexiang. (2012). Facile preparation and photoelectrochemical properties of CdSe/TiO_2 NTAs. *Materials Research Bulletin, 47*(3), 580-585.

Ge, Ming-Zheng, Li, Shu-Hui, Huang, Jian-Ying, Zhang, Ke-Qin, Al-Deyab, Salem S, & Lai, Yue-Kun. (2015a). TiO_2 nanotube arrays loaded with reduced graphene oxide films: facile hybridization and promising photocatalytic application. *Journal of Materials Chemistry A, 3*(7), 3491-3499.

Ge, Mingzheng, Cao, Chunyan, Huang, Jianying, Li, Shuhui, Chen, Zhong, Zhang, Ke-Qin, . . . Lai, Yuekun. (2016). A review of one-dimensional TiO_2 nanostructured materials for environmental and energy applications. *Journal of Materials Chemistry A*.

Ge, Mingzheng, Cao, Chunyan, Li, Shuhui, Zhang, Songnan, Deng, Shu, Huang, Jianying, . . . Lai, Yuekun. (2015b). Enhanced photocatalytic performances of n-TiO_2 nanotubes by uniform creation of p–n heterojunctions with p-Bi_2O_3 quantum dots. *Nanoscale, 7*(27), 11552-11560.

Ghicov, Andrei, & Schmuki, Patrik. (2009). Self-ordering electrochemistry: a review on growth and functionality of TiO_2 nanotubes and other self-aligned MO_x structures. *Chemical Communications*(20), 2791-2808.

González-Pedro, Victoria, Shen, Qing, Jovanovski, Vasko, Giménez, Sixto, Tena-Zaera, Ramon, Toyoda, Taro, & Mora-Seró, Iván. (2013). Ultrafast characterization of the electron injection from CdSe quantum dots and dye N719 co-sensitizers into TiO_2 using sulfide based ionic liquid for enhanced long term stability. *Electrochimica Acta, 100*, 35-43.

Gopakumar, N, Anjana, PS, & Pillai, PK Vidyadharan. (2010). Chemical bath deposition and characterization of CdSe thin films for optoelectronic applications. *Journal of Materials Science, 45*(24), 6653-6656.

Gorczyca, I, Suski, T, Christensen, Niels Egede, & Svane, Axel. (2010). Limitations to band gap tuning in nitride semiconductor alloys. *Applied Physics Letters, 96*(10), 101907.

Grätzel, Michael. (2001). Photoelectrochemical cells. *Nature, 414*(6861), 338-344.

Grimes, Craig A. (2007). Synthesis and application of highly ordered arrays of TiO_2 nanotubes. *Journal of Materials Chemistry, 17*(15), 1451-1457.

Grimes, Craig A, & Mor, Gopal K. (2009). *TiO_2 nanotube arrays: synthesis, properties, and applications*: Springer Science & Business Media.

Grimes, Craig, Varghese, Oomman, & Ranjan, Sudhir. (2007). *Light, water, hydrogen: the solar generation of hydrogen by water photoelectrolysis*: Springer Science & Business Media.

Hagen, Dirk J, Povey, Ian M, Rushworth, Simon, Wrench, Jacqueline S, Keeney, Lynette, Schmidt, Michael, . . . Pemble, Martyn E. (2014). Atomic layer deposition of Cu with a carbene-stabilized Cu (i) silylamide. *Journal of Materials Chemistry C, 2*(43), 9205-9214.

Hahn, R, Macak, JM, & Schmuki, P. (2007). Rapid anodic growth of TiO_2 and WO_3 nanotubes in fluoride free electrolytes. *Electrochemistry Communications, 9*(5), 947-952.

Han, Gill Sang, Lee, Sangwook, Noh, Jun Hong, Chung, Hyun Suk, Park, Jong Hoon, Swain, Bhabani Sankar, . . . Jung, Hyun Suk. (2014). 3-D TiO_2 nanoparticle/ITO nanowire nanocomposite antenna for efficient charge collection in solid state dye-sensitized solar cells. *Nanoscale, 6*(11), 6127-6132.

Hatam, E Gholami, & Ghobadi, N. (2016). Effect of deposition temperature on structural, optical properties and configuration of CdSe nanocrystalline thin films deposited by chemical bath deposition. *Materials Science in Semiconductor Processing, 43*, 177-181.

Hoa, Nguyen Thi Quynh, & Huyen, Duong Ngoc. (2013). Comparative study of room temperature ferromagnetism in undoped and Ni-doped TiO_2 nanowires synthesized by solvothermal method. *Journal of Materials Science: Materials in Electronics, 24*(2), 793-798.

Hoyer, Patrick. (1996). Formation of a titanium dioxide nanotube array. *Langmuir, 12*(6), 1411-1413.

Hu, Yun Hang. (2012). A highly efficient photocatalyst—hydrogenated black TiO2 for the photocatalytic splitting of water. *Angewandte Chemie International Edition, 51*(50), 12410-12412.

HyukáIm, Sang, & HyeokáPark, Jong. (2010). CdS or CdSe decorated TiO_2 nanotube arrays from spray pyrolysis deposition: use in photoelectrochemical cells. *Chemical Communications, 46*(14), 2385-2387.

Ismail, Syahriza, Ahmad, Zainal A, Berenov, Andrey, & Lockman, Zainovia. (2011). Effect of applied voltage and fluoride ion content on the formation of zirconia nanotube arrays by anodic oxidation of zirconium. *Corrosion Science, 53*(4), 1156-1164.

Izumi, Yasuo, Itoi, Takaomi, Peng, Shuge, Oka, Kazuki, & Shibata, Yoshiyuki. (2009). Site structure and photocatalytic role of sulfur or nitrogen-doped titanium oxide with uniform mesopores under visible light. *The Journal of Physical Chemistry C, 113*(16), 6706-6718.

Ji, Yajun, Zhang, Mingdao, Cui, Jiehu, Lin, Keng-Chu, Zheng, Hegen, Zhu, Jun-Jie, & Samia, Anna Cristina S. (2012). Highly-ordered TiO_2 nanotube arrays with double-walled and bamboo-type structures in dye-sensitized solar cells. *Nano Energy, 1*(6), 796-804.

Jitputti, Jaturong, Suzuki, Yoshikazu, & Yoshikawa, Susumu. (2008). Synthesis of TiO_2 nanowires and their photocatalytic activity for hydrogen evolution. *Catalysis Communications, 9*(6), 1265-1271.

Joo, Jin, Kwon, Soon Gu, Yu, Taekyung, Cho, Min, Lee, Jinwoo, Yoon, Jeyong, & Hyeon, Taeghwan. (2005). Large-scale synthesis of TiO_2 nanorods via nonhydrolytic sol-gel ester elimination reaction and their application to photocatalytic inactivation of E. c oli. *The Journal of Physical Chemistry B, 109*(32), 15297-15302.

Kale, RB, & Lokhande, CD. (2005). Systematic study on structural phase behavior of CdSe thin films. *The Journal of Physical Chemistry B*, *109*(43), 20288-20294.

Kasuga, Tomoko, Hiramatsu, Masayoshi, Hoson, Akihiko, Sekino, Toru, & Niihara, Koichi. (1998). Formation of titanium oxide nanotube. *Langmuir, 14*(12), 3160-3163.

Kasuga, Tomoko, Hiramatsu, Masayoshi, Hoson, Akihiko, Sekino, Toru, & Niihara, Koichi. (1999). Titania nanotubes prepared by chemical processing. *Advanced Materials, 11*(15), 1307-1311.

Khare, Chinmay, Sliozberg, Kirill, Meyer, Robert, Savan, Alan, Schuhmann, Wolfgang, & Ludwig, Alfred. (2013). Layered WO_3/TiO_2 nanostructures with enhanced photocurrent densities. *International Journal of Hydrogen Energy, 38*(36), 15954-15964.

Kim, Jin Young, Zhu, Kai, Neale, Nathan R, & Frank, Arthur J. (2014). Transparent TiO_2 nanotube array photoelectrodes prepared via two-step anodization. *Nano Convergence, 1*(1), 1-7.

Kitano, Masaaki, Matsuoka, Masaya, Ueshima, Michio, & Anpo, Masakazu. (2007). Recent developments in titanium oxide-based photocatalysts. *Applied Catalysis A: General, 325*(1), 1-14.

Kreuter, W, & Hofmann, H. (1998). Electrolysis: the important energy transformer in a world of sustainable energy. *International Journal of Hydrogen Energy, 23*(8), 661-666.

Kubacka, Anna, Fernández-García, Marcos, & Colón, Gerardo. (2011). Advanced nanoarchitectures for solar photocatalytic applications. *Chemical Reviews, 112*(3), 1555-1614.

Kudo, Akihiko, & Miseki, Yugo. (2009). Heterogeneous photocatalyst materials for water splitting. *Chemical Society Reviews, 38*(1), 253-278.

Lai, Chin Wei, & Sreekantan, Srimala. (2012). Optimized sputtering power to incorporate WO_3 into C–TiO_2 nanotubes for highly visible photoresponse performance. *Nano, 7*(06), 1250051.

Lai, Chin Wei, & Sreekantan, Srimala. (2013). Single step formation of C-TiO 2 nanotubes: influence of applied voltage and their photocatalytic activity under solar illumination. *International Journal of Photoenergy, 2013*.

Lakshmi, Brinda B, Dorhout, Peter K, & Martin, Charles R. (1997). Sol-gel template synthesis of semiconductor nanostructures. *Chemistry of materials, 9*(3), 857-862.

Lee, Chang Soo, Kim, Jin Kyu, Lim, Jung Yup, & Kim, Jong Hak. (2014a). One-step process for the synthesis and deposition of anatase, two-dimensional, disk-shaped TiO_2 for dye-sensitized solar cells. *ACS Applied Materials & Interfaces, 6*(23), 20842-20850.

Lee, Doh C, Robel, István, Pietryga, Jeffrey M, & Klimov, Victor I. (2010). Infrared-active heterostructured nanocrystals with ultralong carrier lifetimes. *Journal of the American Chemical Society, 132*(29), 9960-9962.

Lee, HyoJoong, Wang, Mingkui, Chen, Peter, Gamelin, Daniel R, Zakeeruddin, Shaik M, Gratzel, Michael, & Nazeeruddin, Md K. (2009). Efficient CdSe quantum dot-sensitized solar cells prepared by an improved successive ionic layer adsorption and reaction process. *Nano Letters, 9*(12), 4221-4227.

Lee, Jiwon, Kim, Dai Hong, Hong, Seong-Hyeon, & Jho, Jae Young. (2011). A hydrogen gas sensor employing vertically aligned TiO_2 nanotube arrays prepared by template-assisted method. *Sensors and Actuators B: Chemical, 160*(1), 1494-1498.

Lee, Sooho, Lee, Kangha, Kim, Whi Dong, Lee, Seokwon, Shin, Do Joong, & Lee, Doh C. (2014b). Thin amorphous TiO_2 shell on CdSe nanocrystal quantum dots enhances photocatalysis of hydrogen evolution from water. *The Journal of Physical Chemistry C, 118*(41), 23627-23634.

Lee, Wai Hong, Lai, Chin Wei, & Hamid, Sharifah Bee Abd. (2015). One-Step Formation of WO_3-Loaded TiO_2 Nanotubes Composite Film for High Photocatalytic Performance. *Materials, 8*(5), 2139-2153.

Leghari, Sajjad Ahmed Khan, Sajjad, Shamaila, Chen, Feng, & Zhang, Jinlong. (2011). WO_3/TiO_2 composite with morphology change via hydrothermal template-free route as an efficient visible light photocatalyst. *Chemical Engineering Journal, 166*(3), 906-915.

Leung, Dennis YC, Fu, Xianliang, Wang, Cuifang, Ni, Meng, Leung, Michael KH, Wang, Xuxu, & Fu, Xianzhi. (2010). Hydrogen production over titania-based photocatalysts. *ChemSusChem, 3*(6), 681-694.

Li, Huaqiong, Lai, Yuekun, Huang, Jianying, Tang, Yuxin, Yang, Lei, Chen, Zhong, . . . Tan, Lay Poh. (2015). Multifunctional wettability patterns prepared by laser processing on superhydrophobic TiO_2 nanostructured surfaces. *Journal of Materials Chemistry B, 3*(3), 342-347.

Li, Hui, Chen, Zhenhua, Tsang, Chun Kwan, Li, Zhe, Ran, Xiao, Lee, Chris, . . . Lu, Jian. (2014a). Electrochemical doping of anatase TiO_2 in organic electrolytes for high-performance supercapacitors and photocatalysts. *Journal of Materials Chemistry A, 2*(1), 229-236.

Li, Ling, Yang, Xichuan, Zhang, Wenming, Zhang, Huayan, & Li, Xiaowei. (2014b). Boron and sulfur co-doped TiO_2 nanofilm as effective photoanode for high efficiency CdS quantum-dot-sensitized solar cells. *Journal of Power Sources, 272*, 508-512.

Li, XZ, Li, FB, Yang, CL, & Ge, WK. (2001). Photocatalytic activity of WOx-TiO_2 under visible light irradiation. *Journal of Photochemistry and Photobiology A: Chemistry, 141*(2), 209-217.

Liang, Yan, Kong, Biao, Zhu, Anwei, Wang, Zhen, & Tian, Yang. (2012). A facile and efficient strategy for photoelectrochemical detection of cadmium ions based on in situ electrodeposition of CdSe clusters on TiO_2 nanotubes. *Chemical Communications, 48*(2), 245-247.

Lieber, Charles M. (1998). One-dimensional nanostructures: chemistry, physics & applications. *Solid state communications, 107*(11), 607-616.

Lim, San Hua, Luo, Jizhong, Zhong, Ziyi, Ji, Wei, & Lin, Jianyi. (2005). Room-temperature hydrogen uptake by TiO_2 nanotubes. *Inorganic Chemistry, 44*(12), 4124-4126.

Liu, Baoshun, Nakata, Kazuya, Sakai, Munetoshi, Saito, Hidenori, Ochiai, Tsuyoshi, Murakami, Taketoshi, . . . Fujishima, Akira. (2012). Hierarchical TiO_2 spherical nanostructures with tunable pore size, pore volume, and specific surface area: facile preparation and high-photocatalytic performance. *Catalysis Science & Technology, 2*(9), 1933-1939.

Liu, Zhaoyue, Zhang, Qianqian, Zhao, Tianyi, Zhai, Jin, & Jiang, Lei. (2011). 3-D vertical arrays of TiO_2 nanotubes on Ti meshes: efficient photoanodes for water photoelectrolysis. *Journal of Materials Chemistry, 21*(28), 10354-10358.

Lokhande, CD, Lee, Eun-Ho, Jung, Kwang-Deog, & Joo, Oh-Shim. (2005). Ammonia-free chemical bath method for deposition of microcrystalline cadmium selenide films. *Materials chemistry and physics, 91*(1), 200-204.

Lopez-Luke, Tzarara, Wolcott, Abraham, Xu, Li-ping, Chen, Shaowei, Wen, Zhenhai, Li, Jinghong, . . . Zhang, Jin Z. (2008). Nitrogen-doped and CdSe quantum-dot-sensitized nanocrystalline TiO_2 films for solar energy conversion applications. *The Journal of Physical Chemistry C, 112*(4), 1282-1292.

Luo, Jingshan, Karuturi, Siva Krishna, Liu, Lijun, Su, Liap Tat, Tok, Alfred Iing Yoong, & Fan, Hong Jin. (2012). Homogeneous photosensitization of complex TiO_2 nanostructures for efficient solar energy conversion. *Scientific Reports, 2*.

Luttrell, Tim, Halpegamage, Sandamali, Tao, Junguang, Kramer, Alan, Sutter, Eli, & Batzill, Matthias. (2014). Why is anatase a better photocatalyst than rutile?-Model studies on epitaxial TiO_2 films. *Scientific Reports, 4*.

Lv, Jun, Wang, Honge, Gao, Huazhen, Xu, Guangqing, Wang, Dongmei, Chen, Zhong, . . . Wu, Yucheng. (2015). A research on the visible light photocatalytic activity and kinetics of CdS/CdSe co-modified TiO_2 nanotube arrays. *Surface and Coatings Technology, 261*, 356-363.

Macak, Jan M, Sirotna, K, & Schmuki, P. (2005). Self-organized porous titanium oxide prepared in Na_2SO_4/NaF electrolytes. *Electrochimica Acta, 50*(18), 3679-3684.

Macak, JM, Tsuchiya, H, Ghicov, A, Yasuda, K, Hahn, R, Bauer, S, & Schmuki, P. (2007). TiO_2 nanotubes: self-organized electrochemical formation, properties and applications. *Current Opinion in Solid State and Materials Science, 11*(1), 3-18.

Martin, David James, Qiu, Kaipei, Shevlin, Stephen Andrew, Handoko, Albertus Denny, Chen, Xiaowei, Guo, Zhengxiao, & Tang, Junwang. (2014). Highly efficient photocatalytic H_2 evolution from water using visible light and structure‐controlled graphitic carbon nitride. *Angewandte Chemie International Edition, 53*(35), 9240-9245.

Martin, David James, Umezawa, Naoto, Chen, Xiaowei, Ye, Jinhua, & Tang, Junwang. (2013). Facet engineered Ag_3PO_4 for efficient water photooxidation. *Energy & Environmental Science, 6*(11), 3380-3386.

Martinson, Alex BF, McGarrah, James E, Parpia, Mohammed OK, & Hupp, Joseph T. (2006). Dynamics of charge transport and recombination in ZnO nanorod array dye-sensitized solar cells. *Physical Chemistry Chemical Physics, 8*(40), 4655-4659.

Masson, DP, Lockwood, DJ, & Graham, MJ. (1997). Thermal oxide on CdSe. *Journal of Applied Physics, 82*, 1632-1639.

Meng, Ze-Da, Zhu, Lei, Ye, Shu, Sun, Qian, Ullah, Kefayat, Cho, Kwang-Youn, & Oh, Won-Chun. (2013). Fullerene modification CdSe/TiO_2 and modification of photocatalytic activity under visible light. *Nanoscale Research Letters, 8*(1), 1-10.

Misra, M, & Raja, KS. (2010). *Ordered titanium dioxide nanotubular arrays as photoanodes for hydrogen generation* (Vol. 1): John Wiley & Sons: Chichester, UK.

Momeni, Mohamad Mohsen, & Ghayeb, Yousef. (2015). Visible light-driven photoelectrochemical water splitting on ZnO–TiO_2 heterogeneous nanotube photoanodes. *Journal of Applied Electrochemistry, 45*(6), 557-566.

Momeni, Mohamad Mohsen, & Ghayeb, Yousef. (2016). Fabrication, characterization and photoelectrochemical performance of chromium-sensitized titania nanotubes as efficient photoanodes for solar water splitting. *Journal of Solid State Electrochemistry, 20*(3), 683-689.

Moniz, Savio JA, Shevlin, Stephen A, Martin, David James, Guo, Zheng-Xiao, & Tang, Junwang. (2015). Visible-light driven heterojunction photocatalysts for water splitting–a critical review. *Energy & Environmental Science, 8*(3), 731-759.

Mor, Gopal K, Varghese, Oomman K, Paulose, Maggie, Shankar, Karthik, & Grimes, Craig A. (2006). A review on highly ordered, vertically oriented TiO_2 nanotube arrays: fabrication, material properties, and solar energy applications. *Solar Energy Materials and Solar Cells, 90*(14), 2011-2075.

More, PD, Shahane, GS, Deshmukh, LP, & Bhosale, PN. (2003). Spectro-structural characterisation of CdSe 1− x Te x alloyed thin films. *Materials Chemistry and Physics, 80*(1), 48-54.

Morgan, Dana L, Zhu, Huai-Yong, Frost, Ray L, & Waclawik, Eric R. (2008). Determination of a morphological phase diagram of titania/titanate nanostructures from alkaline hydrothermal treatment of Degussa P25. *Chemistry of Materials, 20*(12), 3800-3802.

Nakahira, Atsushi, Kubo, Takashi, & Numako, Chiya. (2010). Formation mechanism of TiO_2-derived titanate nanotubes prepared by the hydrothermal process. *Inorganic Chemistry, 49*(13), 5845-5852.

Nam, Chau Thanh, Falconer, John L, & Yang, Wein-Duo. (2014). Morphology, structure and adsorption of titanate nanotubes prepared using a solvothermal method. *Materials Research Bulletin, 51*, 49-55.

Ni, Meng, Leung, Michael KH, Leung, Dennis YC, & Sumathy, K. (2007). A review and recent developments in photocatalytic water-splitting using TiO_2 for hydrogen production. *Renewable and Sustainable Energy Reviews, 11*(3), 401-425.

Nicolau, YF. (1985). Solution deposition of thin solid compound films by a successive ionic-layer adsorption and reaction process. *Applications of Surface Science, 22*, 1061-1074.

Okamoto, Hirotaka, Sugiyama, Yusuke, & Nakano, Hideyuki. (2011). Synthesis and modification of silicon nanosheets and other silicon nanomaterials. *Chemistry–A European Journal, 17*(36), 9864-9887.

Padiyan, D Pathinettam, Marikani, A, & Murali, KR. (2003). Influence of thickness and substrate temperature on electrical and photoelectrical properties of vacuum-deposited CdSe thin films. *Materials Chemistry and Physics, 78*(1), 51-58.

Park, Sang-Sun, Eom, Seon-Mi, Anpo, Masakazu, Seo, Dong-Ho, Jeon, Yukwon, & Shul, Yong-gun. (2011). N-doped anodic titania nanotube arrays for hydrogen production. *Korean Journal of Chemical Engineering, 28*(5), 1196-1199.

Paulose, Maggie, Prakasam, Haripriya E, Varghese, Oomman K, Peng, Lily, Popat, Ketul C, Mor, Gopal K, . . . Grimes, Craig A. (2007). TiO_2 nanotube arrays of 1000 μm length by anodization of titanium foil: phenol red diffusion. *The Journal of Physical Chemistry C, 111*(41), 14992-14997.

Pawar, Sachin A, Devan, Rupesh S, Patil, Dipali S, Moholkar, Annasaheb V, Gang, Myeng Gil, Ma, Yuan-Ron, . . . Patil, Pramod S. (2013). Improved solar cell performance of chemosynthesized cadmium selenide pebbles. *Electrochimica Acta, 98*, 244-254.

Peng, Xinsheng, & Chen, Aicheng. (2006). Large-scale synthesis and characterization of TiO_2 - based nanostructures on Ti substrates. *Advanced Functional Materials, 16*(10), 1355-1362.

Pu, Ying-Chih, Wang, Gongming, Chang, Kao-Der, Ling, Yichuan, Lin, Yin-Kai, Fitzmorris, Bob C, . . . Zhang, Jin Z. (2013). Au nanostructure-decorated TiO2 nanowires exhibiting photoactivity across entire UV-visible region for photoelectrochemical water splitting. *Nano Letters, 13*(8), 3817-3823.

Qiu, Jijun, Yu, Weidong, Gao, Xiangdong, & Li, Xiaomin. (2006). Sol–gel assisted ZnO nanorod array template to synthesize TiO_2 nanotube arrays. *Nanotechnology, 17*(18), 4695.

Ramaiah, K Subba, Su, Yan-Kuin, Chang, Shoou-Jinn, Juang, Fuh-Shyang, Ohdaira, K, Shiraki, Yasuhiro, . . . Bhatnagar, Anil-Kumar. (2001). Characterization of Cu doped CdSe thin films grown by vacuum evaporation. *Journal of Crystal Growth, 224*(1), 74-82.

Ran, Jingrun, Zhang, Jun, Yu, Jiaguo, Jaroniec, Mietek, & Qiao, Shi Zhang. (2014). Earth-abundant cocatalysts for semiconductor-based photocatalytic water splitting. *Chemical Society Reviews, 43*(22), 7787-7812.

Rao, Chintamani Nagesa Ramachandra, Müller, Achim, & Cheetham, Anthony K. (2006). *The chemistry of nanomaterials: synthesis, properties and applications*: John Wiley & Sons.

Reyes-Gil, Karla R, & Robinson, David B. (2013). WO_3-enhanced TiO_2 nanotube photoanodes for solar water splitting with simultaneous wastewater treatment. *ACS Applied Materials & Interfaces, 5*(23), 12400-12410.

Robel, István, Subramanian, Vaidyanathan, Kuno, Masaru, & Kamat, Prashant V. (2006). Quantum dot solar cells. Harvesting light energy with CdSe nanocrystals molecularly linked to mesoscopic TiO_2 films. *Journal of the American Chemical Society, 128*(7), 2385-2393.

Rodenas, Pau, Song, Taesup, Sudhagar, Pitchaimuthu, Marzari, Gabriela, Han, Hyungkyu, Badia‐Bou, Laura, . . . Bisquert, Juan. (2013). Quantum dot based heterostructures for unassisted photoelectrochemical hydrogen generation. *Advanced Energy Materials, 3*(2), 176-182.

Roy, Poulomi, Berger, Steffen, & Schmuki, Patrik. (2011). TiO_2 nanotubes: synthesis and applications. *Angewandte Chemie International Edition, 50*(13), 2904-2939.

Sander, Melissa S, Cote, Matthew J, Gu, Wei, Kile, Brian M, & Tripp, Carl P. (2004). Template-assisted fabrication of dense, aligned arrays of titania nanotubes with well-controlled dimensions on substrates. *Advanced Materials, 16*(22), 2052-2057.

Santos, Laís C, Poli, Alessandra L, Cavalheiro, Carla, & Neumann, Miguel G. (2009). The UV/H2O2-photodegradation of poly (ethyleneglycol) and model compounds. *Journal of the Brazilian Chemical Society, 20*(8), 1467-1472.

Seah, MP. (2001). Summary of ISO/TC 201 Standard: VII ISO 15472: 2001—surface chemical analysis—x-ray photoelectron spectrometers—calibration of energy scales. *Surface and Interface Analysis, 31*(8), 721-723.

Shin, Hyunjung, Jeong, D ‐ K, Lee, JAEGAB, Sung, Myung M, & Kim, JIYOUNG. (2004). Formation of TiO_2 and ZrO_2 nanotubes using atomic layer deposition with ultraprecise control of the wall thickness. *Advanced Materials, 16*(14), 1197-1200.

Solanki, Chetan Singh. (2015). *Solar photovoltaics: fundamentals, technologies and applications*: PHI Learning Pvt. Ltd.

Song, Xiaohui, Wang, Minqiang, Zhang, Hao, Deng, Jianping, Yang, Zhi, Ran, Chenxin, & Yao, Xi. (2013). Morphologically controlled electrodeposition of CdSe on mesoporous TiO 2 film for quantum dot-sensitized solar cells. *Electrochimica Acta, 108*, 449-457.

Sopha, Hanna, Hromadko, Ludek, Nechvilova, Katerina, & Macak, Jan M. (2015). Effect of electrolyte age and potential changes on the morphology of TiO_2 nanotubes. *Journal of Electroanalytical Chemistry, 759*, 122-128.

Spadavecchia, Francesca, Ardizzone, Silvia, Cappelletti, Giuseppe, Falciola, Luigi, Ceotto, Michele, & Lotti, Davide. (2013). Investigation and optimization of photocurrent transient measurements on nano-TiO_2. *Journal of Applied Electrochemistry, 43*(2), 217-225.

Sreekantan, Srimala, Hazan, Roshasnorlyza, & Lockman, Zainovia. (2009). Photoactivity of anatase–rutile TiO_2 nanotubes formed by anodization method. *Thin Solid Films, 518*(1), 16-21.

Su, Lili, Lv, Jun, Wang, Honge, Liu, Lingjuan, Xu, Guangqing, Wang, Dongmei, . . . Wu, Yucheng. (2014). Improved visible light photocatalytic activity of CdSe modified TiO_2 nanotube arrays with different intertube spaces. *Catalysis Letters, 144*(4), 553-560.

Suzuki, Yoshikazu, & Yoshikawa, Susumu. (2004). Synthesis and thermal analyses of TiO_2-derived nanotubes prepared by the hydrothermal method. *Journal of Materials Research, 19*(04), 982-985.

Tan, AW, Pingguan-Murphy, B, Ahmad, R, & Akbar, SA. (2012). Review of titania nanotubes: fabrication and cellular response. *Ceramics International, 38*(6), 4421-4435.

Tanaka, Shin-ichi, Hirose, Norimitsu, & Tanaki, Toshiyuki. (2005). Effect of the temperature and concentration of NaOH on the formation of porous TiO_2. *Journal of The Electrochemical Society, 152*(12), C789-C794.

Tang, Yuxin, Lai, Yuekun, Gong, Dangguo, Goh, Kok‐Hui, Lim, Teik‐Thye, Dong, Zhili, & Chen, Zhong. (2010). Ultrafast synthesis of layered titanate microspherulite particles by electrochemical spark discharge spallation. *Chemistry–A European Journal, 16*(26), 7704-7708.

Taveira, LV, Macak, JM, Tsuchiya, H, Dick, LFP, & Schmuki, P. (2005). Initiation and growth of self-organized TiO_2 nanotubes anodically formed in NH_4F / $(NH_4)_2SO_4$ electrolytes. *Journal of the Electrochemical Society, 152*(10), B405-B410.

Tian, Fang, Zhang, Yupeng, Zhang, Jun, & Pan, Chunxu. (2012). Raman spectroscopy: a new approach to measure the percentage of anatase TiO_2 exposed (001) facets. *The Journal of Physical Chemistry C, 116*(13), 7515-7519.

Tian, Jian, Zhao, Zhenhuan, Kumar, Anil, Boughton, Robert I, & Liu, Hong. (2014). Recent progress in design, synthesis, and applications of one-dimensional TiO_2 nanostructured surface heterostructures: a review. *Chemical Society Reviews, 43*(20), 6920-6937.

Todescato, Francesco, Minotto, Alessandro, Signorini, Raffaella, Jasieniak, Jacek J, & Bozio, Renato. (2013). Investigation into the Heterostructure Interface of CdSe-Based Core–Shell Quantum Dots Using Surface-Enhanced Raman Spectroscopy. *ACS nano, 7*(8), 6649-6657.

Tong, Hua, Ouyang, Shuxin, Bi, Yingpu, Umezawa, Naoto, Oshikiri, Mitsutake, & Ye, Jinhua. (2012). Nano-photocatalytic materials: possibilities and challenges. *Advanced Materials, 24*(2), 229-251.

Turner, John A. (2004). Sustainable hydrogen production. *Science, 305*(5686), 972-974.

VanderHyde, Cephas A, Sartale, SD, Patil, Jayant M, Ghoderao, Karuna P, Sawant, Jitendra P, & Kale, Rohidas B. (2015). Room temperature chemical bath deposition of cadmium selenide, cadmium sulfide and cadmium sulfoselenide thin films with novel nanostructures. *Solid State Sciences, 48*, 186-192.

Vargas‐Hernández, C, Lara, VC, Vallejo, JE, Jurado, JF, & Giraldo, O. (2005). XPS, SEM and XRD investigations of CdSe films prepared by chemical bath deposition. *Physica Status Solidi (b), 242*(9), 1897-1901.

Wang, Congjun, Thompson, Robert L, Baltrus, John, & Matranga, Christopher. (2009). Visible light photoreduction of CO_2 using CdSe/Pt/TiO_2 heterostructured catalysts. *The Journal of Physical Chemistry Letters, 1*(1), 48-53.

Wang, Gongming, Yang, Xunyu, Qian, Fang, Zhang, Jin Z, & Li, Yat. (2010). Double-sided CdS and CdSe quantum dot co-sensitized ZnO nanowire arrays for photoelectrochemical hydrogen generation. *Nano Letters, 10*(3), 1088-1092.

Wang, Peifang, Ao, Yanhui, Wang, Chao, Hou, Jun, & Qian, Jin. (2013). Preparation of graphene-modified TiO_2 nanorod arrays with enhanced photocatalytic activity by a solvothermal method. *Materials Letters, 101*, 41-43.

Wang, Peng, Li, Danzhen, Chen, Jing, Zhang, Xiaoyun, Xian, Jiangjun, Yang, Xue, . . . Shao, Yu. (2014). A novel and green method to synthesize CdSe quantum dots-modified TiO_2 and its enhanced visible light photocatalytic activity. *Applied Catalysis B: Environmental, 160*, 217-226.

Wang, Qiang, Wen, Zhenhai, & Li, Jinghong. (2006). Solvent-controlled synthesis and electrochemical lithium storage of one-dimensional TiO_2 nanostructures. *Inorganic Chemistry, 45*(17), 6944-6949.

Wang, Wenchao, Li, Fang, Zhang, Dieqing, Leung, Dennis YC, & Li, Guisheng. (2016). Photoelectrocatalytic hydrogen generation and simultaneous degradation of organic pollutant via CdSe/TiO_2 nanotube arrays. *Applied Surface Science, 362*, 490-497.

Wu, Feng, Hu, Xiaoyun, Fan, Jun, Liu, Enzhou, Sun, Tao, Kang, Limin, . . . Liu, Hanchen. (2013). Photocatalytic activity of Ag/TiO_2 nanotube arrays enhanced by surface plasmon resonance and application in hydrogen evolution by water splitting. *Plasmonics, 8*(2), 501-508.

Wu, Zhi, Wang, Yingying, Sun, Lan, Mao, Yuxiao, Wang, Mengye, & Lin, Changjian. (2014). An ultrasound-assisted deposition of NiO nanoparticles on TiO_2 nanotube arrays for enhanced photocatalytic activity. *Journal of Materials Chemistry A, 2*(22), 8223-8229.

Xia, Younan, Yang, Peidong, Sun, Yugang, Wu, Yiying, Mayers, Brian, Gates, Byron, . . . Yan, Haoquan. (2003). One-dimensional nanostructures: synthesis, characterization, and applications. *Advanced materials, 15*(5), 353-389.

Xu, Yong, & Schoonen, Martin AA. (2000). The absolute energy positions of conduction and valence bands of selected semiconducting minerals. *American Mineralogist, 85*(4), 543-556.

Xue, Jinbo, Shen, Qianqian, Liang, Wei, Liu, Xuguang, & Yang, Fei. (2013). Photosensitization of TiO_2 nanotube arrays with CdSe nanoparticles and their photoelectrochemical performance under visible light. *Electrochimica Acta, 97*, 10-16.

Xue, Jinbo, Shen, Qianqian, Yang, Fei, Liang, Wei, & Liu, Xuguang. (2014). Investigation on the influence of pH on structure and photoelectrochemical properties of CdSe electrolytically deposited into TiO_2 nanotube arrays. *Journal of Alloys and Compounds, 607*, 163-168.

Yan, Shicheng, Wan, Lijuan, Li, Zhaosheng, & Zou, Zhigang. (2011). Facile temperature-controlled synthesis of hexagonal Zn_2GeO_4 nanorods with different aspect ratios toward improved photocatalytic activity for overall water splitting and photoreduction of CO_2. *Chemical Communications, 47*(19), 5632-5634.

Yang, Lixia, Luo, Shenglian, Liu, Ronghua, Cai, Qingyun, Xiao, Yan, Liu, Shaohuan, . . . Wen, Lingfei. (2010a). Fabrication of CdSe nanoparticles sensitized long TiO_2 nanotube arrays for photocatalytic degradation of anthracene-9-carbonxylic acid under green monochromatic light. *The Journal of Physical Chemistry C, 114*(11), 4783-4789.

Yang, Min, Ji, Ying, Liu, Wei, Wang, Ying, & Liu, Xiaoyang. (2014). Facile microwave-assisted synthesis and effective photocatalytic hydrogen generation of Zn_2GeO_4 with different morphology. *RSC Advances, 4*(29), 15048-15054.

Yang, Min, Shrestha, Nabeen K, & Schmuki, Patrik. (2010b). Self-organized CdS microstructures by anodization of Cd in chloride containing Na_2S solution. *Electrochimica Acta, 55*(26), 7766-7771.

Yao, Huizhen, Fu, Wuyou, Yang, Haibin, Ma, Jinwen, Sun, Meiling, Chen, Yanli, . . . Li, Meijing. (2014). Vertical growth of two-dimensional TiO_2 nanosheets array films and enhanced photoelectrochemical properties sensitized by CdS quantum dots. *Electrochimica Acta, 125*, 258-265.

Yasuda, Kouji, Macak, Jan M, Berger, Steffen, Ghicov, Andrei, & Schmuki, Patrik. (2007). Mechanistic aspects of the self-organization process for oxide nanotube formation on valve metals. *Journal of the electrochemical society, 154*(9), C472-C478.

Ye, Meidan, Gong, Jiaojiao, Lai, Yuekun, Lin, Changjian, & Lin, Zhiqun. (2012). High-efficiency photoelectrocatalytic hydrogen generation enabled by palladium quantum dots-sensitized TiO_2 nanotube arrays. *Journal of the American Chemical Society, 134*(38), 15720-15723.

Yu, Kehan, & Chen, Junhong. (2009). Enhancing solar cell efficiencies through 1-D nanostructures. *Nanoscale Research Letters, 4*(1), 1-10.

Yu, Xiao-Yun, Lei, Bing-Xin, Kuang, Dai-Bin, & Su, Cheng-Yong. (2012). High performance and reduced charge recombination of CdSe/CdS quantum dot-sensitized solar cells. *Journal of Materials Chemistry, 22*(24), 12058-12063.

Zhang, Dongbai, Qi, Limin, Ma, Jiming, & Cheng, Humin. (2002). Formation of crystalline nanosized titania in reverse micelles at room temperature. *J. Mater. Chem., 12*(12), 3677-3680.

Zhang, Juan, Du, Rong-Gui, Lin, Ze-Quan, Zhu, Yan-Feng, Guo, Ya, Qi, Hai-Qing, . . . Lin, Chang-Jian. (2012a). Highly efficient CdSe/CdS co-sensitized TiO_2 nanotube films for photocathodic protection of stainless steel. *Electrochimica Acta, 83*, 59-64.

Zhang, Jun, Yu, Jiaguo, Zhang, Yimin, Li, Qin, & Gong, Jian Ru. (2011). Visible light photocatalytic H_2-production activity of CuS/ZnS porous nanosheets based on photoinduced interfacial charge transfer. *Nano Letters, 11*(11), 4774-4779.

Zhang, Miao, Xu, Yanyan, Lv, Jianguo, Yang, Lei, Jiang, Xishun, He, Gang, . . . Sun, Zhaoqi. (2014). Capability of coupled CdSe/TiO_2 heterogeneous structure for photocatalytic degradation and photoconductivity. *Nanoscale Research Letters, 9*(1), 1-7.

Zhang, Zhonghai, Zhang, Lianbin, Hedhili, Mohamed Nejib, Zhang, Hongnan, & Wang, Peng. (2012b). Plasmonic gold nanocrystals coupled with photonic crystal seamlessly on TiO2 nanotube photoelectrodes for efficient visible light photoelectrochemical water splitting. *Nano Letters, 13*(1), 14-20.

Zhao, Jingyong, Yao, Jianxi, Zhang, Yongzhe, Guli, Mina, & Xiao, Li. (2014). Effect of thermal treatment on TiO_2 nanorod electrodes prepared by the solvothermal method for dye-sensitized solar cells: surface reconfiguration and improved electron transport. *Journal of Power Sources, 255*, 16-23.

Zhao, Yu, Yan, Zhiqiang, Liu, Jun, & Wei, Aixiang. (2013). Synthesis and characterization of CdSe nanocrystalline thin films deposited by chemical bath deposition. *Materials Science in Semiconductor Processing, 16*(6), 1592-1598.

Zhou, Ru, Zhang, Qifeng, Tian, Jianjun, Myers, Daniel, Yin, Min, & Cao, Guozhong. (2013). Influence of cationic precursors on CdS quantum-dot-sensitized solar cell prepared by successive ionic layer adsorption and reaction. *The Journal of Physical Chemistry C, 117*(51), 26948-26956.

Zwilling, Valérie, Darque-Ceretti, Evelyne, Boutry-Forveille, Annick, David, Daniel, Perrin, Michel-Yves, & Aucouturier, Marc. (1999). Structure and physicochemistry of anodic oxide films on titanium and TA6V alloy. *Surface and Interface Analysis*, *27*(7), 629-637.

LIST OF PUBLICATIONS AND PAPERS PRESENTED

ISI-Cited Publications:

Kung Shiuh Lau, Chin Wei Lai, You Sing Lim, Sharifah Bee Abd Hamid, Electrochemical growth of self-organized anodic TiO2 nanotubes for better photocatalytic degradation reaction, Materials Research Innovations, 18(S6), pp. S6-462-S6-464, (2014).

Conference Proceedings:

1. Chin Wei Lai*, Joon Ching Juan, **Kung Shiuh Lau**, Nur Azimah Binti Abd Samad, Soon Weng Chong, Sharifah Bee Abd Hamid. Investigation on Potential Solar-activated Photoelectrode for Direct Water Electrolysis Hydrogen Generation in a Tandem Photoelectrochemical Cell. Presented at 5th international Conference on Solid State Science and Technology 2015 (ICSSST 2015), Bayview Hotel, Langkawi (13rd to 15th December 2015)

2. Chin Wei Lai*, **Kung Shiuh Lau**, Nur Azimah Binti Abd Samad, Joon Ching Juan, Sharifah Bee Abd Hamid. Development of Hybrid WO3-TiO2 Nanotubes Film for Solar Hydrogen Generation via Water Electrolysis in a Custom-designed Water Splitter. Energy Materials Nanotechnology (EMN) Hong Kong Meeting 2015, Eaton Hotel, Kowloon, Hong Kong, China (9th to 12nd December 2015)

3. Chin Wei Lai*, **Kung Shiuh Lau**. Development of Hybrid WO3-TiO2 Nanotubes for Solar Hydrogen Generation via Water Electrolysis. Presented at Malaysia-Japan International Conference on Nanoscience, Nanotechnology and Nanoengineering 2014 (NANO-SciTech 2014 & IC-NET 2014), UiTM Shah Alam, (28th Feb- 3rd Mac 2014)

4. **Kung Shiuh Lau**, Chin Wei Lai*, You Sing Lim, Sharifah Bee Abd Hamid. Electrochemical growth of self-organized anodic TiO_2 nanotubes for better photocatalytic degradation reaction. Presented at 1st International Conference on The Science and Engineering of Materials 2013 (ICoSEM 2013), Sunway Putra Hotel, Kuala Lumpur (13th to 14th November 2013).